CHAPTER - 5

RESULTS AND DISCUSSION

Chapter 5 consists of detailed results and discussion on the experiments performed in the laboratory fabricated direct sodium borohydride fuel cell (DSBFC) using laboratory synthesized PVA based alkaline membrane electrolyte. The current chapter is divided into two parts, i.e., based on pristine PVA-TEOS alkaline membrane electrolyte (**Part-I**) and physically crosslinked PVA-TEOS membrane electrolyte (**Part-II**). **Part I** and **Part II**, focus on synthesizing NaOH doped PVA-TEOS alkaline membrane electrolyte. Initially, **Part I** consists of detailed discussion on the characterizations of NaOH doped pristine PVA-TEOS membrane electrolyte through various types of physical characterization and electrochemical characterization. The physical characterizations consist of water and NaOH uptake, ion exchange capacity (IEC), SEM, XRD, FTIR and mechanical strength. Whereas, electrochemical characterization consists of cyclic voltammetry (V) and electrochemical impedance spectroscopy (EIS). At the end of the **Part-I**, the performance study of the NaOH doped pristine PVA-TEOS membrane electrolyte in the direct sodium borohydride fuel cell (DSBFC) is discussed.

Similarly, **Part-II** consists of detailed characterizations of NaOH doped physically crosslinked PVA-TEOS membrane electrolytes using physical and electrochemical characterization techniques. The important physical characterizations were water and NaOH uptake, XRD, FTIR, SEM, swelling ratio and mechanical strength test. Same electrochemical characterization as adopted in **Part-I**, also used in **Part-II**. The performance study of NaOH doped physically crosslinked PVA-TEOS membrane electrolyte in DSBFC is discussed in detail in **Part-II**. The optimization of the process parameters of DSBFC using best membrane electrolyte i.e., NaOH

doped physically crosslinked membrane electrolyte in DSBFC using response surface methodology is discussed in Part II. Finally, the efficiency and stability of DSBFC are discussed in **Part II**.

5.1 NaOH doped pristine PVA-TEOS membrane electrolyte: Part-I

5.1.1 Membrane Characterization

5.1.1.1 Water and NaOH uptake

The prepared PVA based membrane as discussed in the **Chapter 3 Experimental** section (page no. 60) was subjected to water and NaOH uptake tests. The pristine PVA-TEOS membrane obtained was transparent, homogeneous, and flexible in nature. At the end of the manufacturing process, the thickness of the dry PVA membranes recorded was in the order of 200 ± 10 μm. The water uptake and NaOH uptake of the synthesized membrane are the essential parameters whose presence in adequate quantity with the proper balance between these two parameters ensures the better ionic conductivity of the membrane electrolyte and thus, the fuel cell performance. Too high NaOH uptake may reduce the membrane conductivity due to poor ionic mobility (Gupta and Pramanik 2019a, An et al. 2012). Similarly, excessively high water uptake will impact the other properties of the membrane, such as swelling of the membrane alongwith mechanical and thermal stability also. The sol-gel-prepared pristine PVA-TEOS composite membrane showed higher water uptake than pristine PVA membrane due to the hygroscopic nature of silica present in the PVA matrix. **Figure 5.1** shows the water and NaOH uptake of the pristine PVA and pristine PVA-TEOS membrane soaked in various concentrations of NaOH at the room temperature of 30 ^{o}C. The water uptake of the PVA-TEOS membrane in water/0M NaOH was recorded as highest i.e., 161.2 wt. % at temperature of 30 ^{o}C whereas, pristine PVA membrane showed little water uptake

of 142.16 wt. % when soaked in water only (0 M NaOH) at the same temperature of 30 ºC. The PVA-TEOS membrane always absorbed more water than pristine PVA for all concentrations of NaOH. As already mentioned, it may be due to the presence of hygroscopic silica in the pristine PVA-TEOS membrane matrix. The water uptake decreases as the concentration of NaOH increases, irrespective of the type of membrane as it is clearly seen in **Figure 5.1**. The relative concentration of water decreases with an increase in NaOH concentration and thus, the water uptake is decreasing with increase in NaOH (Yadav and Pramanik 2023). The NaOH uptake of both pristine PVA and PVA-TEOS membrane increases with the increase in NaOH concentration upto 6 M. However, further increase in NaOH concentration beyond 6 M, NaOH uptake of the membrane decreases. The maximum NaOH uptake of pristine PVA and pristine PVA-TEOS were 32.64 wt. % and 39.16 wt. %, respectively when doped with 6 M NaOH.

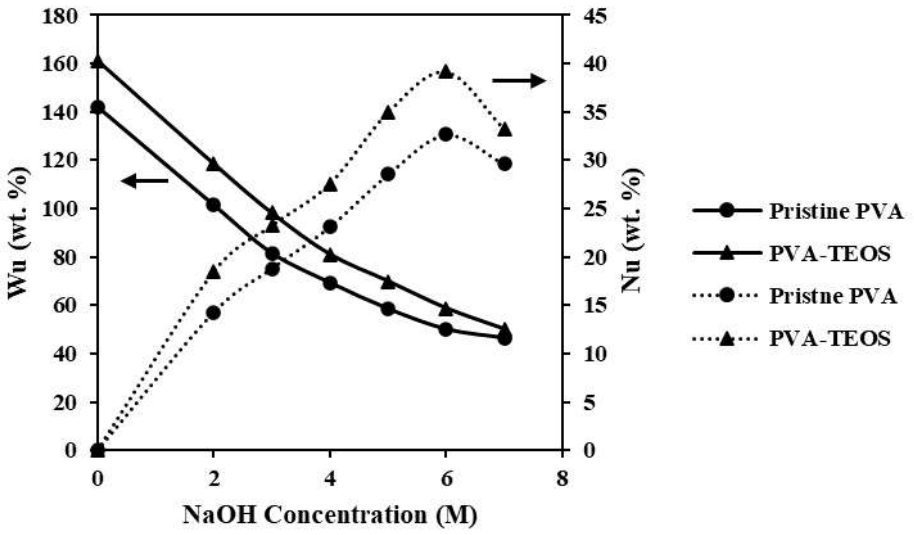

Figure 5.1 Water uptake (Wu) and NaOH uptake (Nu) of pristine PVA and PVA-TEOS membranes doped in different NaOH concentrations.

The initial increase in NaOH uptake may be due to an increase in NaOH concentration. Initially, there is no NaOH present in the membrane matrix due to which there must be the transportation of NaOH from high concentration to low concentration. However, with the subsequent increase in NaOH concentration beyond 6 M, the mobility of NaOH decreases due to increased solution viscosity. This prevented the addition of further NaOH to the polymer matrix (Gupta and Pramanik 2019a, An et al. 2012). Thus, the maximum amount of NaOH uptake is observed for both the PVA and PVA-TEOS membranes doped with 6 M NaOH concentration as the membrane gets saturated at this concentration (**Figure 5.1**). However, the determination of ionic conductivity through EIS study of the membrane electrolyte is essential to find out optimum doping concentration of NaOH.

5.1.1.2 Ion exchange capacity (IEC)

The ion exchange capacity (IEC) of membrane electrolyte demonstrates its suitability for the use as a solid electrolyte in a fuel cell. The ion exchange capacity indicates the number of exchangeable groups in the membrane. In general, better ionic conductivity is associated with a higher IEC. The IEC is a critical parameter for determining the nature of the ionic charge of membrane electrolytes in terms of the equivalent of ionic functional groups present per unit dry weight of membrane electrolyte (Gupta and Pramanik 2018). **Figure 5.2** shows the ion exchange capacity of the pristine PVA-TEOS membrane as a function of NaOH concentration. A similar trend of IEC with varying NaOH concentration is observed here, as it was seen in the case of NaOH uptake with varying NaOH concentrations which has already been discussed earlier in **section 5.1.1.1** (page no. 83). It is seen from the **Figure 5.2** that the IEC increases with the increase in NaOH concentration up to 6 M. However, further increase in NaOH concentration, the IEC of the PVA-TEOS membrane decreases. It should be noted that the IEC depends on the amount of NaOH present in the

membrane matrix and thus, the IEC is changing with NaOH concentration. The maximum IEC of 1.14 meq/g was recorded for 6 M NaOH concentration (**Table 5.1**).

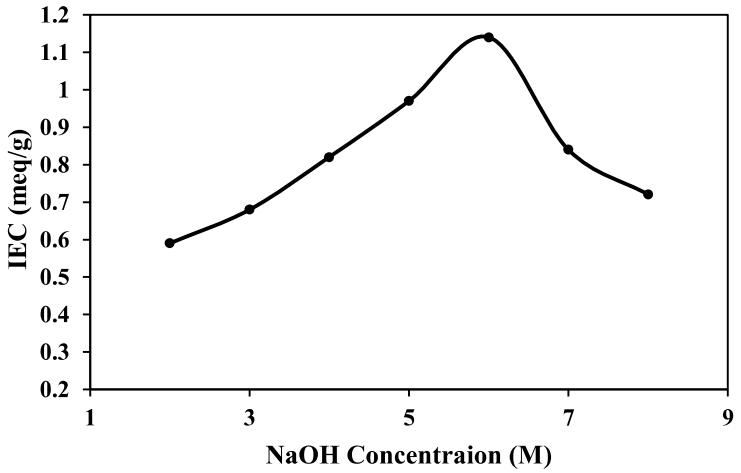

Figure 5.2 Ion exchange capacity of PVA-TEOS membrane as a function of NaOH concentration at room temperature 30 ºC.

Table 5.1 IEC of the PVA-TEOS Membrane doped in different NaOH concentrations at the room temperature of 30 ºC.

NaOH doping concentration	2M	3M	4M	5M	6M	7M	8M
IEC (meq/g)	0.59±0.02	0.68±0.04	0.82±0.01	0.97±0.02	1.14±0.03	0.84±0.05	0.72±0.04

5.1.1.3 Ionic Conductivity of PVA-TEOS membrane electrolyte

The ionic conductivity of the synthesized membrane electrolytes was measured using the electrochemical impedance spectroscopy (EIS) in a two probe system as discussed in the **Chapter 3 Experimental** (page no. 64). The ionic conductivity of the membrane electrolyte was measured with the varying temperature and doping concentration of NaOH keeping the membrane thickness and contact area fixed value of 200±10 μm and 1 cm^2 (1 cm × 1 cm), respectively. The EIS of all

synthesized membranes doped with various concentrations of NaOH at the temperature of 25 ^{o}C are presented in **Figure 5.3**. The membrane samples of 6 cm^2 (2 cm × 3 cm) surface area were dipped in various concentrations of NaOH for 24 h prior to the EIS measurements for varying concentration of NaOH doping. Two distinct zones could be observed in typical EIS spectra, namely the high frequency zone and low frequency zone (**Figure 5.3**). The high frequency zone is related to the ionic conductivity of the solid electrolyte membrane. The electrode and electrolyte interface of the two probe arrangements can be considered as capacitance. An ideal capacitance should display a vertical spike in an impedance diagram. In the present analysis, instead of a vertical spike, an angled spike with an angle of less than 90^{o} was detected. The non-homogeneous or roughness of the electrode and electrolyte interface is the major cause of this non-ideal behavior (Yang et al. 2006). Generally, the EIS characteristics give information about the bulk resistance (R) of the PVA-TEOS membrane electrolyte. The intercept on the real axis (Z') on the higher frequency zone gives the value of R (**Figure 5.3**). The intercept of EIS in the real axis is also presented in the onset for better clarity. The ionic conductivity of the membrane electrolyte was calculated from Equation 3.5 **Chapter 3** (page no. 65). It is seen from **Figure 5.3** that the ionic conductivity of the PVA-TEOS membrane depends on the quantity of NaOH doped in the membrane and water uptake both. Initially, the ionic conductivity of PVA-TEOS membrane increases with the increase in NaOH concentration up to 4 M and then starts decreasing when NaOH concentration was increased beyond 4 M.

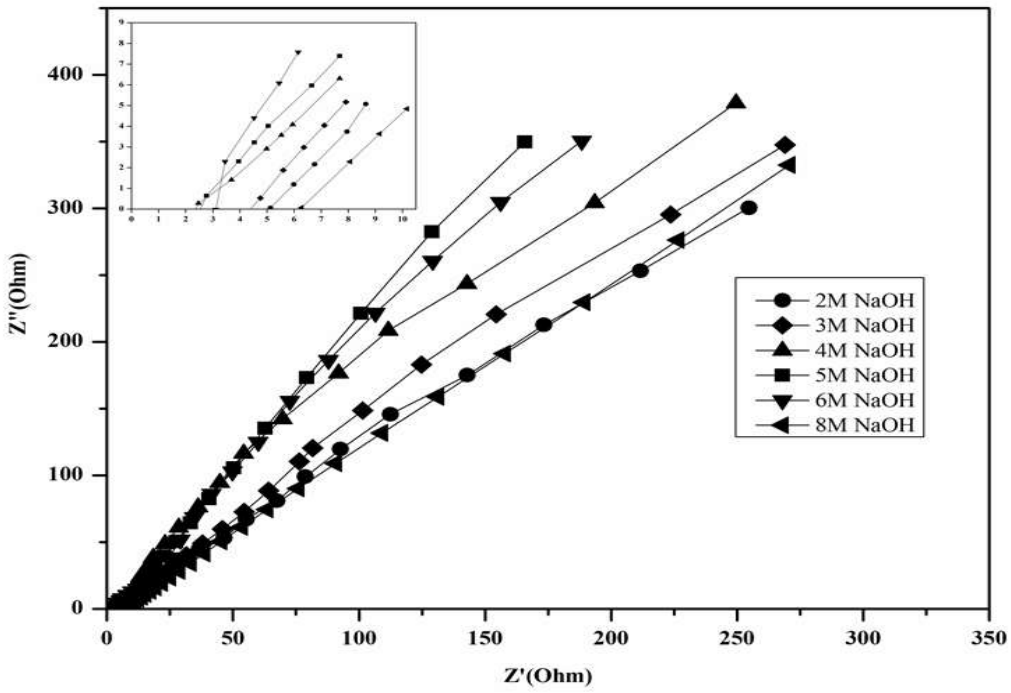

Figure 5.3 EIS characteristics of PVA-TEOS membrane doped with various NaOH concentrations at 25 ^{o}C temperature.

The highest ionic conductivity of $9.09 \pm 0.5 \times 10^{-3}$ S/cm was obtained for the membrane electrolyte doped with 4 M NaOH i.e., PVA-TEOS-(4M) (**Table 5.2**). However, membrane electrolytes doped with a very high concentration of NaOH i.e., 8 M, resulted in the lowest ionic conductivity of $3.27 \pm 0.3 \times 10^{-3}$ S/cm. The reason for such high ionic conductivity of PVA-TEOS-(4M) membrane electrolyte, may be due to the relatively higher water content (81.03 wt. %) (Kim et al. 2004) and moderate NaOH uptake of 27.58 wt. % which makes a proper balance to give rise to the highest ionic mobility within the membrane matrix (Yadav and Pramanik 2023). Thus, the PVA-TEOS-(4M) showed the highest ionic conductivity ($9.09 \pm 0.5 \times 10^{-3}$ S/cm). On the other side, the PVA-TEOS-(6M) membrane with the highest NaOH uptake (39.16 wt. %) shows lower conductivity of $6.23 \pm 0.3 \times 10^{-3}$ S/cm and it may be due to low water content (58.74 wt. %) and very high NaOH

uptake (39.16 wt. %) in the membrane matrix and thus, it results in poor ionic mobility (An at al. 2012).

Table 5.2 Ionic conductivity of PVA-TEOS membrane doped in various concentrations of NaOH at the temperature of 25 ^{o}C.

NaOH doping concentration	**2 M**	**3 M**	**4 M**	**5 M**	**6 M**	**8 M**
Ionic Conductivity ($\times 10^{-3}$) (S/cm)	3.90 ± 0.4	4.70 ± 0.3	**9.09 ± 0.5**	8.26 ± 0.4	6.23 ± 0.3	3.27 ± 0.3

The effect of temperature on the ionic conductivity of the best membrane electrolyte of ionic conductivity 9.09 ± 0.5 × 10^{-3} S/cm i.e., PVA-TEOS-(4M) was also studied. **Figure 5.4** shows the EIS characteristics of the PVA-TEOS-(4M) membrane electrolyte at different temperature ranging from 25 ^{o}C to 55 ^{o}C. It is observed from **Table 5.3** that the ionic conductivity of the membrane electrolyte increases with the increase in temperature. The highest ionic conductivity of 9.98±0.3×10^{-3} S/cm was obtained at the temperature of 50 ^{o}C for the membrane electrolyte PVA-TEOS-(4M). It should be noted that the PVA-TEOS membrane electrolyte got damaged and started beyond 55 oC i.e., at the temperatute of 60 ^{o}C. It is well known that the moisture content of the membrane electrolyte also plays an important role in controlling the ionic conductivity of the membrane electrolyte. The proper amount of moisture must be present during the cell experiment. The lack of moisture or dehydration can lead to an increase in the measured resistance of membrane electrolyte (Diaz et al. 2023). Moreover, the water content or water uptake of the membrane is also temperature dependent. It is seen from the water uptake study with varying temperature (**Table 5.3**) that the water uptake increases with the increase in temperature and thus, the ionic conductivity also increases (Yan et al. 2007). In addition to water content in the

membrane matrix, the enhancement in the ionic conductivity may be due to increased thermal motion of polymer chain segment at higher temperature, increasing the speed of ions transport and the number of transport tunnels (Wu et al. 2008). Moreover, when the temperature rises, the structural relaxation of the polymer chains increases free-volume, contributing to an improvement in ion migration capacity (Wu et al. 2008). Furthermore, viscosity and diffusion resistance significantly impacted ionic transport, and they obviously decreased with rising temperature, which enhanced the ionic conductivity of the membrane electrolyte to some extent (Popa et al. 2017).

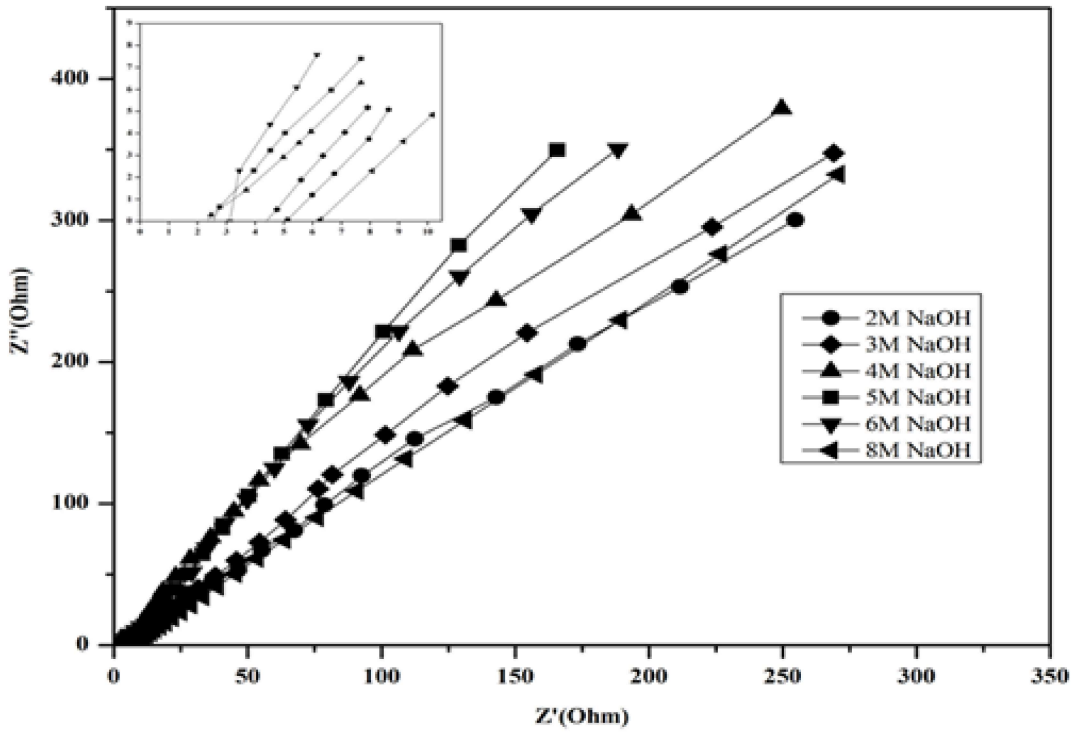

Figure 5.4 EIS characteristics of PVA-TEOS-(4M) membrane electrolyte at various temperatures.

Table 5.3 Ionic conductivity of PVA-TEOS-(4M) membrane electrolyte at various temperatures.

Temperature (°C)	25	35	45	55
Water Uptake (wt. %)	81.03	109.12	128.43	142.26
Ionic Conductivity ($\times 10^{-3}$) (S/cm)	9.09±0.5	9.41±0.2	9.72±0.6	9.98±0.3

5.1.1.4 Scanning electron microscopy (SEM) analysis

The surface morphology of some selective membranes like pristine PVA, PVA-TEOS, PVA-TEOS-(4M) and PVA-TEOS-(6M) are presented in the **Figure 5.5** for comparison of surface prperties using Nova Nano SEM 450, FEI Company, USA device. **Figure 5.5**(a) shows the surface morphology of pristine PVA where cracks and holes are visible on the surface of the pristine PVA membrane. The cracks are uniformly distributed over the surface of the membrane. On the other hand, no such cracks and holes are observed on the surface of the pristine PVA-TEOS composite membrane (**Figure 5.5**(b)). It is clearly seen in **Figure 5.5(b)** that the silica particles from TEOS are uniformly distributed over the surface of the membrane. The uniform distribution of silica particles on the surface of the cast membrane indicating a good degree of reaction between PVA and TEOS. **Figure 5.5**(c) and **Figure 5.5**(d) show the surface morphology of PVA-TEOS-(4M) and PVA-TEOS-(6M), respectively. The membrane electrolyte PVA-TEOS-(4M) shows the highest conductivity ($9.09 \pm 0.5 \times 10^{-3}$ S/cm) for ion transport with a NaOH uptake of 27.58 wt. % which is lower than the NaOH uptake of membrane PVA-TEOS-(6M) (29.16 wt. %). However, PVA-TEOS-(6M) came up with lower conductivity ($6.23 \pm 0.3 \times 10^{-3}$ S/cm) in spite of highest NaOH uptake and IEC (1.14 meq/g). Thus, it is essential to know the surface morphology of both the membrane electrolytes.

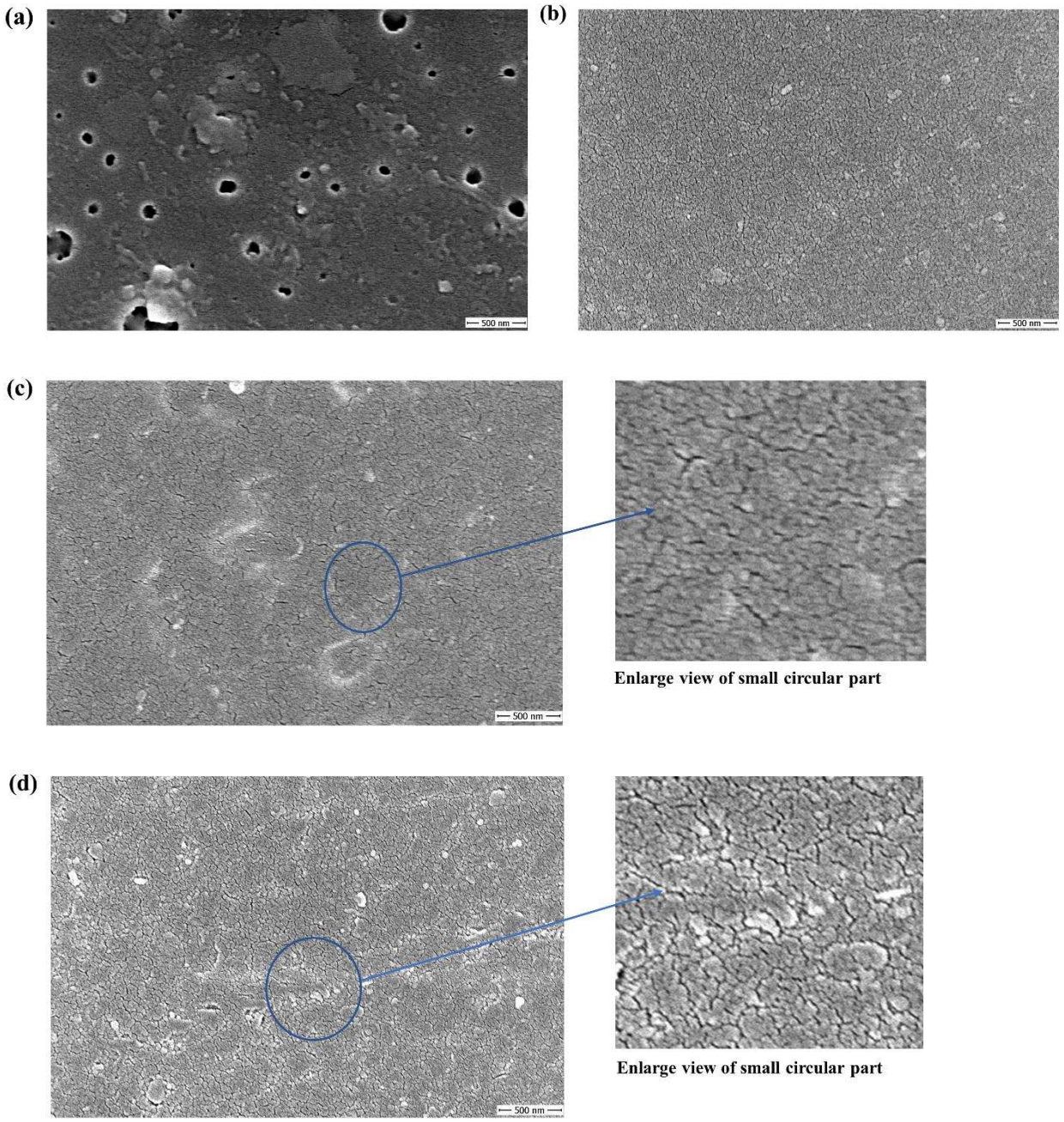

Figure 5.5 FE-SEM images of the surface of (a) pristine PVA, (b) PVA-TEOS (c) PVA-TEOS-(4M) (d) PVA-TEOS-(6M).

It is seen from **Figure 5.5**(c), the surface of the membrane electrolyte is very uniform and in the inset of **Figure 5.5**(c) does not show any aggregation of white mass of NaOH. Thus, the membrane electrolyte PVA-TEOS-(4M) exhibits the highest ionic conductivity of $9.09 \pm 0.5 \times 10^{-3}$ S/cm for better ionic mobility without any NaOH depositing on the membrane surface. However, the inset enlarged view of **Figure 5.5** (d) shows the white deposit of NaOH on the surface of the PVA-TEOS-(6M) membrane. It may be due to the highest NaOH uptake (39.16 wt. %) within the membrane. This very high NaOH content in the membrane matrix with low water content (58.74 wt. %) resulting in relatively low ionic conductivity.

5.1.1.5 FT-IR Analysis

The important functional groups present within the synthesized membrane electrolyte matrix were determined using FT-IR analysis. The FT-IR spectra of pristine PVA, pristine PVA-TEOS and PVA-TEOS-(4M) membranes in the range of 500-4000 cm^{-1} are shown in **Figure 5.6**. The broad absorption peak in the range of 3200-3400 cm^{-1}(**region-a**) demonstrates the presence of a large number of -OH groups of bound water in all the synthesized membrane electrolytes (Kim et al. 2004). The intense peak at 1643 cm^{-1} for PVA-TEOS-(4M) (**region-c)** was due to H–O–H bending vibration of water (Wang et al. 2022). The peak at 2950 cm^{-1} (**region-b**) and 1440 cm^{-1}(**region-d**) were corresponds to C-H stretching (Attaran et al. 2015). The stretching vibration of C–O groups in PVA-TEOS appears in the range of around 1350 (**region-e**) and 1000–1100 cm^{-1} (**region-f**) (An et al. 2012, Sahin 2018). In the synthesized PVA-TEOS composite membranes, the silanol groups engage strongly with the hydroxyl group in the repeating units of PVA to build covalent and hydrogen connections. The PVA-TEOS composite formation in the membrane matrix was determined by the formation of siloxane (Si–O–Si) and Si–O–C linkages. The peaks at 833 cm^{-1}

(**region-g**) and 610 cm^{-1} (**region-h**) were attributed to the development of siloxane linkages, Si-O stretching and Si-O-C formation, respectively (Mahreni et al. 2009). The Si-O-C linkages make it easier for the organic and inorganic phases to coexist.

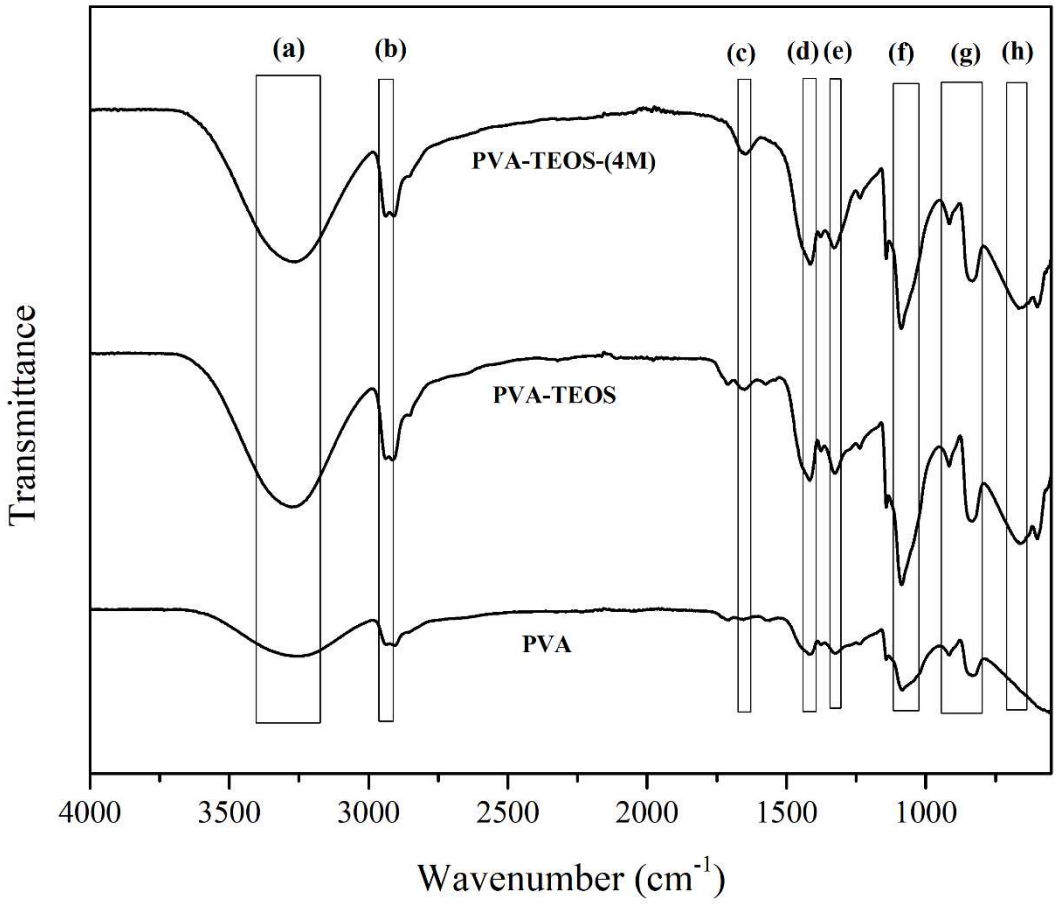

Figure 5.6 FT-IR spectra of membranes pristine PVA, PVA-TEOS and PVA-TEOS-(4M) membrane electrolyte.

5.1.1.6 X-ray diffraction analysis

The X-ray diffraction (XRD) of pristine PVA, PVA-TEOS composite membrane, PVA-(4M) and PVA-TEOS-(4M) composite membrane were performed to further characterize the structural alterations caused by the presence of silica domains. When a polymer comprises a crystalline area, the XRD peaks are crisp and intense, whereas they are broad and diffuse in an amorphous polymer

(Kim et al. 2009). **Figure 5.7** shows the XRD characteristics of pristine PVA, PVA-(4M), PVA-TEOS and PVA-TEOS-(4M) membrane electrolytes. The semi-crystalline structure of the PVA polymer is well known and it exhibits a significant peak at a 2θ angle of about 20^{o} and a tiny peak at 40^{o} (Gupta and Pramanik 2019a, Fu et al. 2010). It is clearly seen from **Figure 5.7** that a prominent and intense peak appears at a 2θ angle of 19.26^{o} (110) and a small peak was observed at 40^{o} (041) (ICDD No. 00-061-1401) for all membrane electrolytes However, the peak intensity and shape was varying with membrane types. The peak position does not shift with the addition of silica in the polymer matrix of the PVA-TEOS membrane. The changes that occur is in the shape of the peak which becomes wider than the pristine PVA. This widening of the peak implies the increase in the amorphous nature of the membrane on the incorporation of silica. The crystallinity of pristine PVA is due to the presence of its side-chain hydroxyl groups. However, by incorporation of silica in PVA by mixing with TEOS through the sol-gel process, the hydroxyl groups of the PVA reacted with silica and thus, reducing the crystallinity of the PVA-TEOS composite membrane (Kittur et al. 2013). It is also seen from **Figure 5.7**, with the incorporation of NaOH in pristine PVA and PVA-TEOS i.e., PVA-(4M) and PVA-TEOS-(4M), the intensity of peak decreases and it indicates the amorphous nature of membrane. The local structural relaxation and segmental motions of the polymer in the amorphous domain, cation and anion transport in the polymer matrix and ion transport in the solvent may all contribute to the explanation of the ionic conductivity of the polymer electrolyte (Fu et al. 2010). It should be noted that the lowest peak height at 2θ of 20^{o} was observed for PVA-TEOS-(4M) membrane electrolyte. Thus, it can be concluded that the incorporation of silica and NaOH in PVA would increase the ionic conductivity of the membrane. The EIS study also shows the highest conductivity of $9.09 \pm 0.5 \times 10^{-3}$ S/cm for the PVA-TEOS-(4M) membrane. The XRD and SEM investigation of the synthesized membrane

confirms that PVA-TEOS-(4M) would come up with better performance as the electrolyte in the single cell DSBFC study.

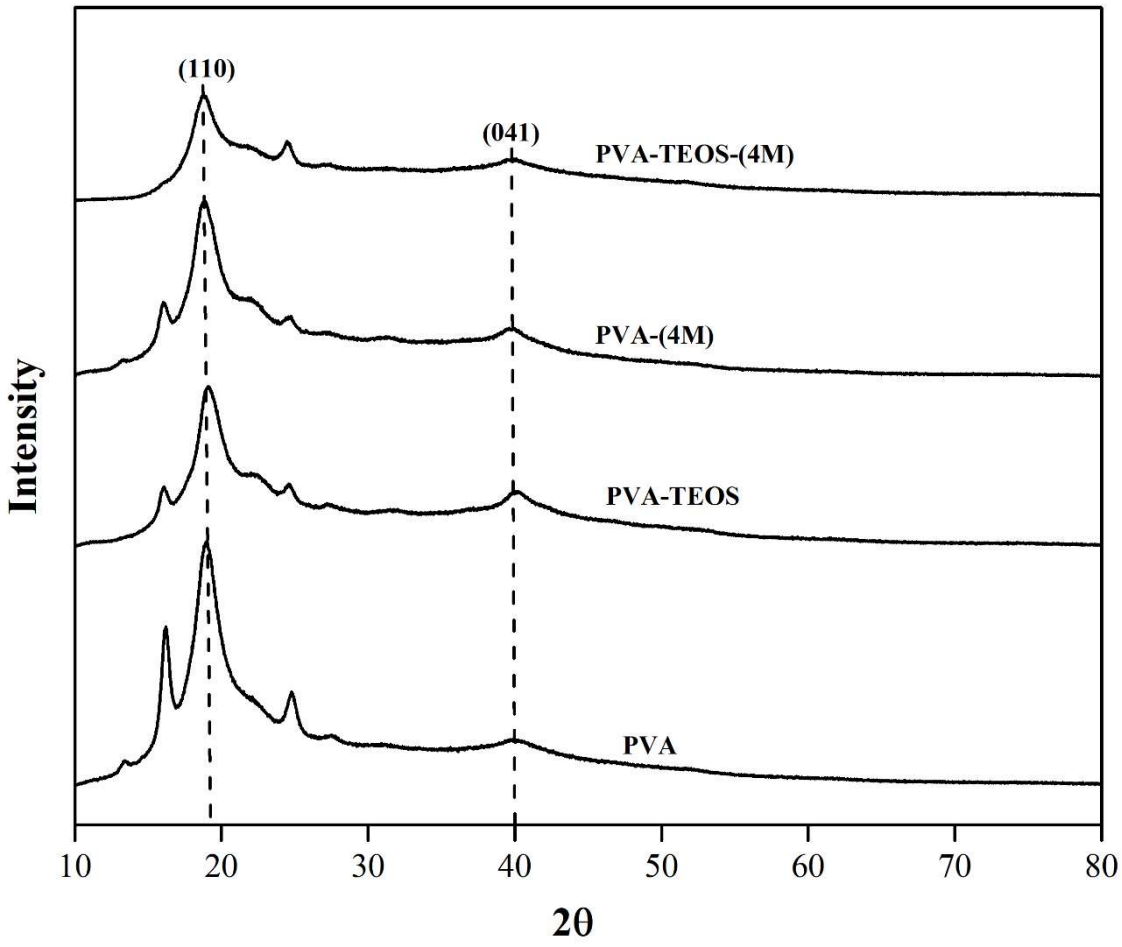

Figure 5.7 The XRD spectra of the synthesized pristine PVA, PVA-(4M) (PVA membrane doped with 4 M NaOH), PVA-TEOS and PVA-TEOS-(4M) membranes.

5.1.1.7 Mechanical strength study

The mechanical strength of the synthesized membrane electrolyte is measured using an ASTM D0882 using UTM AEC1112-ACD, Asian Engineers Company, India, testing machine as discussed in the **Chapter 3** (page no. 67). **Figure 5.8** shows the stress-strain curve of the pristine PVA, PVA-TEOS and PVA-TEOS-(4M) membrane. The mechanical strength of pristine PVA-

TEOS membrane is higher than the pristine PVA (**Figure 5.8**) and it may be due to the addition of TEOS in PVA matrix, the membrane strength gets enhanced (Tong et al. 2017).

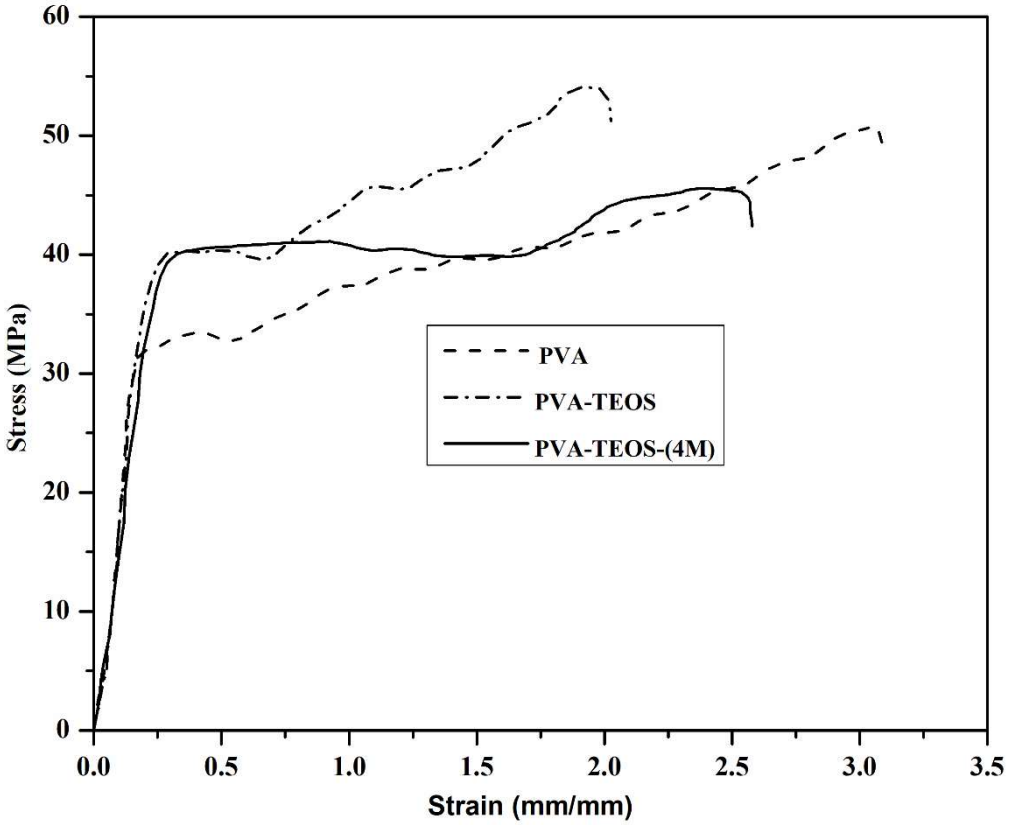

Figure 5.8 Stress-strain curve for the pristine PVA, PVA-TEOS and PVA-TEOS-(4M) membrane.

The tensile strength exhibited by the pristine PVA and PVA-TEOS were 31.26 MPa and 38.80 MPa, respectively. However, PVA-TEOS exhibited less elongation than PVA as the elasticity of the PVA-TEOS membrane decreases and become brittle in nature on the addition of the TEOS to PVA matrix (Jessie et al. 2007) (**Figure 5.8**). The mechanical strength of PVA-TESO doped with 4M NaOH i.e., PVA-TEOS-(4M) was also tested. The tensile strength of PVA-TEOS-(4M) was found in the order of 37.89 MPa and it indicates that the mechanical strength of PVA-TEOS is not much affected by doping with 4 M NaOH. However, the elongation of the PVA-TEOS-(4M)

is higher than PVA-TEOS as it can be clearly seen in **Figure 5.8.** It may be due to the presence of NaOH which simultaneously acted as plasticizer (Jessie et al. 2007).

5.1.2 Cyclic voltammetry (CV) of Pt/C_{HSA} anode

The electrocatalytic activity of anode electrode (Pt/C_{HSA}) for the electrooxidation of $NaBH_4$ in NaOH electrolyte was investigated through the CV study in a half cell. The effects of scan rate and fuel concentration were investigated through the CV study for $NaBH_4$ fuel in alkaline medium.

5.1.2.1 Scan rate study

Typical cyclic voltammograms of a Pt/C_{HSA} based electrode in 0.005 M $NaBH_4$ mixed with 2 M NaOH solution at various scan rates in the range of 20 mV/s - 50 mV/s are shown in **Figure 5.9**. In the forward scan, the $NaBH_4$ electrooxidation peaks are visible in the potential window of -0.15 V to 0.2 V and the CV characteristics shifted upward with the increase in scan rate (**Figure 5.9**). As the $NaBH_4$ is consumed during its electrooxidation, a diffusion barrier is created by the concentration gradient that develops between the electrode surface and the bulk phase of electrolyte (Pramanik and Rathoure 2017). The scan rate or the applied voltage per unit time determines the thickness of the diffusion barrier. When the scan rate is slow (20 mV/s), the diffusion barrier has enough time to develop a thicker barrier than the faster scan rate. Thus, at a slow scan rate, the mass transfer resistance towards the $NaBH_4$ molecules will be significant, resulting in a low peak current density (Pramanik and Rathoure 2017, Panjiara and Pramanik 2020b). On the other hand, at a high scan rate, the diffusion layer will be thinner, resulting in a larger peak current density due to the low resistance of $NaBH_4$ molecules transfer to the electrode surface. The higher scan rate of 40 mV/s was found to be ideal for further CV investigation since it produces a significant current peak at low potential.

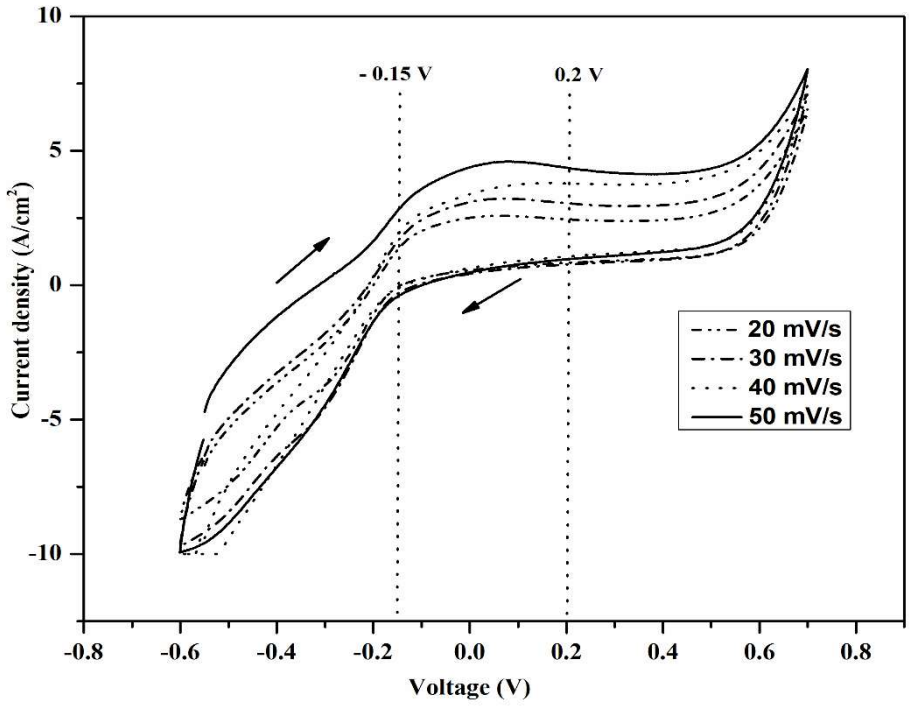

Figure 5.9 Cyclic voltammetry for 0.00 5 M $NaBH_4$ in 2 M NaOH at different scan rates on Pt (40 wt. %)/C_{HSA} anode loading of 1 mg/cm^2; temperature 30 ^oC.

5.1.2.2 Electrooxidation study of sodium borohydride

The cyclic voltammograms of Pt (40 wt. %)/C_{HSA} electrode for different concentrations of $NaBH_4$ mixed with 2 M NaOH at the scan rate of 40 mV/s are shown in **Figure 5.10**. The presence of $NaBH_4$ in 2 M NaOH solution causes anodic currents due to the electrooxidation of $NaBH_4$ on the Pt/C_{HSA} electrodes potentials greater than -0.15 V. The prominent pick was observed in the forward scan only for the $NaBH_4$ concentrations ranging from 0.005 M to 0.015 M. It is seen from literature review that the peak observed between 0 V to 0.1 V is due to direct oxidation of BH_4^- (Equation 2.1) (Tarozaite et al. 2009, Gyenge 2004, Martins and Nunes 2008). Thus, the electrooxidation of $NaBH_4$ in NaOH solution represented in **Figure 5.10** may be due to direct oxidation route. At a higher concentration of 0.02 M $NaBH_4$ the electrooxidation peak begins to disappear. The

maximum current density of 8.6 mA/cm^2 at a potential of 0.045 V was obtained for 0.015 M $NaBH_4$. However, the electrooxidation peak for the very high concentration of $NaBH_4$ i.e., 0.02 M gets flattened. It is similar to the behavior as reported by Aytac et al. 2011, and Pramanik and Rathoure 2017 for the electrooxidation study of $NaBH_4$ in an alkaline medium. The reason for such a trend may be due to the increase in $NaBH_4$ concentration, the relative concentration of NaOH to $NaBH_4$ decreases. It is also reported in various literature that at a low NaOH to $NaBH_4$ ratio, the hydrolysis of $NaBH_4$ predominates which (Pramanik and Rathoure 2017, Yu et al. 2011) resulting in the reduction of the peak current density of sodium borohydride electrooxidation.

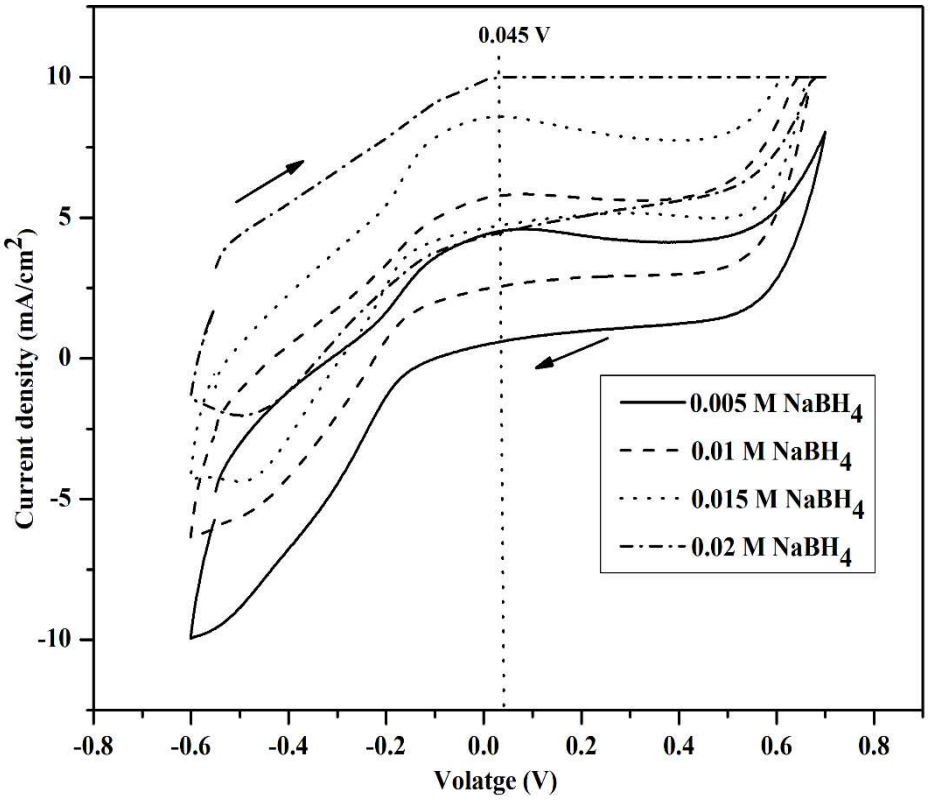

Figure 5.10 CV for different concentrations of $NaBH_4$ in 2 M NaOH on Pt/ (40 wt. %)/C_{HSA} at a scan rate of 40 mV/s; Temperature 30 ^oC.

5.1.2.3 Cyclic voltammetry (CV) of Pt/C_{HSA} cathode

The oxygen reduction reaction on Pt/C_{HSA} electrocatalyst in alkaline medium was studied using cyclic voltammetry. **Figure 5.11**a shows the cyclic voltammetry of the electrochemical reduction reaction of oxygen saturated 1 M NaOH solution at scan rate of 50 mV/s. The loading of Pt/C_{HSA} electrocatalyst was 1 mg/cm^2. It is seen from **Figure 5.11**a that two distinct peaks in the backward scan were observed which indicate the two-step two-electron mechanism route of oxygen reduction reaction in 1 M NaOH solution (Equation 2.6 and 2.7). The two distinct peaks were observed at -0.53 V and at -0.92 V (**Figure 5.11**a). Similar two-step two-electron mechanism route of oxygen reduction in alkaline medium was also observed by Rathoure and Pramanik 2016 and Jin et al. 2010.

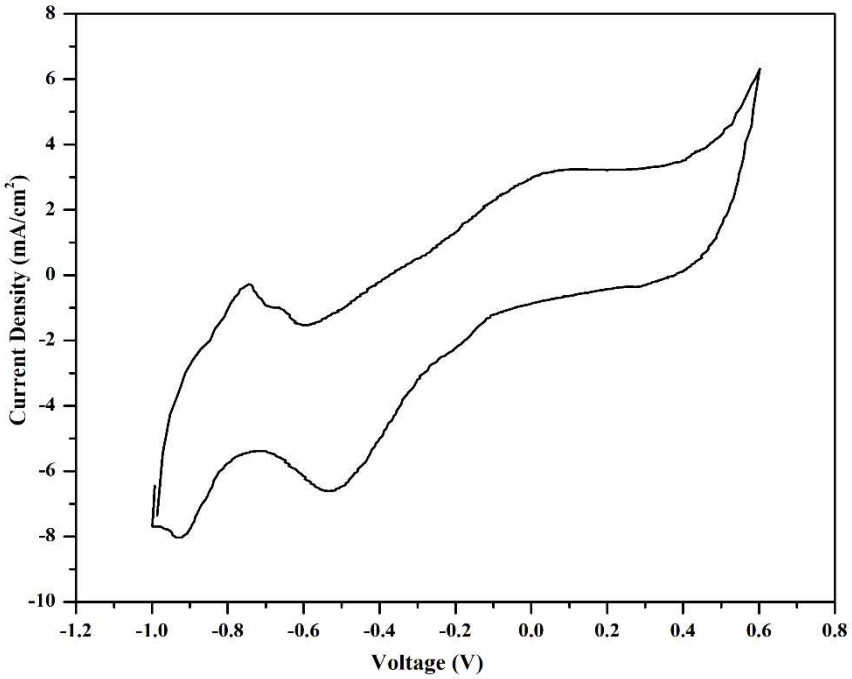

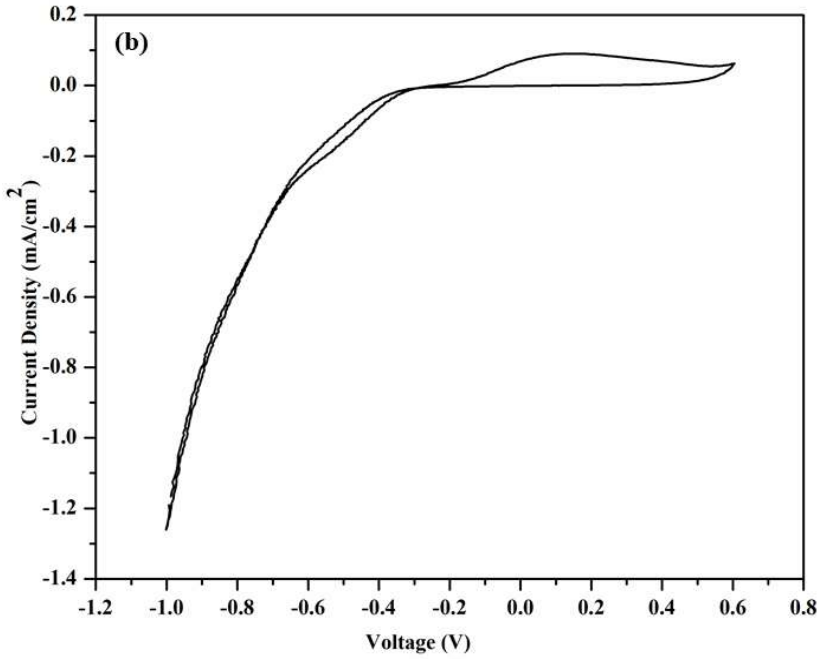

Figure 5.11 Cyclic voltammetry for (a) Pt/C_{HSA} cathode at loading 1 mg/cm^2 (b) blank GDL as half-cell electrode without an electrocatalyst at scan rate of 50 mV/s in oxygen saturated 1 M NaOH solution.

The peak current density of 6.61 mA/cm^2 and 8.64 mA/cm^2 were obtained at the applied voltage of -0.53 V and -0.92 V, respectively, in the backward scan of ORR (**Figure 5.11**a). **Figure 5.11**b shows the CV curve of a blank GDL as a working electrode without an electrocatalyst in a saturated 1 M NaOH solution. It is clearly seen that no oxygen reduction reaction (ORR) peak was observed due to the absence of electrocatalyst.

5.1.3 Single DSBFC performance

5.1.3.1 Effect of cathode electrocatalyst loading

Figure 5.12 shows the current density vs cell voltage and current density vs power density curves for the varying cathode loading ranging from 0.5 mg/cm^2 to 2.5 mg/cm^2 and fixed anode loading of 1 mg/cm^2. The single-cell test of the DSBFC was done using the membrane electrolyte PVA-

TEOS-(4M) with highest ionic conductivity of $9.09 \pm 0.5\times10^{-3}$ S/cm. The fuel used was 1 M $NaBH_4$ mixed in 4 M NaOH solution at a flow rate of 1.5 ml/min. The commercial Pt (40 wt. %)/C_{HSA} was used as both, anode electrocatalyst as well as a cathode. The cathode side was exposed to pure oxygen that had been humidified. The DSBFC cell was kept at a room temperature of 25 ^oC. It is seen from **Figure 5.12** that polarization and power density curves shifted upward with the increase in cathode loading up to 2 mg/cm^2. The initial zone of polarization curves (Zone-I), where activation overpotential mainly predominates, the fall in cell voltage is low for the loading of 2 mg/cm^2 Pt/C_{HSA} at the cathode. It may be due to the low activation loss at 2 mg/cm^2. As per the literature, roughness and loading of electrocatalysts improve kinetics or electrochemical reaction rate at the electrode and reduce activation loss also (Celik et al. 2008, Srinivasan et al. 1991). At a very high loading of 2.5 mg/cm^2, the cell voltage falls rapidly for all three regions viz. Zone-I, II and III where predominant losses are activation, ohmic and concentration polarization, respectively. It may be because of low available surface area which arises from more contact between the particles. Moreover, the particles get agglomerated at very high loading and thus, low cathode reduction kinetics and high activation loss at very high loading is observed. The ohmic loss and mass transfer losses are also very high for very high loading of 2.5 mg/cm^2 as the cathode becomes thicker and compact than the optimum loading of 2 mg/cm^2 . Thus, the voltage losses are very high in these regions i.e., Zone-II and Zone-III also. **Figure 5.13**a and **Figure 5.13**b show the SEM images of the catalyst layer of 2 mg/cm^2 and 2.5 mg/cm^2. It is clearly seen from **Figure 5.13**b that at higher loading of 2.5 mg/cm^2, the agglomeration of the catalyst is high and compact whereas, no such high agglomeration is observed in the catalyst layer of 2 mg/cm^2 **Figure 5.13**a. Due to this reason the polarization and power density curves for 2 mg/cm^2 always remain above all other loadings in the regions of ohmic and concentration polarization also (Yadav and Pramanik

2023). The maximum power density of 54.91 mW/cm^2 at the current density of 128 mA/cm^2 was obtained for the loading of 2 mg/cm^2 whereas, the highest loading of 2.5 mg/cm^2 produced maximum power density 26.84 mW/cm^2 at the current density of 57.6 mA/cm^2. The optimum cathode loading of 2 mg/cm^2 produced the highest power density (54.91 mW/cm^2) than any other cathode loading. It should be noted that the cathode loading lower than 2 mg/cm^2 i.e., 0.5 mg/cm^2, 1 mg/cm^2, and 1.5 mg/cm^2 produced a maximum power density of 20.45 mW/cm^2, 24.36 mW/cm^2 and 32.48 mW/cm^2, respectively (Yadav and Pramanik 2023).

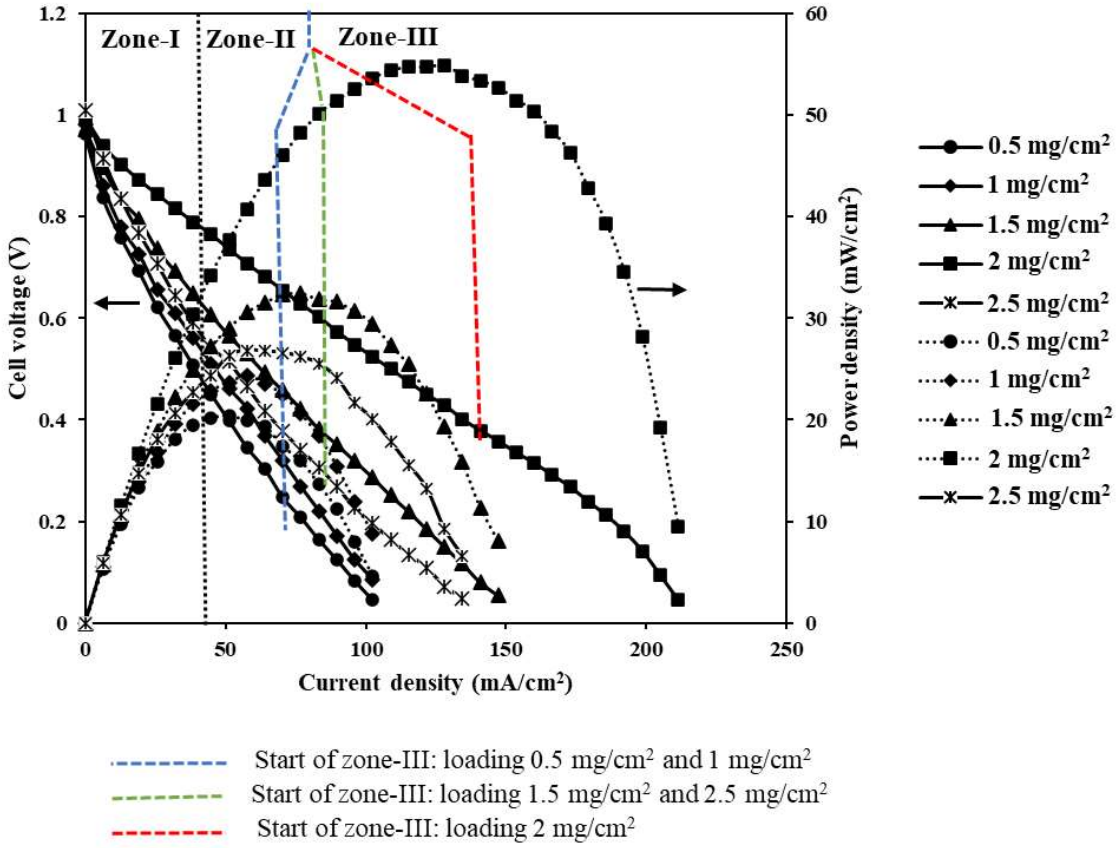

Figure 5.12 The polarization and power density curve of DSBFC using 1 M $NaBH_4$ mixed in 4 M NaOH for different cathode loading at a room temperature of 25 ^oC; solid line-polarization curves; dotted line-power density curves.

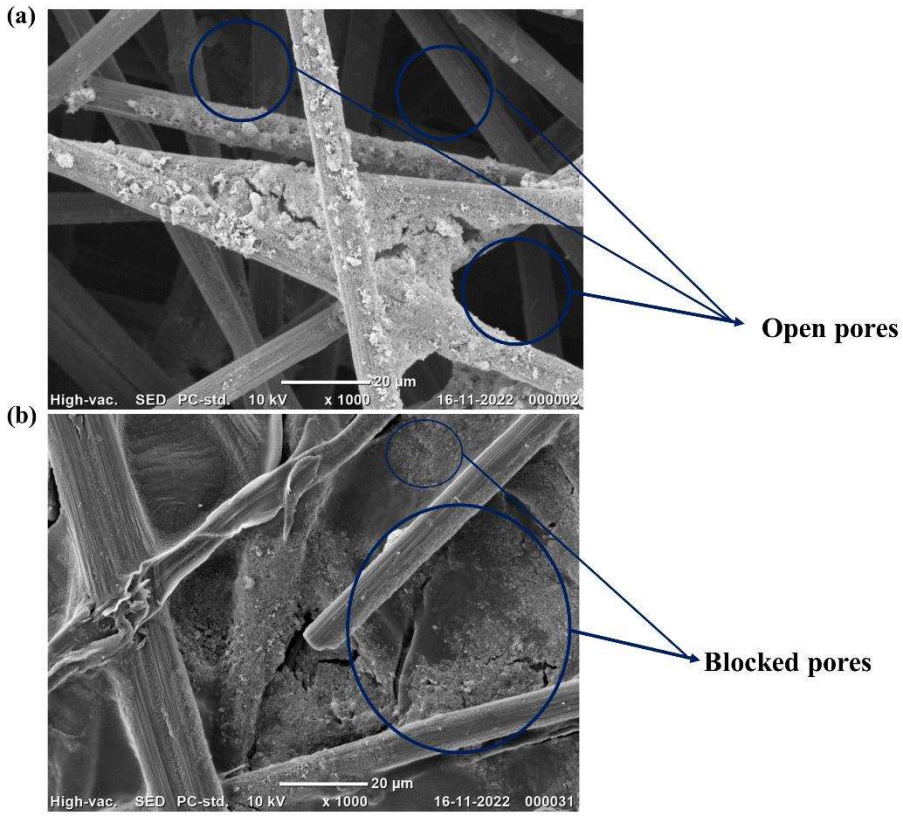

Figure 5.13 The SEM images for the electrocatalyst surface for (a) 2 mg/cm^2 and (b) 2.5 mg/cm^2 loading.

5.1.3.2 Effect of anode electrocatalyst loading

Figure 5.14 shows the effect of anode (Pt /C_{HSA}) loading on polarization and power density curves using varying anode loading ranging from 0.5 mg/cm^2 to 2 mg/cm^2. The cathode loading was kept fixed at optimum value of 2 mg/cm^2. The cell was operated at the room temperature of 25 ^{o}C to optimize the anode loading. It is seen from **Figure 5.14** that the power density increased from 44.53 mW/cm^2 to 54.91 mW/cm^2 with the increase in anode loading from 0.5 mg/cm^2 to 1 mg/cm^2 and beyond the loading 1 mg/cm^2, the cell performance starts decreasing. The highest power density of 54.91 mW/cm^2 was obtained at the current density of 128 mA/cm^2 for the optimum anode loading of 1 mg/cm^2. The maximum power density of 45.13 mW/cm^2 and 42.84 mW/cm^2

were obtained for the higher anode loading of 1.5 mg/cm^2 and 2 mg/cm^2, respectively. The decrease in performance at very high loading was due to an increase in ohmic resistance and hindrance in the mass transport of borohydride fuel at the anode electrocatalyst layer as discussed earlier for the varying cathode loading (**section 5.1.3.1**) (page no. 102).

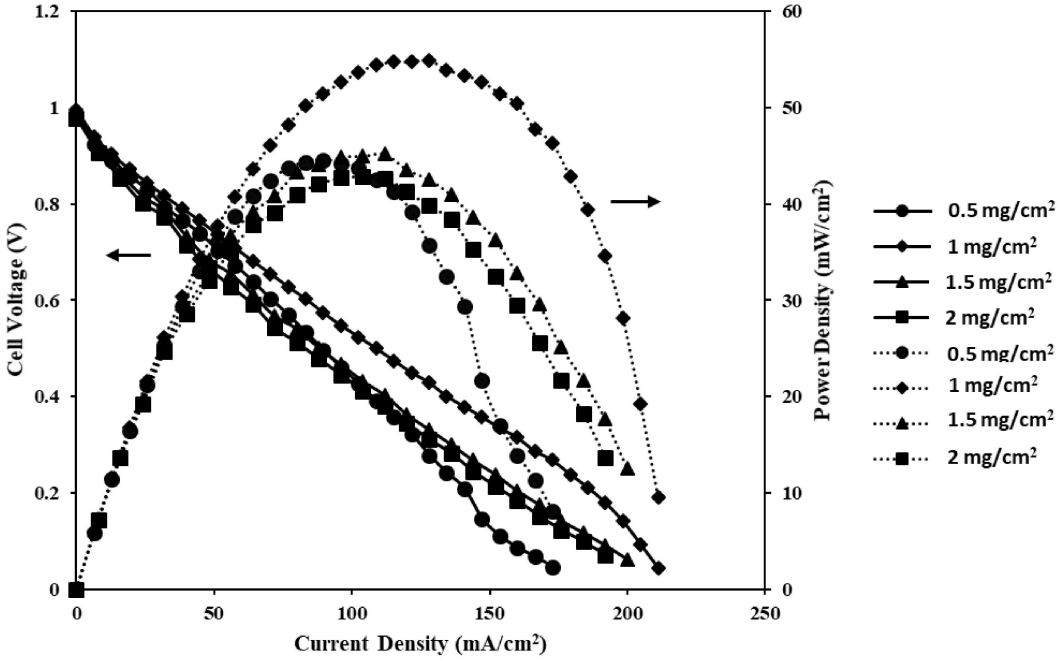

Figure 5.14 The polarization and power density curves of DSBFC using 1 M $NaBH_4$ mixed in 4 M NaOH for different anode loading at a room temperature of 25 ^oC; Membrane electrolyte PVA-TEOS-(4M); solid line-polarization curves; dotted line-power density curves.

5.1.3.3 Effect of $NaBH_4$ concentration

Figure 5.15 shows the effect of sodium borohydride concentration on the performance of a single DSBFC at the room temperature of 25 ^oC. It is seen rom **Figure 5.15**, the cell performance in terms of power density and current density increases with the increase in $NaBH_4$ concentration from 0.5 M $NaBH_4$ to 1 M $NaBH_4$. However, the cell performance decreases beyond the fuel $NaBH_4$ concentration of 1 M. The maximum power density of 54.91 mW/cm^2 was obtained at the current

density 128 mA/cm^2 for 1 M $NaBH_4$ concentration. However, the maximum power density of 44.91 mW/cm^2 and 42.04 mW/cm^2 were obtained at the current density of 112 mA/cm^2 and 96 mA/cm^2 for the higher concentration of 1.5 M and 2 M $NaBH_4$, respectively. The highest power density of 54.91 mW/cm^2 was obtained for the optimum concentration of 1 M $NaBH_4$, whereas 0.5 M $NaBH_4$ produced the lowest power density of 40.24 mW/cm^2.

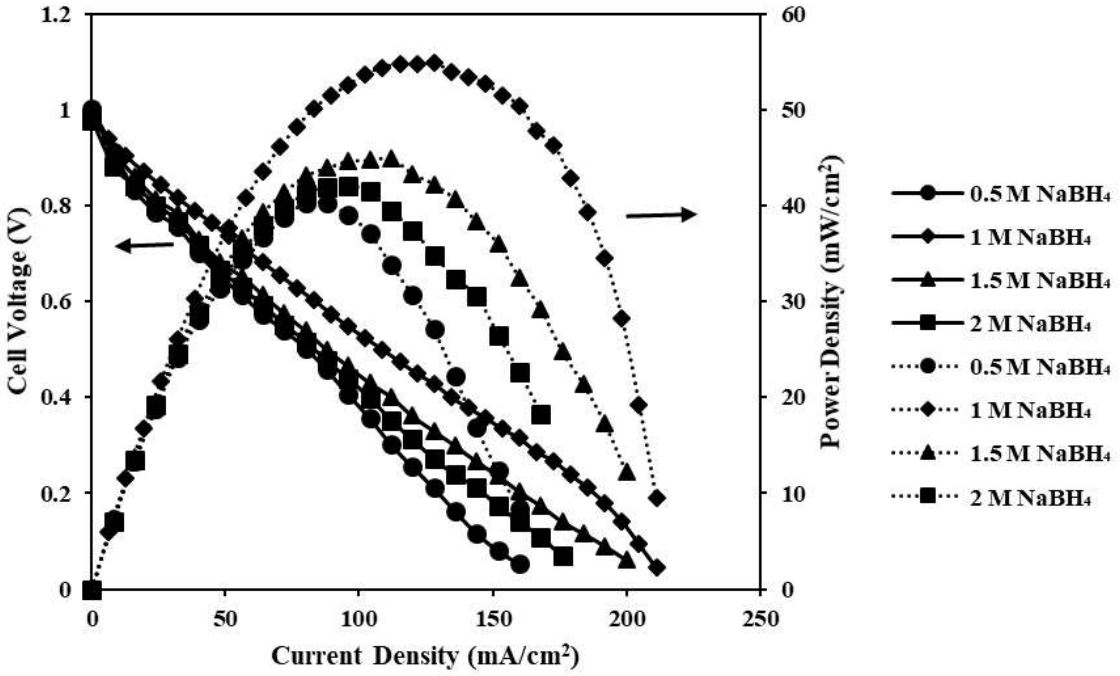

Figure 5.15 The polarization and power density curve of DBHFC using various concentrations of $NaBH_4$ mixed in 4 M NaOH at a temperature of 25 ^oC; Membrane electrolyte PVA-TEOS-(4M); Solid line-polarization curves; dotted line-power density curves.

The reasons for the improvement in the cell performance for the initial increase in $NaBH_4$ concentration from 0.5 M to 1 M, may be due to the availability of more molecules of $NaBH_4$, electrooxidation kinetics at anode gets improved (Cheng et al. 2006b). On the other hand, the decrease in the cell performance beyond 1 M $NaBH_4$ concentration may be due to an increase in $NaBH_4$ hydrolysis and the fuel crossover from anode to cathode (Celik et al. 2010). The effect of

$NaBH_4$ concentration on the performance of the DSBFC trend is similar to the behavior as reported by Choudhary et al. 2005.

5.1.3.4 Effect of NaOH doping in PVA-TEOS membrane

The presence of NaOH in the PVA-TEOS matrix is responsible for ion transport in the fuel cell during its operation. **Figure 5.16** shows the polarization and power density curves for varying NaOH concentrations doped in pristine PVA-TEOS membrane electrolyte. The anode and cathode loading were kept fixed at their optimum values of 1 mg/cm^2 and 2 mg/cm^2 of Pt/C_{HSA}, respectively. The fuel 1 M $NaBH_4$ mixed in 4 M NaOH was fed at the anode and humidified oxygen was fed to the cathode side as oxidant at a room temperature of 25 ^oC. It can be observed from **Figure 5.16**, the polarization and power density curves shifted upward with the increase in NaOH concentration upto 4 M NaOH and then shifted downward when the NaOH concentration was increased beyond 4 M. The highest power density of 54.91 mW/cm^2 at the current density of 128 mA/cm^2 was obtained for membrane electrolytes with 4 M NaOH concentration (PVA-TEOS-(4M)). On the other side, the maximum power densities of 33.02 mW/cm^2, 46.89 mW/cm^2 and 44.34 mW/cm^2 were obtained for the membrane electrolyte PVA-TEOS-(2M), PVA-TEOS-(6M) and PVA-TEOS-(8M), respectively. Initially, NaOH concentration affects the cell performance due to an increase in NaOH uptake of the membrane with the increase in NaOH concentration. Although, the highest NaOH uptake (39.16 wt. %) of the PVA-TEOS membrane was observed at 6 M NaOH (PVA-TEOS-(6 M) (**Figure 5.1**), the highest power density was recorded for the PVA-TEOS membrane doped with 4M NaOH (PVA-TEOS-(4M)).

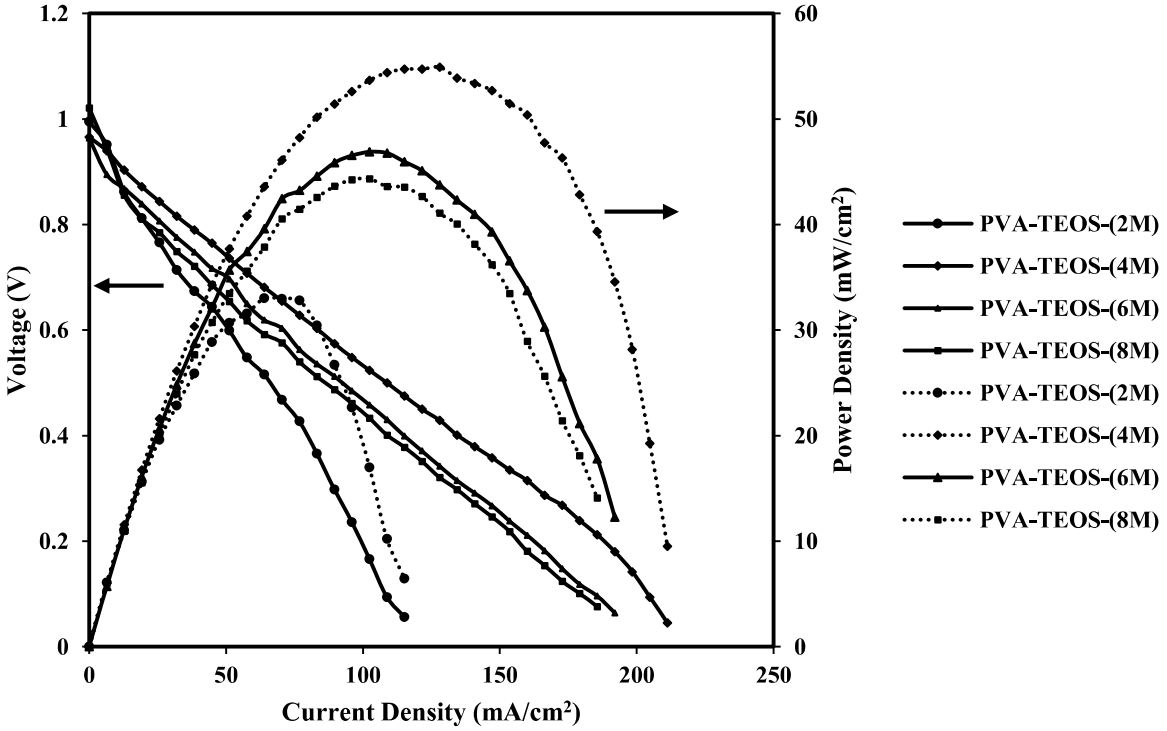

Figure 5.16 The polarization and power density curve of DSBFC using 1 M $NaBH_4$ mixed with 4M NaOH for different membrane electrolyte concentrations at the fixed anode and cathode loading of 1 mg/cm^2 and 2 mg/cm^2, respectively; cell temperature 25 ^oC; solid line-polarization curves; dotted line-power density curves.

The increase in power density is mainly due to improvements in ionic conductivity which was found to be highest (9.09 ± 0.5×10^{-3} S/cm) for PVA-TEOS-(4M) membrane as shown in **Table 5.2** (page no. 89). On the other side, the ionic conductivity of the PVA-TEOS-(6M) membrane comes up with a lower magnitude of 6.23 ± 0.3×10^{-3} S/cm. As already discussed, the reason for such dependency of the ionic conductivity of membrane electrolytes with NaOH concentration may be the very high ionic mobility of hydroxyl ions at a moderate NaOH concentration of 4 M with an adequate quantity of water (81.03 wt. %). The ionic mobility may be low for very high NaOH uptake (39.16 wt. %) when PVA-TEOS was doped with 6 M NaOH and thus, ionic

conductivity was low which is resulting in the low performance of the membrane electrolyte in DSBFC. The surface morphology of the PVA-TEOS-(6M) membrane in SEM images also showed many patches of white deposits of NaOH on the membrane surface at a very high concentration of NaOH doping (**Figure 5.5**(d)). It may result in high ohmic resistance which is prominent for PVA-TEOS-(6M) membrane electrolyte. Whereas, the surface morphology of PVA-TEOS-(4M) (**Fig. 5.5**(c)) appears to be a uniform surface of the membrane without white deposits of NaOH on the membrane electrolyte surface. This ensures the absorption of NaOH within the membrane matrix only and thus, ohmic resistance is also low for this membrane electrolyte. The XRD study of PVA-TEOS-(4M) membrane electrolyte showed promising results i.e., more amorphous nature and thus, better ionic conductivity (**Figure 5.7**). It should be noted that the alkali solution inhaled into the membrane material is quite stable. The TEOS incorporated into the membrane material greatly enhances NaOH retention (Yang et al. 2011).

5.1.3.5 Effect of DSBFC temperature

Figure 5.17 depicts the effect of cell temperature on DSBFC performance in terms of current density and power density for the PVA-TEOS-(4M) membrane electrolyte using optimum loading at anode and cathode. It is seen from **Fig. 5.17**, the maximum power density of DSBFC increases with the increase in cell temperature upto 55 ^{o}C. Further, increase in cell temperature to 60 ^{o}C, the cell performance falls significantly (**Figure 5.17**). The maximum power densities were 54.91 mW/cm^2, 69.73 mW/cm^2, 75.51 mW/cm^{2,} and 79.87 mW/cm^2 at the cell temperature of 25 ^{o}C, 35^{o}C, 45 ^{o}C, and 55 ^{o}C, respectively. The improvement in power density with temperature is due to a reduction in activation loss (Celic et al. 2008) and higher reaction kinetics at both electrodes; thus, polarization curves shift upward with the increase in cell temperature. Furthermore, the ionic

mobility is improved and anolyte viscosity gets lower with the increase in cell temperature (Yadav and Pramanik 2023). The conductivity test of the membrane electrolyte PVA-TEOS-(4M) with varying temperature also shows the increasing trend of ionic conductivity with the increase in temperature in two probe system (externally) (**Figure 5.4**) and within the single cell also (**Figure 5.18**) (Wen et al. 2022, Coowar et al. 2008]. The maximum conductivity of the DSBFC obtained was 4.56±0.03×10^{-3} S/cm at the cell temperature of 55 ^{o}C (**Figure 5.17**). The conductivity at the cell temperature of 25 ^{o}C, 35 ^{o}C and 45 ^{o}C were 2.89±0.02×10^{-3} S/cm, 3.53±0.04×10^{-3} S/cm and 3.80±0.06×10^{-3} S/cm, respectively as is shown in **Table 5.4**. The mass transfer loss also declines as the diffusion coefficient rises. As a result, electrolyte conductivity rises and ohmic losses fall (Celik et al. 2008).

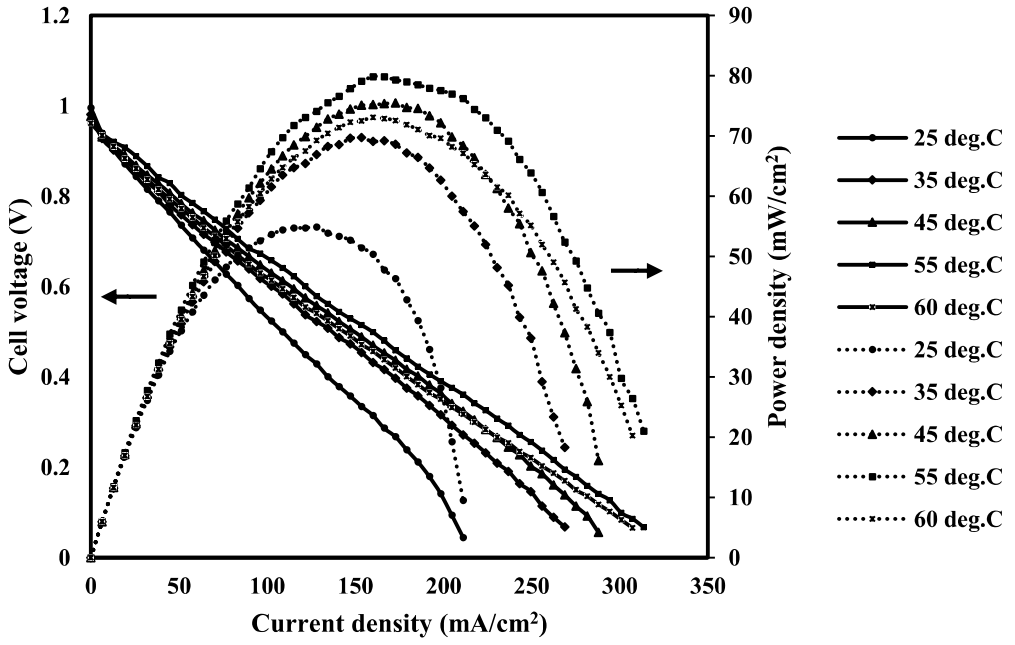

Figure 5.17 The polarization and power density curve of DBHFC using 1 M $NaBH_4$ and 4 M NaOH for varying cell temperature at the fixed anode and cathode loading of 1 mg/cm^2 and 2 mg/cm^2, respectively; solid line-polarization curves; dotted line-power density curves.

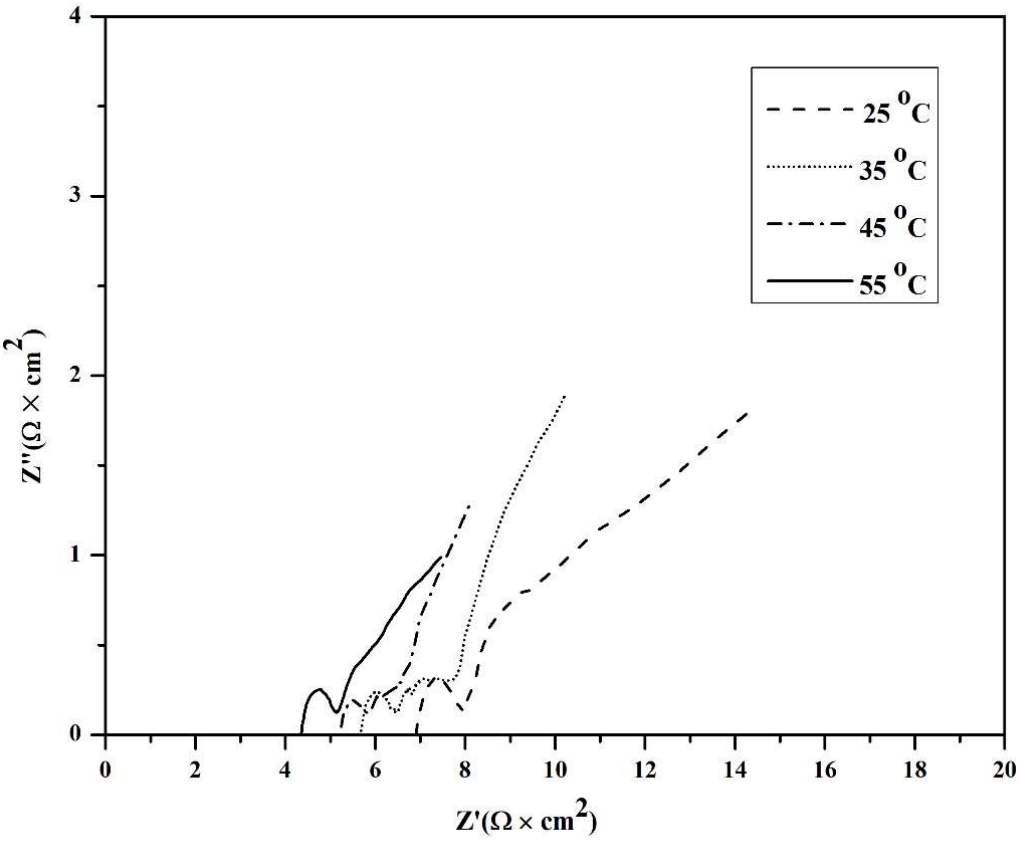

Figure 5.18 The EIS characteristics of the single DSBFC using PVA-TEOS-(4M) and OCV of 0.9 V at the different cell temperature.

Table 5.4 The ionic conductivity of the single DSBFC using PVA-TEOS-(4M) at the different cell temperature.

Cell Temperature (^oC)	25	35	45	55
Ionic Conductivity ($\times 10^{-3}$) (S/cm)	2.89±0.02	3.53±0.04	3.80±0.06	4.56±0.03

It should be noted that the DSBFC temperature was not increased beyond 60 ^oC to operate the cell from room temperature to moderate temperature for saving energy consumption of cell heating. Moreover, the decline in DSBFC performance was observed when the cell temperature increased

beyond 55 ^{o}C. It may be due to other adverse effects come into existence such as borohydride crossover and hydrolysis of borohydride at the higher temperature of 60 ^{o}C (Cheng et al. 2006b). Furthermore, as the temperature rises, the membrane electrolyte and cathode electrocatalyst layer dryness occur, resulting in higher cell resistance and thereby cell performance. It should also be noted that the membrane electrolyte gets damaged at a higher temperature of 60 ^{o}C, as it is shown in **Figure 5.19**. In view of this, operating the developed DSBFC at a moderate temperature range, i.e., from room temperature (25 ^{o}C) to moderate temperature (55 ^{o}C) is recommended.

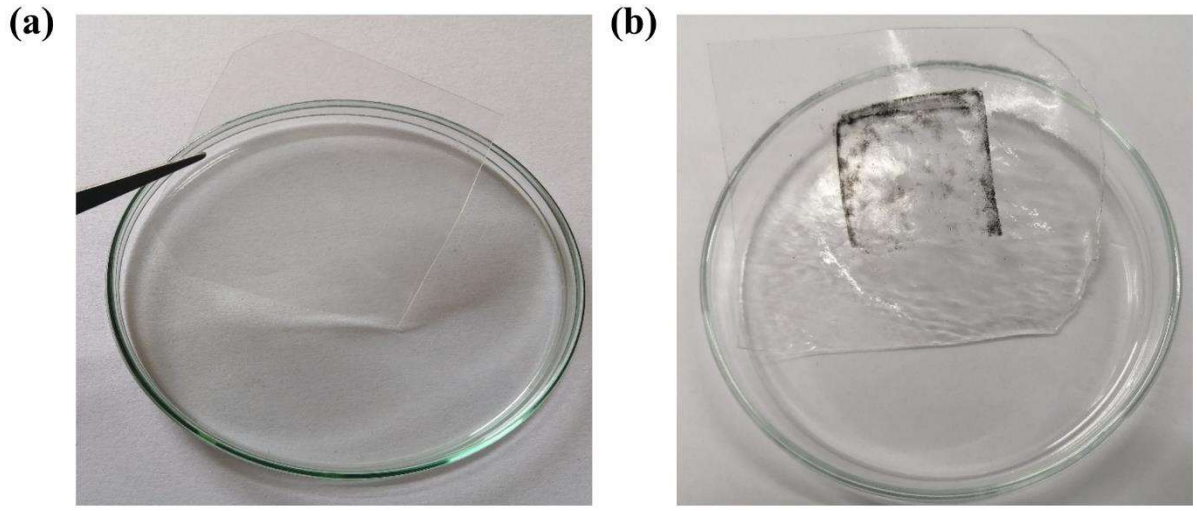

Figure 5.19. Photograph of PVA-TEOS (4M) membrane electrolyte (a) fresh and (b) used at a cell temperature of 60 ^{o}C.

5.2 Performance evaluation of NaOH doped physically crosslinked PVA-TEOS membrane electrolyte: Part II

5.2.1 Membrane characterization

5.2.1.1 Water uptake and NaOH uptake

5.2.1.1.1 Effect of freeze-thaw cycle

The synthesized NaOH doped physically crosslinked PVA-TEOS membrane electrolyte were subjected to water uptake and NaOH uptake tests as discussed in **Chapter 3 Experimental section 3.2.3.1** (page no. 62). The water uptake and NaOH uptake of $PT_{5wt.\%}$-0Cy (pristine), $PT_{5wt.\%}$-3Cy, $PT_{5wt.\%}$-5Cy, $PT_{5wt.\%}$-7Cy and $PT_{5wt.\%}$-9Cy were estimated using Equation 3.1 (page no. 63) and Equation 3.2 (page no. 63). The doping content of TEOS in the membrane electrolyte was varied from 5 wt. % to 15 wt. %. The membrane considered here was doped with 5 wt. % TEOS. The effect of doping concentration of TEOS on membrane properties presented in the preceding **section 5.2.1.1.2** (page no. 118) was also studied. The thickness of the synthesized dry membrane was in the order of 200 ± 10 um. The presence of water and NaOH in the PVA-TEOS membrane matrix are the key factors for providing conducting network within the solid membrane electrolyte. The presence of a suitable amount of water and NaOH within the membrane matrix is responsible for higher ionic conductivity, which results in better fuel cell performance. As already mentioned in the previous **Part-I** (page no. 88), too high water and low NaOH cause low ionic conductivity due to a lesser number of available OH^- ions. Similarly, too low water and high NaOH also causes low ionic conductivity due to poor ionic mobility of OH^- ions (Gupta and Pramanik 2019a). Thus, a delicate balance between the amount of water and NaOH is essential to ensure very better ionic conductivity of the synthesized membrane electrolyte. The degree of physical crosslinking of the PVA-TEOS membrane depends on the number of freeze-thaw cycle used, which effect the water

uptake and NaOH uptake capacity. It is seen from the published literature that the water and NaOH uptake of the physically crosslinked membrane is always less than the pristine PVA-TEOS. In pristine PVA-TEOS, a large number of hydrophilic (–OH) groups are present, which can easily form hydrogen bond with water molecules. Thus, water can easily penetrate into space between PVA crystallites (Gonzalez et al. 2011). Moreover, the molecules remain relatively at a larger distance in the pristine membrane electrolyte. However, during physical crosslinking via freeze-thaw process, when the freezing process of 18 h is performed, the molecule comes closer and thus, the intermolecular interaction of PVA occurs, probably leading to hydrogen bond formation. Finally, it leads to a physical entangled zone in the physically crosslinked PVA-TEOS matrix (Ru-yin et al. 2008). Due to the availability of less space between the PVA crystallites may lead to a decrease in water uptake and NaOH uptake of the physically crosslinked membrane. The number of freeze-thaw cycle also affects the membrane characteristics. The PVA molecular chains are loosely connected with hydrogen bonds when the membrane is crosslinked via lower freeze-thaw cycle. As the cycle increases, the PVA molecular chain aggregate more, form stronger hydrogen bond (Hatakeyema et al. 2005). At a higher freeze-thaw cycle, many entangled zones formed; thus, the membrane matrix eventually becomes more rigid.

The water uptake and NaOH uptake of $PT_{5wt.\%}$-0Cy, $PT_{5wt.\%}$-3Cy, $PT_{5wt.\%}$-5Cy, $PT_{5wt.\%}$-7Cy and $PT_{5wt.\%}$-9Cy are presented in Appendix B (**Figure B1)**. It is clearly observed from **Figure B1** that the water uptake decreases with the increase in NaOH doping concentration, irrespective of the freeze-thaw cycle and it may be due to poor diffusion of water in the PVA membrane matrix due to a decrease in the relative concentration of water, leaving less space for water molecule to occupy the pore volume in the membrane matrix. Moreover, water uptake also decreases with the increase in the freeze-thaw cycle, irrespective of doping concentration. The maximum water uptake of the

synthesized membrane $PT_{5wt.\%}$-0Cy (pristine), $PT_{5wt.\%}$-3Cy, $PT_{5wt.\%}$-5Cy, $PT_{5wt.\%}$-7Cy and $PT_{5wt.\%}$-9Cy were 161.20 wt. % 152.12 wt. %, 141.23 wt. %, 133.87 wt. %, and 128.43 wt. %, respectively, when dipped in 0 M NaOH/pure water (**Table 5.5**).

Table 5.5 Water and NaOH uptake of the physically crosslinked synthesized membrane in different NaOH doping concentration**.**

Membrane Type	NaOH (0 M)		NaOH (2 M)		NaOH (3 M)		NaOH (4 M)		NaOH (5 M)		NaOH (6 M)		NaOH (7 M)	
	Wu (wt.%)	Nu (wt.%)	Wu (wt.%)	Nu (wt.%)	Wu (wt.%)	Nu (wt.%)	Wu (wt.%)	Nu (wt.%)	Wu (wt.%)	Nu (wt.%)	Wu (wt.%)	Nu (wt.%)	Wu (wt.%)	Nu (wt.%)
$PT_{5wt.\%}$-0Cy	161.20	0	118.49	18.49	98.14	23.25	81.03	27.58	69.93	34.96	58.84	39.16	50.12	33.24
$PT_{5wt.\%}$-3Cy	152.12	0	109.67	17.12	92.27	21.38	75.62	26.09	64.18	32.04	53.62	37.16	47.71	30.64
$PT_{5wt.\%}$-5Cy	141.23	0	98.41	16.23	**85.22**	**19.60**	**70.78**	**24.13**	**59.85**	**30.16**	49.07	35.48	44.47	28.73
$PT_{5wt.\%}$-7Cy	133.87	0	89.44	14.50	**79.27**	**18.16**	**65.80**	**22.38**	**52.88**	**28.10**	45.66	33.64	41.78	26.38
$PT_{5wt.\%}$-9Cy	128.43	0	80.53	12.90	70.69	16.37	60.91	18.82	48.43	24.71	42.14	28.79	38.62	23.62

The lowest water uptake of 128.43 wt. % was observed for the membrane $PT_{5wt.\%}$-9Cy and it may be due to the highly intermolecular interaction of PVA-TEOS and the formation of the large number of entangled zone in the membrane matrix for the highest freeze-thaw cycle 9 (Ru-yin et al. 2008, Adelnia et al. 2021). It should be noted that the NaOH uptake also decreases with the increase in freeze-thaw cycles same as that of water uptake for all doping concentrations of NaOH. However, the NaOH uptake of the pristine PVA-TEOS (0 cycle) and physically crosslinked membrane electrolyte increased when the concentration of NaOH increased upto 6 M and beyond 6 M NaOH concentration, the NaOH uptake decreases irrespective of freeze-thaw cycle used (**Table 5.5**). The maximum NaOH uptake of $PT_{5wt.\%}$-0Cy (pristine), $PT_{5wt.\%}$-3Cy, $PT_{5wt.\%}$-5Cy, $PT_{5wt.\%}$-7Cy and $PT_{5wt.\%}$-9Cy were 39.16 wt %, 37.16 wt %, 35.48 wt %, 33.64 wt % and 28.79 wt %, respectively when doped with 6 M NaOH concentration. The increase in NaOH uptake upto 6 M NaOH concentration may be due to the increase in NaOH concentration, the more NaOH molecules are available for moving from bulk to the solid electrolyte matrix. However, beyond the 6 M concentration of NaOH, the solution viscosity is highly enhanced, reducing the mobility of NaOH molecules into the polymer matrix. The membrane gets saturated at a very high concentration of NaOH (An et al. 2012) and thus, highest NaOH uptake was observed at 6 M for all types of membrane obtained through various cycles. It should be noted that the NaOH uptake gets reduced with the increase in freeze-thaw cycles for all concentrations of NaOH solution. The optimum concentration of 6 M NaOH was recorded at which NaOH uptake was highest. However, the measurement of the ionic conductivity of membrane electrolytes is essential to find out the best combination of the freeze-thaw cycle and NaOH doping concentration which will give suitable value of NaOH uptake and water uptake in the membrane with the highest ionic conductivity. The very high NaOH uptake of 37.16 wt. % for $PT_{5wt.\%}$-3Cy physically crosslinked membrane may not

show very high conductivity for the synthesized membrane. As the ionic mobility within the membrane matrix depends on the delicate balance between the presence of water and NaOH uptake of the membrane.

Moreover, these two important parameters, water uptake and NaOH uptake, depend on the number of freeze-thaw cycles and weight percent (wt. %) of TEOS impregnated in the membrane matrix. Thus, TEOS concentration in the PVA-TEOS matrix needs to be optimized further. It is clearly seen from **Table 5.5** that water uptake and NaOH uptake are in the intermediate range for the freeze-thaw cycle of 5 and 7, and the NaOH doping concentration of 3 M, 4 M and 5 M which are marked with dotted line. Thus, it is expected that the PVA-TEOS membrane with all these doping concentrations of NaOH electrolytes enclosed with bold dotted line in the **Table 5.6** might result in better ionic conductivity.

5.2.1.1.2 Effect of TEOS wt. % on water and NaOH uptake of the membrane electrolyte

Table 5.6 shows the water uptake and NaOH uptake of PVA-TEOS physically crosslinked membrane with varying TEOS concentrations of 5 wt. %, 10 wt. % and 15 wt. % for freeze-thaw cycle of 5 and 7. It is observed from **Table 5.6** that the water uptake increases as the TEOS amount increases from 5 wt. % to 10 wt. % for all NaOH doping concentrations. Further, increase in TEOS concentration beyond 10 wt. %, the water uptake decreases. The increase in water uptake of the membrane may be due to the hydrophilic characteristics of TEOS and its increased content in the membrane matrix (Mahreni et al. 2009). The highest water uptake of 146.6 wt. % and 136.54 wt. % were observed for $PT_{10wt.\%}$-5Cy and $PT_{10wt.\%}$-7Cy membranes, respectively, when dipped in distilled water only (0 M NaOH). The decreasing trend in water uptake of the synthesized membrane was observed beyond 10 wt. % TEOS, irrespective of the doping concentration of

NaOH for both the freeze-thaw cycles. The decrease in water uptake at very high concentrations (15 wt. %) of TEOS may be due to an increase in a high degree of crosslinking at higher TEOS content which enhances the hydrophobicity of membrane (Das eta l. 2015).

Table 5.6 Water and NaOH uptake of the physically crosslinked membrane of intermediate cycle 5 and 7 with varying TEOS concentration/loading in membrane.

Membrane Types	NaOH (0 M)		NaOH (2 M)		NaOH (3 M)		NaOH (4 M)		NaOH (5 M)		NaOH (6 M)		NaOH (7 M)	
	Wu (wt.%)	Nu (wt.%)	Wu (wt.%)	Nu (wt.%)	Wu (wt.%)	Nu (wt.%)	Wu (wt.%)	Nu (wt.%)	Wu (wt.%)	Nu (wt.%)	Wu (wt.%)	Nu (wt.%)	Wu (wt.%)	Nu (wt.%)
$PT_{5wt.\%}$-5Cy	141.23	0	98.41	16.23	85.22	19.60	70.78	24.13	59.85	30.16	49.07	35.48	44.47	28.73
$PT_{10wt.\%}$-5Cy	143.61	0	102.54	17.47	89.75	21.30	74.68	26.25	65.81	33.36	**55.43**	**37.24**	49.42	30.37
$PT_{15wt.\%}$-5Cy	135.34	0	95.72	15.31	82.46	17.89	68.12	21.58	57.87	27.78	46.93	32.92	41.67	27.1
$PT_{5wt.\%}$-7Cy	133.87	0	89.44	14.5	79.28	18.16	65.80	22.38	52.88	28.10	45.66	33.64	41.78	26.38
$PT_{10wt.\%}$-7Cy	136.54	0	93.81	15.42	84.31	19.13	68.64	24.88	55.23	30.72	**48.61**	**35.32**	43.28	28.57
$PT_{15wt.\%}$-7Cy	130.59	0	87.36	13.16	76.24	17.14	62.53	20.82	50.12	25.79	42.04	30.23	38.64	25.01

The lower freeze-thaw cycle 5 absorbed more water than 7 cycles for the fixed amount of TEOS loading. It may be due to the formation of more ordered structure of membrane matrix at a higher freeze-thaw cycle resulting in lower amount of void space available for water uptake. However, water uptake consistently decreases with the increase in NaOH doping concentration irrespective of the TEOS wt. % incorporated in the membrane for both freeze-thaw cycles i.e., $PT_{5wt.\%}$-5Cy, $PT_{10wt.\%}$-5Cy and $PT_{15wt.\%}$-5Cy or $PT_{5wt.\%}$-7Cy, $PT_{10wt.\%}$-7Cy and $PT_{15wt.\%}$-7Cy membrane types. As already mentioned, the decrease in water content with an increase in NaOH concentration may be due to the relative decrease of water concentration, which has a lower chance of occupying the pore space in the membrane matrix (Huang et al. 2016). It is seen from the literature and previous studies that the intermediate values of water uptake always give better membrane conductivity and membrane stability (Kim et al. 2004). Thus, it is expected that TEOS doping concentration 10 wt. % with the intermediate range of water uptake 84.31 wt. %, 68.64 wt. % and 55.23 wt. % for $PT_{10wt.\%}$-7Cy and water uptake of 89.75 wt. %, 74.68 wt. % and 65.81 wt. % for $PT_{10wt.\%}$-5Cy may result in good membrane conductivity (Yadav and Pramanik 2024a). It is also seen from **Table 5.6**, that the NaOH uptake increases with an increase in the doping concentration of NaOH up to 6 M, irrespective of the TEOS concentration/loading for both the freeze-thaw cycles. However, the NaOH uptake decreases with the further increase in NaOH doping concentration beyond 6 M. The reason for such a trend with increased NaOH doping concentration has already been discussed in **5.2.1.1.1** (page no. 114). The highest NaOH uptake of 35.32 wt. % was found for the $PT_{10wt.\%}$-7Cy with TEOS loading of 10 wt. %. Whereas, $PT_{5wt.\%}$-7Cy and $PT_{15wt.\%}$-7Cy for the TEOS loading of 5 wt. % and 15 wt. % came up with lower NaOH uptake of 33.64 wt. % and 30.23 wt. % when the PVA-TEOS membrane was doped with 6 M NaOH. It is clearly seen from **Table 5.6**, the NaOH uptake increases with the increase in TEOS loading up to 10 wt. % and then NaOH

uptake goes down when TEOS loading is increased to 15 wt. % for the freeze-thaw cycles with 5 and 7 both. This consistent trend in NaOH uptake of the membrane electrolytes at varying NaOH doping concentrations was found for both the freeze-thaw cycles 5 and 7.

As already mentioned, the highest NaOH uptake of 35.32 wt. % was found for the 6 M doping concentration of NaOH with TEOS loading of 10 wt. % ($PT_{10wt.\%}$-7Cy). Whereas, lower NaOH uptake of 30.72 wt. % and 28.57 wt. % were observed for the NaOH doping concentration of 5 M and 7 M, respectively, for the same membrane $PT_{10wt.\%}$-7Cy. The membrane electrolyte with 5 freeze-thaw cycles ($PT_{10wt.\%}$-5Cy) showed higher NaOH uptake of 37.24 wt. % than the higher freeze-thaw cycle 7 (35.32 wt. %) at the NaOH doping concentration of 6 M. The NaOH uptake is a little lower for the higher freeze-thaw cycle. It may be due to more ordered structure of the PVA-TEOS matrix at higher cycle and thus, relatively less void space available for NaOH uptake. Although, NaOH uptake is higher for 5 cycle, the stability of the membrane is better for 7 cycles due to more crosslinking and more ordered (Adelnia et al. 2021).

The crystallinity of the PVA-TEOS matrix might change from semi-crystalline to amorphous in nature at higher cycles, which might result in better ionic conductivity of the synthesized membrane electrolyte. Thus, XRD studies and subsequently, EIS studies are essential to ensure the best cycles at which the highest ionic conductivity of the membrane electrolyte is obtained. It should be noted that the highest NaOH uptake at 6 M doping concentration does not ensure the highest conductivity, as the sufficient water content in the membrane matrix is also very essential. Thus, the intermediate NaOH uptake i.e., 19.13 wt. %, 24.88 wt. % and 30.72 wt. % are expected to exhibit better ionic conductivity with an intermediate range of water uptake for 7 cycle and

21.30 wt. %, 26.25 wt. % and 33.36 wt. % for 5 cycles which are marked with bold line in the **Table 5.6**.

5.2.1.2 FT-IR analysis of the membrane electrolyte

The FT-IR characteristics of the pristine PVA and PVA-TEOS for the range of 500 - 4000 cm^{-1} are already shown in **Figure 5.6** (page no. 94). The important functional groups present in the pristine PVA and pristine PVA-TEOS membrane are already discussed in detail.

Figure 5.20 shows the FTIR spectra of physically crosslinked PVA-TEOS membrane i.e., $PT_{5wt.\%}$-0Cy, $PT_{5wt.\%}$-3Cy, $PT_{5wt.\%}$-5Cy, $PT_{5wt.\%}$-7Cy and $PT_{5wt.\%}$-9Cy. As discussed earlier that during the freezing process, the molecule of the membrane comes together for a longer time which enhance the possibility of the formation of stronger bond between PVA and TEOS. It is seen from the **Figure 5.20** that the intensity of the -OH broad band (region-a), gradually decreased from the membrane with the increase in the freeze-thaw cycle from $PT_{5wt.\%}$-3Cy to $PT_{5wt.\%}$-9Cy indicating that part of –OH groups of PVA were involved in a condensation reaction with silanol groups of TEOS, creating covalent crosslink between polymer segments (Kittur et al. 2013). The increase in the intensity of the Si-O-C band was observed with the freeze-thaw cycle (region-b) which indicates the formation of stronger bond between organic and inorganic phase. The FT-IR characteristics of the membrane $PT_{10wt.\%}$-5Cy for 5 cycle and $PT_{10wt.\%}$-7Cy for 7 cycle are also compared and is shown in the Appendix B (**Figure B2)**. The TEOS loading of 10 wt. % shows better compatibility with the PVA and there is strong bond formation between PVA and TEOS as indicated by the peak at 610 cm^{-1} for Si-O-C in the **Figure B2.** It should be noted that the intensity of the peak 610 cm^{-1} is high for $PT_{10wt.\%}$-7Cy.

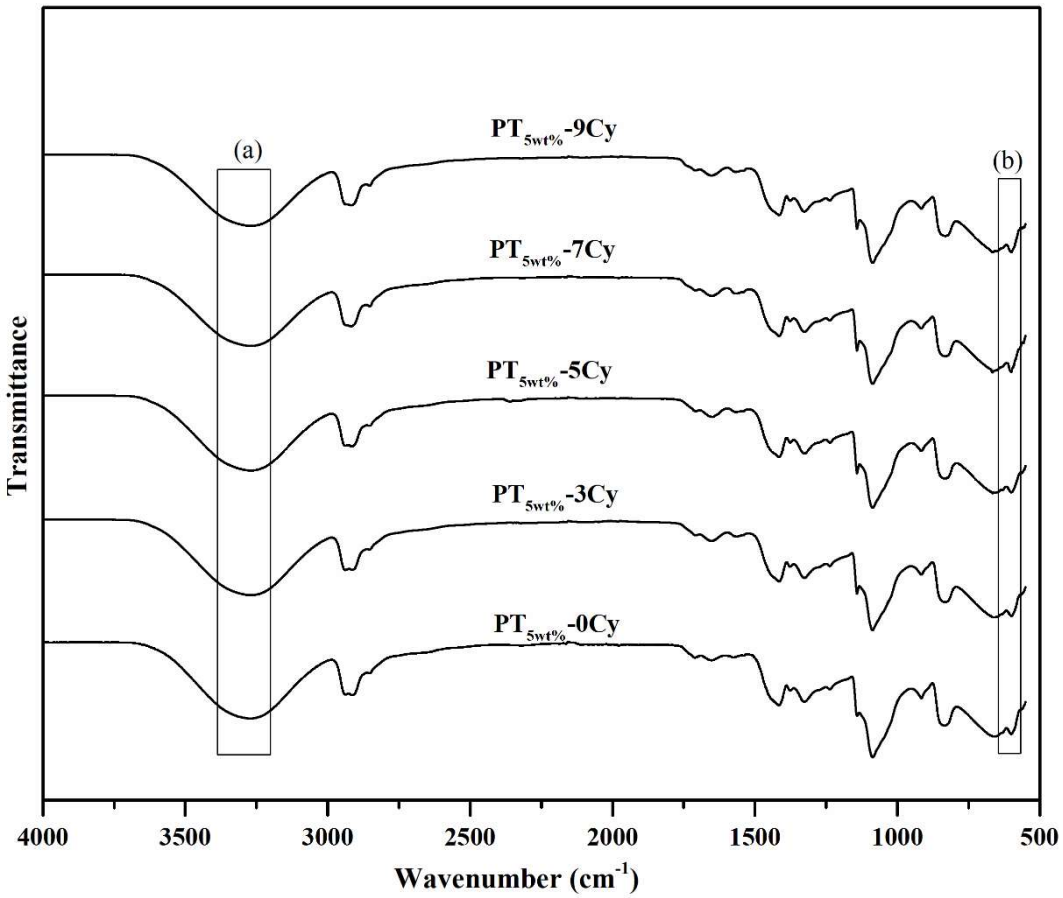

Figure 5.20 FT-IR spectra of the $PT_{5wt.\%}$-0Cy, $PT_{5wt.\%}$-3Cy, $PT_{5wt.\%}$-5Cy, $PT_{5wt.\%}$-7Cy and $PT_{5wt.\%}$-9Cy.

5.2.1.3 XRD analysis of membrane electrolyte

Figure 5.21 shows the XRD characteristics of the synthesized pristine PVA and various PVA-TEOS membranes with 5 wt.% TEOS loading and different freeze-thaw cycles i.e., $PT_{5wt.\%}$-0Cy, $PT_{5wt.\%}$-3Cy, $PT_{5wt.\%}$-5Cy, $PT_{5wt.\%}$-7Cy and $PT_{5wt.\%}$-9Cy. The XRD pattern for the membrane electrolytes of optimum TEOS loading/concentration of 10 wt. % i.e., $PT_{10wt.\%}$-5Cy and $PT_{10wt.\%}$-7Cy as obtained from water and NaOH uptake studies for intermediate freeze-thaw cycle 5 and 7 were compared (**Appendix B, Figure B3**).

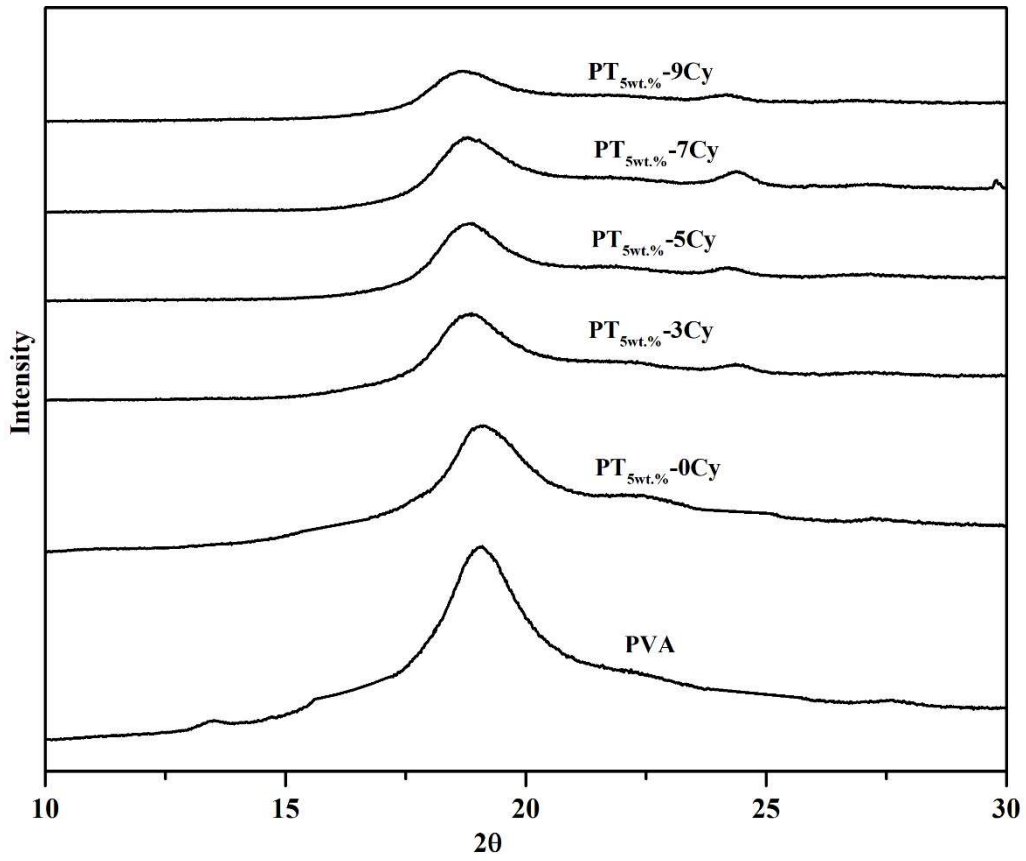

Figure 5.21 XRD spectra of the pristine PVA, $PT_{5wt.\%}$-0Cy, $PT_{5wt.\%}$-3Cy, $PT_{5wt.\%}$-5Cy, $PT_{5wt.\%}$-7Cy and $PT_{5wt.\%}$-9Cy**.**

It is seen in the published literature that the XRD analysis shows a prominant peak for pristine PVA at a 2θ angle of about 19°-20° and a small peak at around 2θ angle of 40° (Aziz et al. 2020, Abral et l. 2020) due to the semi-crystalline nature of PVA pristine membrane. In the present study, the pristine PVA film shows a prominent peak at 19.01° which indicates the semi-crystalline nature of the film. When TEOS is added to the PVA matrix, the $PT_{5wt.\%}$-0Cy (pristine) membrane shows a little lower peak intensity at the same 2θ angle of 19.01° as observed for the pristine PVA membrane also. However, the peak for the $PT_{5wt.\%}$-0Cy (pristine) is wider than pristine PVA. It may be due to an increase in the amorphous nature of the $PT_{5wt.\%}$-0Cy membrane due to the

incorporation of TEOS. The physical crosslinking of the PVA-TEOS membrane with 5 wt. % TEOS showed decreasing trend in peak height at 2θ of 18.89° for $PT_{5wt.\%}$-3Cy, 18.82° for $PT_{5wt.\%}$-5Cy, 18.71° for $PT_{5wt.\%}$-7Cy and 18.67° for $PT_{5wt.\%}$-9Cy, with the increase in freeze-thaw cycle upto 9 cycle. The decrease in peak height with the increase in freeze-thaw cycles indicates that the semi-crystalline nature of the PVA-TEOS (PT) membrane disappeared and became more amorphous in nature when the freeze-thaw cycle was increased. The peak intensity of the physically crosslinked membrane also shifted towards the left side with the increase in the number of freeze-thaw cycle. The shifting of the peak position in the left side indicates an increase in lattice plane spacing of the PVA structure, which occurred during the freeze-thaw process (Hong et al. 2010). The rise in d-spacing in the physical crosslink membrane could be due to the fact that the breakage of the PVA main polymer chains during the freeze-thaw process may have resulted in new crosslinkages and the creation of 3D structures of the membranes (Hernandez et al. 2002). It is well known that the amorphous nature gives better ionic conductivity of the membrane electrolyte (Wei et al. 2012). As the water uptake was found to be highest for the PVA-TEOS membrane with 10 wt. % TEOS loading of intermediate cycle 5 and 7 (**Table 5.6**) (page no. 119) and thus, the XRD characteristics of $PT_{10wt.\%}$-5Cy and $PT_{10wt.\%}$-7Cy were also compared and it is shown in the **Figure B3 (Appendix B)**. The peak intensity of the membrane $PT_{10wt.\%}$-7Cy was found to be lower than the $PT_{10wt.\%}$-5Cy. It may be due to the more amorphous nature of the PVA-TEOS membrane with 7 freeze-thaw cycle.

5.2.1.4 Ionic conductivity of physically crosslinked PVA-TEOS membrane

5.2.1.4.1 Effect of NaOH doping concentration

The electrochemical impedance spectroscopy (EIS) technique in a two probe system as mentioned in **Chapter 3 Figure 3.2 (**page no. 65), was used to measure the ionic conductivity of physically crosslinked PVA-TEOS membrane electrolyte. **Figure 5.22** shows the EIS characteristics of $PT_{5wt.\%}$-7Cy membrane doped with different concentrations of NaOH. In the EIS characteristics, there are two distinct zones: the high frequency zone and the low frequency zone. The ionic conductivity of the membrane electrolyte can be measured from Equation (3.5) (page no. 65), where the value of membrane resistance R was determined from the intercept of EIS curve on the real axis (Z') in high frequency zone. The enlarged image is also presented in the onset for better clarity of the EIS intercept on the real axis. It is well known that the ionic conductivity of $PT_{5wt.\%}$-7Cy depends on the amount of NaOH and water present in the membrane matrix. NaOH in the membrane matrix is responsible for hydroxyl ion (OH^-) transport and a suitable amount of water must be present in the membrane matrix for better ionic conductivity of the membrane. The highest ionic conductivity obtained was $9.26\pm0.03 \times 10^{-3}$ Scm^{-1} when the membrane was doped with 4 M NaOH ($PT_{5wt.\%}$-7Cy -(4M)). It is seen from **Table 5.7** that the ionic conductivity increases with the increase in the doping concentration of NaOH of 4 M. The increase in ionic conductivity from 2 M to 4 M NaOH doping in the membrane electrolyte is due to the increase in NaOH uptake in the membrane matrix. Although the NaOH uptake is highest for 6 M NaOH doping concentration, the ionic conductivity for the $PT_{5wt.\%}$-7Cy-(6M) obtained was $6.37\pm0.04\times 10^{-3}$ Scm^{-1} which is lower than $PT_{5wt.\%}$-7Cy-(4M). The reason for the highest ionic conductivity of $PT_{5wt.\%}$-7Cy-(4M) membrane electrolyte may due to the presence of little high water (65.80 wt. %) and a moderate amount of NaOH (23.38 wt. %) in the membrane matrix, probably giving better ionic mobility

within the membrane matrix. Whereas, the NaOH uptake was very high (33.64 wt. %) and the water uptake was a little low 45.66 wt.% for the membrane electrolyte $PT5_{wt.\%}$-7Cy-(6M) and thus, ionic mobility might be low. As already mentioned, the ionic conductivity of the membrane electrolyte depends upon the delicate balance between water uptake and NaOH uptake and the presence of a suitable amount of water and NaOH in the membrane matrix is required for better ionic conductivity (Kim et al. 2004).

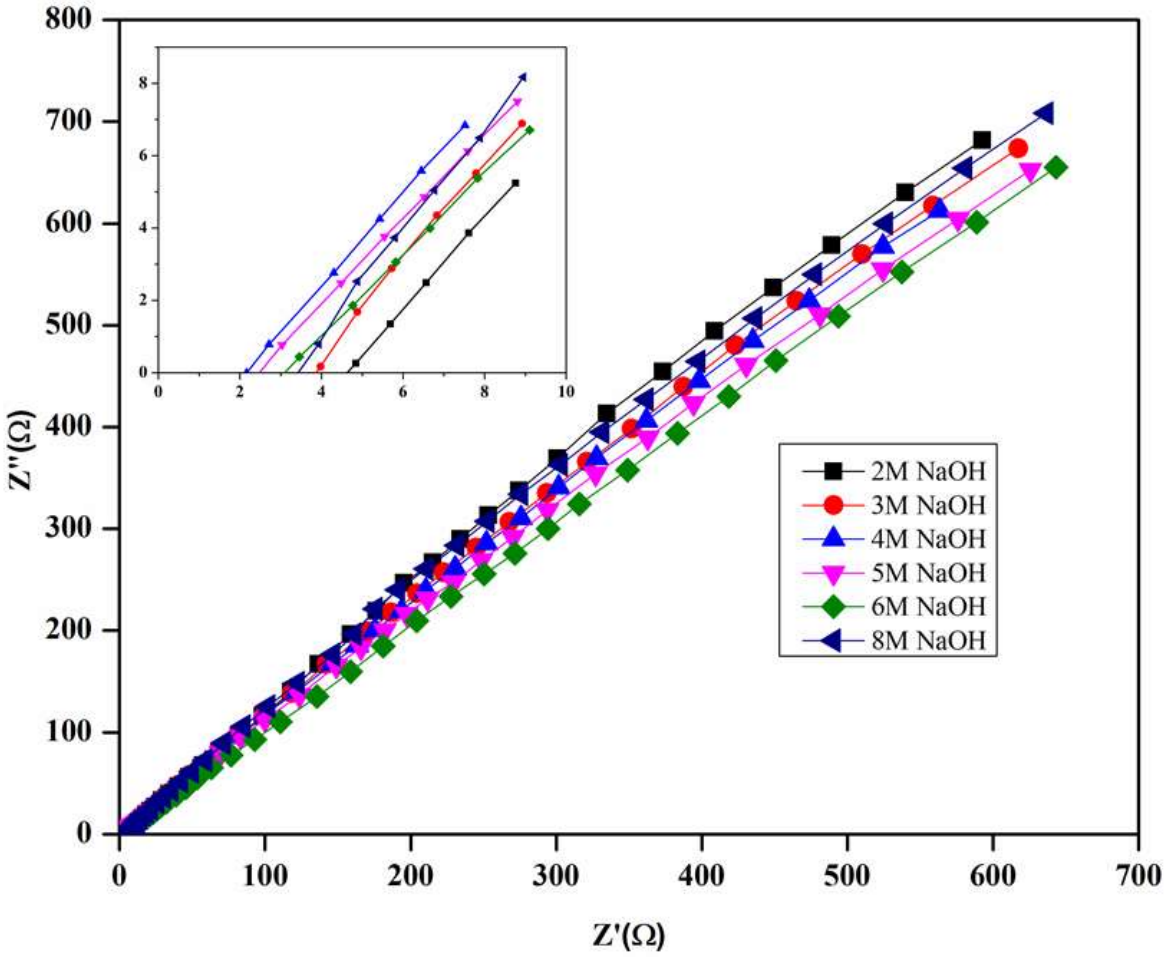

Figure 5.22 EIS spectra of the $PT_{5wt.\%}$-7Cy-(X) membrane electrolyte doped in various concentration of NaOH at the temperature of 30 °C.

Table 5.7 The ionic conductivity of the $PT_{5wt.\%}$-7Cy membrane electrolyte doped in various doping concentrations of NaOH at the temperature of 30 ^{o}C**.**

NaOH doping concentration	2 M	3 M	4 M	5 M	6 M	8 M
Ionic conductivity ($\times 10^{-3}$ Scm^{-1})	4.12±0.03	5.13±0.04	**9.26±0.03**	8.15±.02	6.37±0.04	5.71±0.02

The optimum NaOH doping concentration was found to be 4 M as it gives the highest ionic conductivity (9.26±0.03 × 10^{-3} Scm^{-1}**)**. The EIS characteristics of the freeze-thaw cycle of 5 doped with varying NaOH concentration, i.e., $PT_{5wt.\%}$-5Cy-(X) (where X = 2 M, 3 M, 4 M, 5 M, 6 M and 8 M) were also studied and is given in the Appendix B (**Figure B4**). The same NaOH doping concentration of 4 M was found to be optimum and the maximum ionic conductivity of 8.47±0.04× 10^{-3} Scm^{-1} was obtained for $PT_{5wt.\%}$-5Cy-(4M) membrane electrolyte. The ionic conductivity of $PT_{5wt.\%}$-5Cy in various NaOH doping concentrations is given in **Table B1**.

5.2.1.4.2 Effect of freeze-thaw cycles

The freeze-thaw cycle also modifies the microstructure of the (PT) membrane electrolyte and thus, EIS of the membrane electrolyte with an optimum doping concentration of 4 M with various freeze-thaw cycles were compared. **Figure 5.23** shows the ionic conductivity of the membrane electrolyte, physically crosslinked by different freeze-thaw cycle and dipped in optimum 4 M concentration of NaOH i.e., $PT_{5wt.\%}$-3Cy-(4M), $PT_{5wt.\%}$-5Cy-(4M), $PT_{5wt.\%}$-7Cy-(4M) and $PT_{5wt.\%}$-9Cy-(4M). The highest ionic conductivity of 9.26±0.03 × 10^{-3} Scm^{-1} was observed for $PT_{5wt.\%}$-7Cy-(4M). However, the lower ionic conductivity of 7.81±0.02 × 10^{-3} Scm^{-1} and 8.47±0.04 × 10^{-3} Scm^{-1} were observed for $PT_{5wt.\%}$-3Cy-(4M) and $PT_{5wt.\%}$-5Cy-(4M), respectively (**Table 5.8**). It is clearly seen from **Table 5.8** and **Fig. 5.23** was observed that the ionic conductivity increases with

the increase in the freeze-thaw cycle from 3 to 7 of the synthesized PVA-TEOS membrane electrolyte dipped in 4 M NaOH. Such increase in ionic conductivity may be due to the increase in the amorphous nature of the membrane electrolyte upto 7 freeze-thaw cycle as it is explained in XRD analysis also (**Figure 5.21**). The increase in the amorphous region helped the PVA chain segmental move locally, which enhanced the movement of ions and hence, improved ionic conductivity (Wei et al. 2012, Fan et al. 2018, Fu et al. 2010). The lowest ionic conductivity of $6.43\pm0.06 \times 10^{-3}$ Scm^{-1} was obtained for the very high freeze-thaw cycle 9 i.e., membrane electrolyte $PT_{5wt.\%}$-9Cy-(4M) (**Table 5.8**).

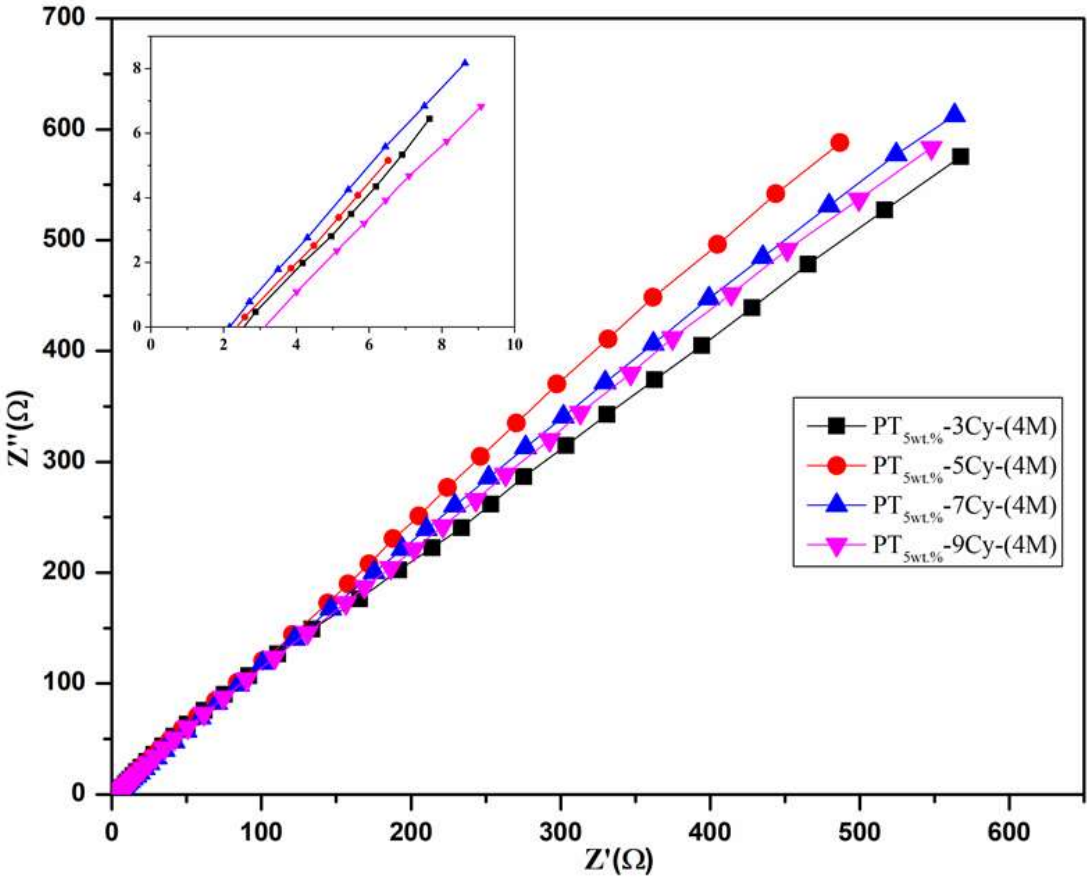

Figure 5.23 EIS characteristics of the different freeze-thaw cycle PVA-TEOS (5 wt. %) membrane electrolyte doped in 4 M NaOH concentration at the temperature of 30 ºC.

Table 5.8 The ionic conductivity of the different freeze-thaw cycle PVA-TEOS membrane electrolyte doped in 4 M NaOH concentration at the temperature of 30 ^{o}C.

Membrane electrolyte	$PT_{5wt.\%}$-**3Cy-**(4M)	$PT_{5wt.\%}$-**5Cy-**(4M)	$PT_{5wt.\%}$-**7Cy-**(4M)	$PT_{5wt.\%}$-**9Cy-**(4M)
Ionic conductivity ($\times 10^{-3}$ Scm^{-1})	7.81±0.02	8.47±0.04	**9.26±0.03**	6.43±0.06

The decrease in the ionic conductivity for the highest freeze-thaw cycle 9 may be due to the presence of relatively low water content (60.91 wt. %) and low uptake of NaOH (18.82 wt. %) in the membrane matrix. The optimum freeze thaw cycle and NaOH doping concentration were found to be 7 and 4 M, respectively as the $PT_{5wt.\%}$-7Cy-(4M) gives the highest ionic conductivity. The membrane electrolyte with 7 freeze-thaw cycle and 4 M NaOH doping concentration was also compared for various TEOS loading to find out the optimum loading/concentration of TEOS in the membrane. The amount of TEOS was also be optimized to obtain better performance of the DSBFC as discussed in the following section.

5.2.1.4.3 Effect of TEOS loading/concentration in membrane

Figure 5.24 shows the EIS characteristics of physically crosslinked PVA-TEOS membrane electrolytes containing different loadings of TEOS, varying from 5 wt. % to 15 wt. % for the optimum freeze-thaw cycle 7 and optimum NaOH concentration 4 M. Very low loading of TEOS causes low interaction with the PVA matrix and a higher amount of TEOS leads to higher interaction with the PVA matrix, which can affect the important characteristics of membrane electrolyte such as water uptake, NaOH uptake, crystallinity and ionic conductivity (Kittur et al. 2013, Das et al. 2015). In view of this, the ionic conductivity of the membrane electrolyte containing different loading of TEOS was measured from the EIS characteristics (**Figure 5.24**). It

is seen from **Table 5.9** that the ionic conductivity of the membrane electrolyte increases with an increase in TEOS loading upto 10 wt. % and then conductivity decreases with the increase in TEOS loading beyond 10 wt. %. The highest ionic conductivity of 9.67±0.04 × 10^{-3} Scm^{-1} was obtained for the membrane electrolyte $PT_{10wt.\%}$-7Cy-(4M). Whereas, lower ionic conductivity of 9.26±0.03 × 10^{-3} Scm^{-1}, and 7.29±0.05 × 10^{-3} Scm^{-1} were obtained for $PT_{5wt.\%}$-7Cy-(4M), and $PT_{15wt.\%}$-7Cy-(4M), respectively (**Table 5.9**). The initial increase in the ionic conductivity is due to the TEOS surface containing many hydroxyl groups, which considerably improve the NaOH retaining ability (Yang etal. 2011). The decrease in the membrane ionic conductivity beyond 10 wt. % of TEOS loading may be due to the higher degree of crosslinking between PVA and TEOS, which causes the membrane electrolyte to be very compact leaving less void space. Thus, the water uptake (62.53 wt.%) and KOH uptake (20.82 wt. %) both become low for the membrane electrolyte $PT_{15wt.\%}$-7Cy-(4M) beyond 10 wt % TEOS loading.

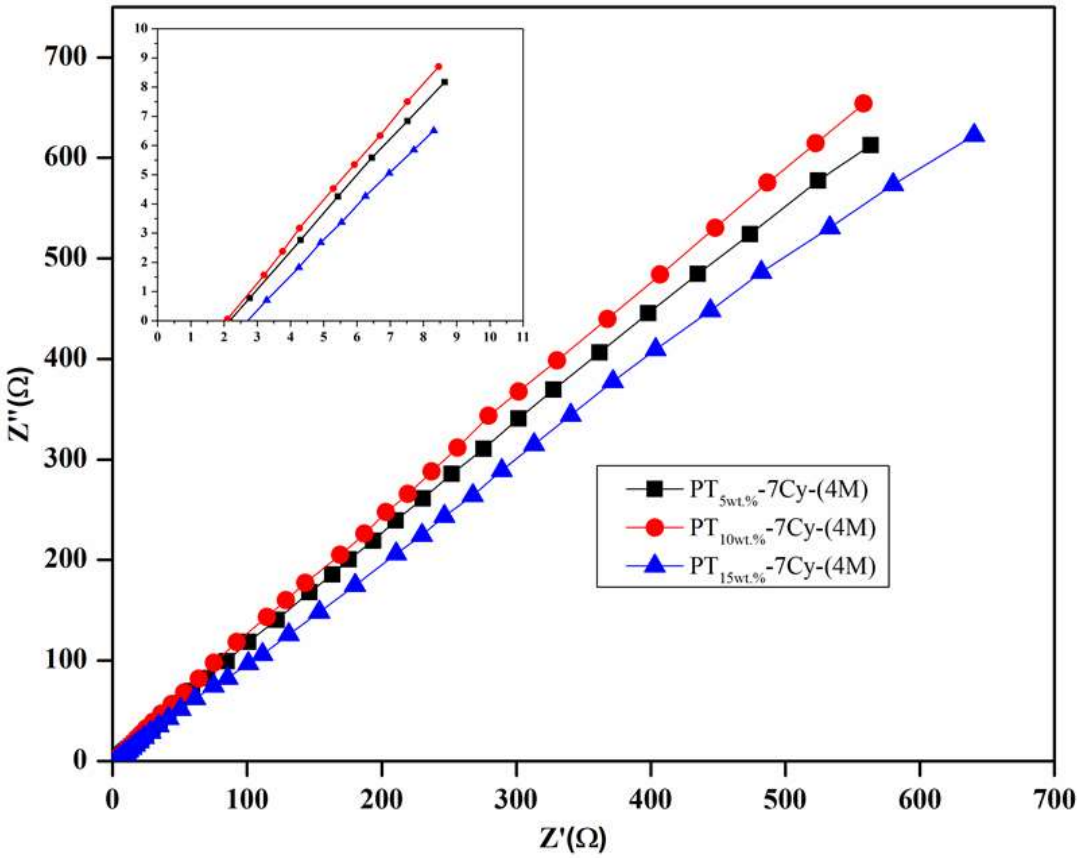

Figure 5.24 EIS characteristics of $PT_{Wwt.\%}$-7Cy with different TEOS content dipped in 4 M NaOH concentration at the temperature of 30 ^{o}C.

Table 5.9 Ionic conductivity of the membrane electrolyte having different TEOS loading at 30 ^{o}C temperature.

Membrane electrolyte	$PT_{5wt.\%}$-7Cy-(4M)	$PT_{10wt.\%}$-7Cy-(4M)	$PT_{15wt.\%}$-7Cy-(4M)
Ionic conductivity ($\times 10^{-3}$ Scm^{-1})	9.26±0.03	**9.67±0.04**	7.29±0.05

5.2.1.5 Surface morphology analysis of synthesized membrane

The surface morphology of the physically crosslinked PVA-TEOS membrane was analyzed using the SEM (SEM Quanta 200 F, USA). **Figure 5.25** shows the surface morphology of the

synthesized membrane for the varying freeze-thaw cycle from 0 to 9, i.e., $PT_{5wt.\%}$-0Cy, $PT_{5wt.\%}$-3Cy, $PT_{5wt.\%}$-5Cy, $PT_{5wt.\%}$-7Cy and $PT_{5wt.\%}$-9Cy. It is seen from **Figure 5.25**a that the surface of $PT_{5wt.\%}$-0Cy/pristine membrane is homogeneous and silica particles are not seen on the membrane surface. It may be due to uniform dispersion of TEOS derived silica particles in PVA matrix. **Figure 5.25**b shows the surface morphology of the physically crosslinked membrane by 3 freeze-thaw cycle i.e., $PT_{5wt.\%}$-3Cy. During the freeze-thaw cycle, the PVA and TEOS molecule comes closer to each other and interaction between PVA and TEOS takes place. However, the time required for 3 freeze-thaw cycle is comparatively less than the higher cycle. The interaction time between PVA and TEOS is less and thus, some TEOS deposites remain on the surface of $PT_{5wt.\%}$-3Cy membrane (**Figure 5.25**b**).** More uniform surface morphology was obtained when the freeze-thaw cycle is increased to 7 cycle ($PT_{5wt.\%}$-7Cy), and it may be due to more interaction between PVA and TEOS (**Figure 5.25**d). The surface of $PT_{5wt.\%}$-7Cy membrane is compact and has more uniformity than $PT_{5wt.\%}$-3Cy. The same phenomenon as observed for the 5 cycle, was also noticed for the higher freeze-thaw cycle of 9 (**Figure 5.25**e), i.e., $PT_{5wt.\%}$-9Cy membrane. The membrane surface becomes more uniform and compact for highe cycles than the membrane obtained through lower freeze-thaw cycle. The XRD analysis (**Figure 5.21**) also showed the more interaction between PVA and TEOS occurs as freeze-thaw increases which eventually increases the amorphous nature of the membranes.

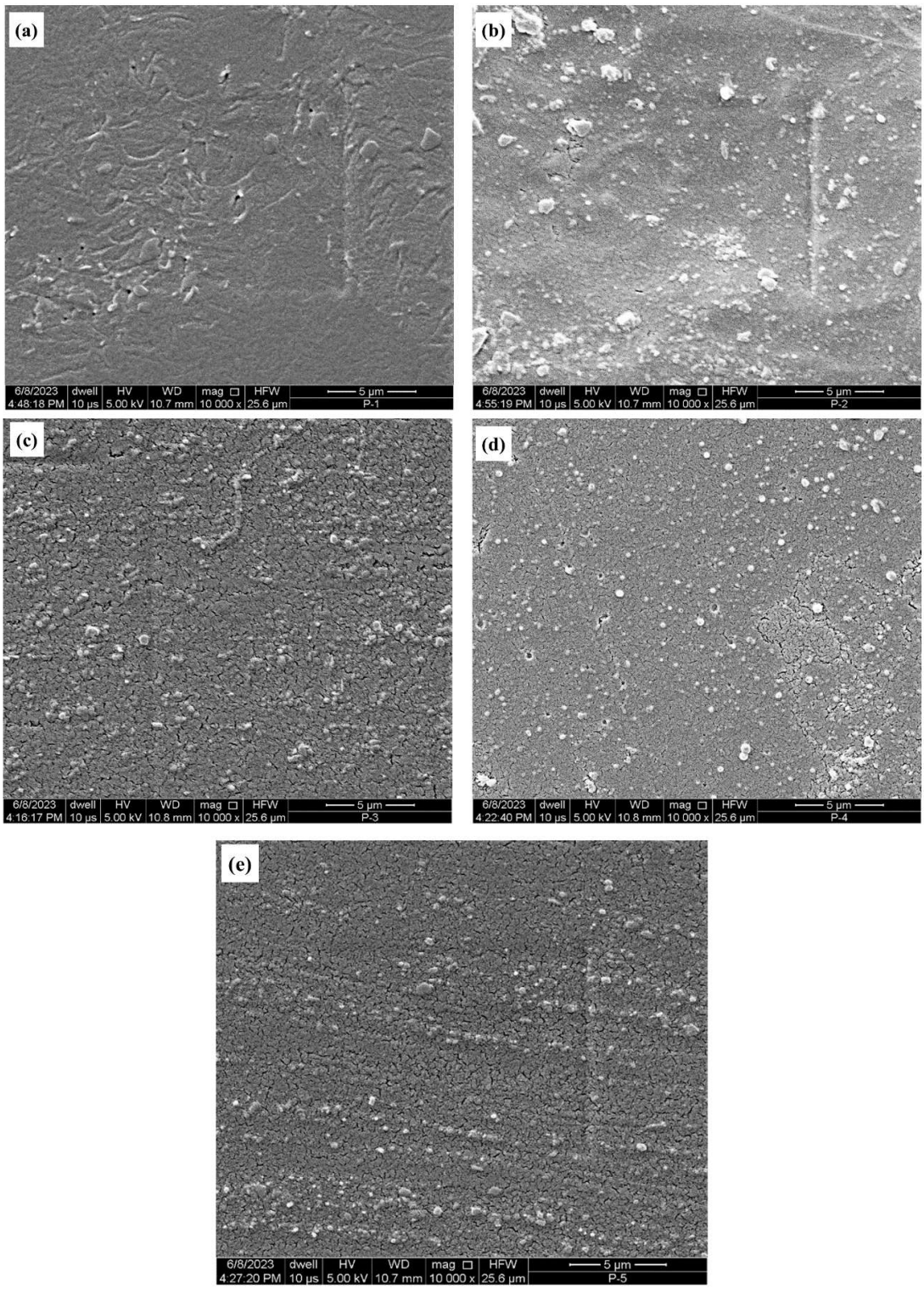

Figure 5.25 SEM images of the surface of (a) $PT_{5wt.\%}$-0Cy (b) $PT_{5wt.\%}$-3Cy (c) $PT_{5wt.\%}$-5Cy (d) $PT_{5wt.\%}$-7Cy and $PT_{5wt.\%}$-9Cy.

Figure 5.26 shows the surface morphology of the synthesized membrane i.e., $PT_{5wt.\%}$-7Cy, $PT_{10wt.\%}$-7Cy and $PT_{15wt.\%}$-7Cy for the fixed and optimum 7 freeze-thaw cycle and different TEOS loading ranging from 5 wt. % to 15 wt. %.

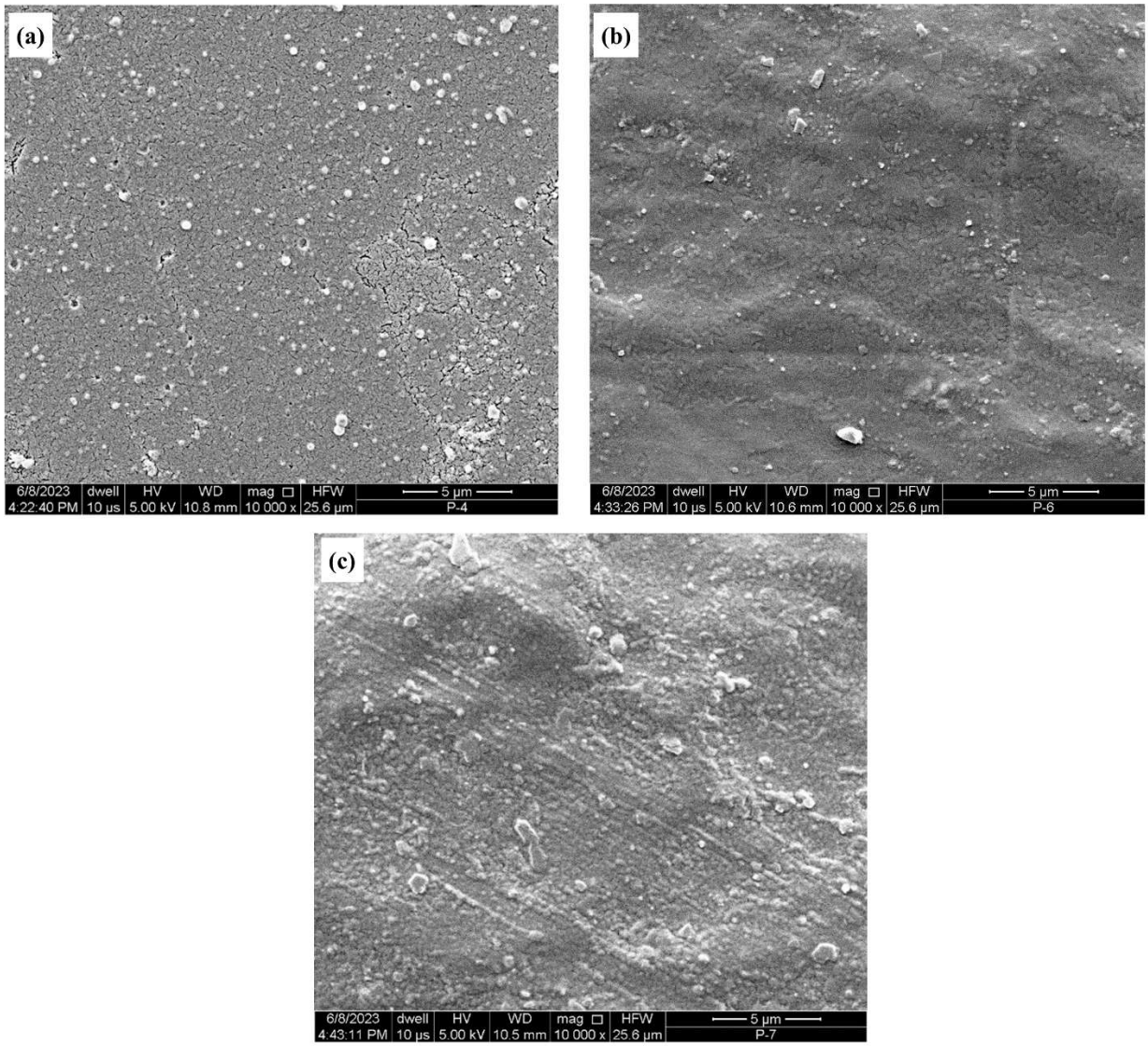

Figure 5.26 SEM images of the surface of (a) $PT_{5wt.\%}$-7Cy (b) $PT_{10wt.\%}$-7Cy and (c) $PT_{15wt.\%}$-7Cy.

It is observed from **Figure 5.26**a that the surface of the $PT_{5wt.\%}$-7Cy shows homogeneous surface and uniform distribution of TEOS particles. However, the surface becomes more compact and homogeneous as the TEOS loading increases from 5 wt. % to 10 wt. % (**Figure 5.26**b). **Figure 5.26**c shows the surface morphology of $PT_{15wt.\%}$-7Cy which is highly compact and rigid structure along with the deposition of the silica layer on the membrane surface due to the very high loading of TEOS of 15 wt %. Thus, the water and NaOH uptake of the $PT_{15wt.\%}$-7Cy membrane get reduced (**Table 5.6**) (page no. 119).

5.2.1.6 Swelling ratio and mechanical strength of the synthesized membrane

Table 5.10 shows the swelling ratio of the various synthesized membrane. The pristine PVA exhibited maximum swelling ratio of 83.33 %, as it is highly hydrophilic in nature. However, the swelling ratio decreases with the increase in the freeze-thaw cycle for the same TEOS loading of 5 wt. %. The decrease in the swelling ratio of the membranes from 0 freeze-thaw cycle/ pristine to 9 cycle may be due to the decrease in water uptake as the freeze-thaw cycle increases (**Table 5.5**). The swelling ratio of the PVA-TEOS membrane electrolyte for the optimum freeze-thaw cycle of 7 and varying TEOS loading i.e., $PT_{5wt.\%}$-(7Cy), $PT_{10wt.\%}$-(7Cy) and $PT_{15wt.\%}$-(7Cy) were 27.27 %, 19.86 % and 14.28, respectively. The similar trend in swelling ratio as observed for the varying freeze-thaw cycle, was also noticed when the TEOS loading was increased from 5 wt % to 15 wt%. However, the membrane $PT_{10wt.\%}$-(7Cy) shows a lower swelling ratio than the membrane $PT_{5wt.\%}$-(7Cy), despite having relatively higher water uptake by the $PT_{10wt.\%}$-(7Cy) membrane. It may be due to the higher crosslinking between PVA and TEOS of $PT_{10wt.\%}$-(7Cy) membrane matrix, which resulted in a more compact structure (Yuan et al. 2014). Thus, it is expected that the synthesized membrane $PT_{10wt.\%}$-(7Cy) would exhibit better mechanical stability which is presented

in the next section. The swelling ratio of the synthesized membrane with varying doping concentrations of NaOH is also presented in the supplementary **Table B2.** It is seen from the **Table B2** that the swelling ratio of $PT_{5wt.\%}$-7Cy, $PT_{10wt.\%}$-7Cy and $PT_{15wt.\%}$-7Cy membrane decrease with increase in NaOH doping concentration. It may be due to decrease in water uptake with increase in NaOH concentration irrespective of the membrane types (**Table 5.6**).

Table 5.10 Swelling ratio of the synthesized membrane using varying freeze-thaw cycle and varying TEOS composition.

Membrane Type	Swelling ratio (%)
PVA	83.33
$PT_{5wt.\%}$-0Cy	58.84
PT $_{5wt.\%}$-3Cy	46.15
PT $_{5wt.\%}$-5Cy	35.71
PT $_{5wt.\%}$-7Cy	27.27
PT $_{5wt.\%}$-9Cy	23.67
PT $_{10wt.\%}$-7Cy	19.86
PT $_{15wt.\%}$-7Cy	15.28

The tensile strength of the synthesized membrane electrolyte was tested using ASTM D0882 using UTM AEC1112-ACD, Asian Engineers Company, India, testing machine. **Figure 5.27** shows the stress-strain curves of the pristine PVA, pristine PVA-TEOS and physically crosslinked PVA-TEOS membrane with different cycle ranging from 0 to 9. The tensile strength of the pristine PVA and $PT_{5wt.\%}$-0Cy/pristine, PT $_{5wt.\%}$-3Cy, PT $_{5wt.\%}$-5Cy, PT $_{5wt.\%}$-7Cy and PT $_{5wt.\%}$-9Cy were 31.26 MPa, 38.80 MPa, 42.40 MPa, 46.23 MPa, 51.35 MPa and 54.72 MPa, respectively (**Table 5.11**). The higher tensile strength of PVA-TEOS pristine membrane i.e., $PT_{5wt.\%}$-0Cy in comparison to pristine PVA, may be due to the addition of TEOS to the PVA matrix, which enhanced the mechanical strength (Tong et al. 2017).

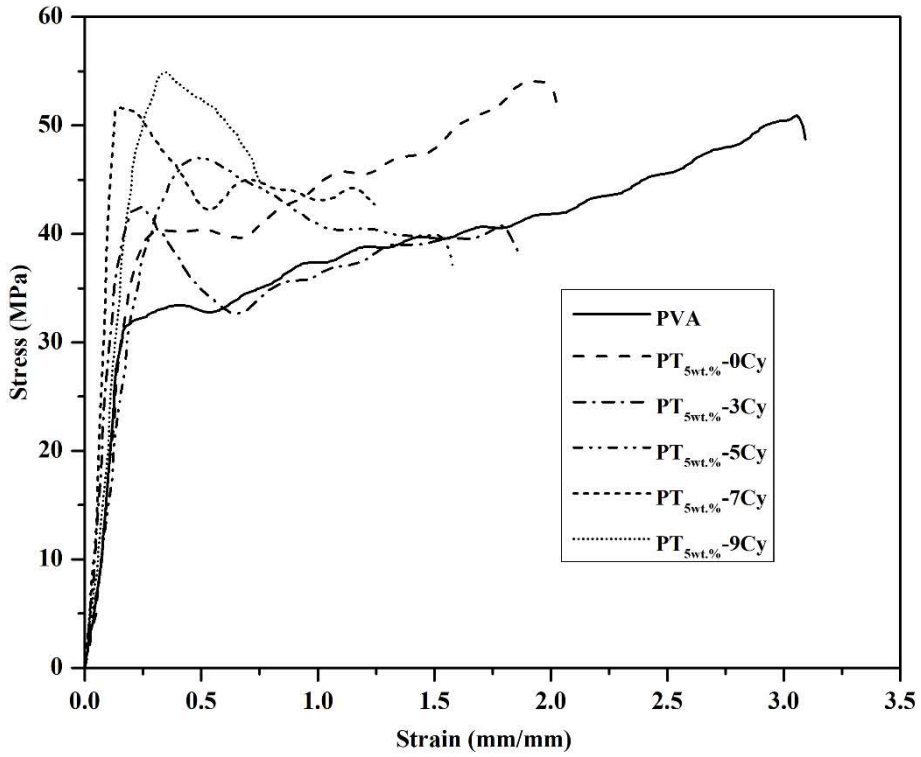

Figure 5.27 Stress-strain curve for the pristine PVA and physically crosslinked PVA-TEOS membrane from 0 to 9 freeze-thaw cycle.

It is also seen from the **Figure 5.27** that the tensile strength of the physically crosslinked membrane increases with the increase in the freeze-thaw cycle. The highest tensile strength of 54.72 MPa was observed for $PT_{5wt.\%}$-9Cy membrane. Although, the membrane $PT_{5wt.\%}$-9Cy shows highest mechanical strength, the membrane becomes more brittle in nature due to lesser membrane strain as compared to other types of membrane.

Figure 5.28 shows the stress-strain curve of the PVA-TEOS membrane obtained with different TEOS weight percent in PVA-TEOS and physically crosslinked by optimum freeze-thaw cycle 7. The tensile strength of $PT_{5wt.\%}$-7Cy, $PT_{10wt.\%}$-7Cy and $PT_{15wt.\%}$-7Cy were 51.35 MPa, 60.88 MPa and 72.18 MPa, respectively (**Table 5.11**). The increase in tensile strength of the membrane with

an increase in TEOS content from 5 wt.% to 15 wt. % in the membrane matrix may due to higher interaction between PVA and TEOS resulted in more stronger structure (Jessie et al. 2007).

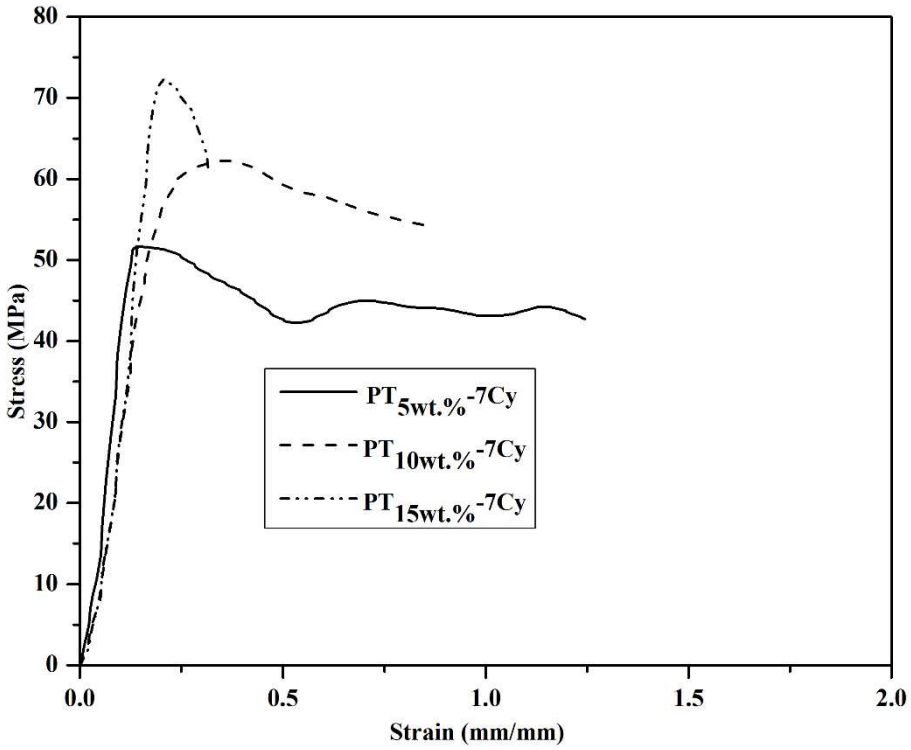

Figure 5.28 Stress-strain curve of the $PT_{5wt.\%}$-7Cy, $PT_{10wt.\%}$-7Cy and $PT_{15wt.\%}$-7Cy membrane electrolyte.

Table 5.11 Tensile strength of the synthesized membrane using varying freeze-thaw cycle and varying TEOS composition.

Membrane Type	Tensile Strength (%)
PVA	31.26
$PT_{5wt.\%}$-0Cy	38.80
PT $_{5wt.\%}$-3Cy	42.40
PT $_{5wt.\%}$-5Cy	46.23
PT $_{5wt.\%}$-7Cy	51.35
PT $_{5wt.\%}$-9Cy	54.72
PT $_{10wt.\%}$-7Cy	60.88
PT $_{15wt.\%}$-7Cy	72.18

5.2.2 Performance study of PVA-TEOS membrane electrolyte in single DSBFC

5.2.2.1 Effect of freeze-thaw cycle

Figure 5.29 shows the current density vs cell voltage and current density vs power density curves for different freeze-thaw cycles ranging from 3 to 9 of PVA-TEOS membrane electrolyte doped in 4 M NaOH. The physically crosslinked PVA-TEOS membrane with TEOS loading of 5 wt. % doped in 4 M NaOH was used as a solid electrolyte in the single cell test of DSBFC. The fuel used was 1 M $NaBH_4$ mixed in 4 M supporting NaOH electrolyte at the flow rate of 1.5 ml/min and the oxidant used was pure oxygen at the flow rate of 65 ml/min. The NaOH doping concentration of 4 M was considered in optimizing the freeze-thaw cycle as the ionic conductivity of the synthesized membrane electrolyte doped with 4 M NaOH was found to be the highest. It is seen from **Figure 5.29** that the highest power density of 61.81 mW/cm^2 at the current density of 140.8 mA/cm^2 was obtained for $PT_{5wt.\%}$-7Cy-(4M) membrane electrolyte at the cell temperature of 30 ^oC. However, the maximum power density of 48.24 mW/cm^2, 53.37 mW/cm^2 and 42.88 mW/cm^2 at the current density of 120 mA/cm^2, 128 mA/cm^2 and 80 mW/cm^2 were obtained for $PT_{5wt.\%}$-

3Cy-(4M), $PT_{5wt.\%}$-5Cy-(4M) and $PT_{5wt.\%}$-9Cy-(4M), respectively (**Table 5.12**). The increase in power density was observed from 3 freeze-thaw cycle to 7 cycle. It may be due to an increase in ionic conductivity of the membrane electrolyte from $7.81\pm0.02 \times 10^{-3}$ Scm^{-1} for $PT_{5wt.\%}$-3Cy-(4M) to $9.26\pm0.03 \times 10^{-3}$ Scm^{-1} for $PT_{5wt.\%}$-7Cy-(4M). Also, the amorphous nature of the PVA-TEOS membrane matrix increased with the increase in freeze-thaw cycle upto 7, as it clearly observed in XRD analysis (**Figure 5.21**).

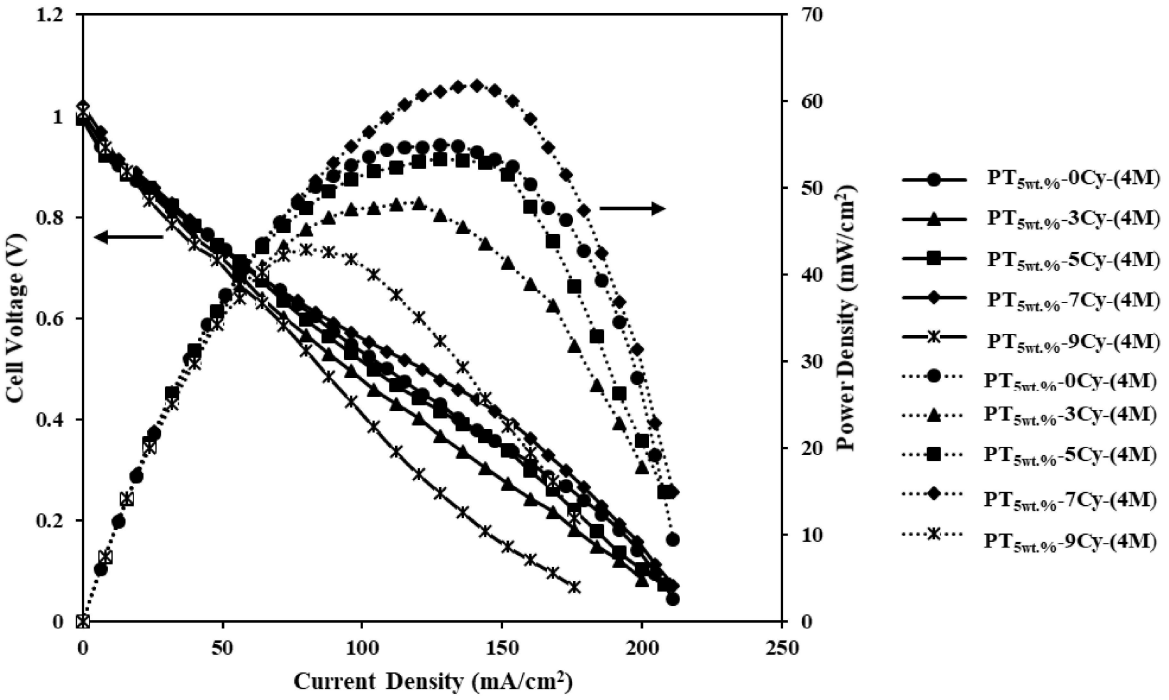

Figure 5.29 Polarization and power density curves of DSBFC for different freeze-thaw cycle using 4 M NaOH doped PVA-TEOS membrane electrolyte at the temperature of 30 ^{o}C; Anode and cathode loading was 1 mg/cm^2 and 2 mg/cm^2, respectively. Solid line-polarization curve; dotted line- power density curve.

Table 5.12 Maximum power density and current density at maximum power density for membrane electrolyte with varying freeze-thaw cycle.

Type of Membrane	Maximum power density (mW/cm^2)	Current density at maximum power density (mA/cm^2)
$PT_{5wt.\%}$-**0Cy-**(4M) / Pristine	54.91	128
$PT_{5wt.\%}$-**3Cy-**(4M)	48.24	120
$PT_{5wt.\%}$-**5Cy-**(4M)	53.37	128
$PT_{5wt.\%}$-**7Cy-**(4M)	**61.81**	**140.8**
$PT_{5wt.\%}$-**9Cy-**(4M)	42.88	80

The EIS study shows the highest ionic conductivity of $9.26\pm0.03 \times 10^{-3}$ Scm^{-1} for $PT_{5wt.\%}$-7Cy-(4M) membrane electrolyte. The decrease in power density was observed beyond 7 freeze-thaw cycle and it may be due to very low water uptake (60.91 wt. %) and NaOH (18.82 wt. %) uptake in the membrane matrix, which resulted in low ionic conductivity (6.43 ± 0.06 10^{-3} Scm^{-1}).

5.2.2.2 Effect of NaOH doping concentration in PVA-TEOS

The conductivity of hydroxyl ion in PVA-TEOS membrane was possible due to the presence of NaOH amount in the membrane matrix by doping it in NaOH solution of varying concentration for 24 h. The freeze-thaw cycle of the synthesized membrane electrolyte of 7 showed better performance in the DSBFC study. Thus, the optimum freeze-thaw cycle of 7 was fixed for optimizing the NaOH doping concentration in the physically crosslinked PVA-TEOS membrane in the DSBFC study. **Figure 5.30** shows the performance of the membrane electrolyte using different NaOH concentrations varying from 2 M to 8 M i.e., $PT_{5wt.\%}$-7Cy-(2M), $PT_{5wt.\%}$-7Cy-(4M), $PT_{5wt.\%}$-7Cy-(6M) and $PT_{5wt.\%}$-7Cy-(8M) in DSBFC at the cell temperature of 30 ^oC. It is seen from **Figure 5.30** that the power density of the DSBFC increases as the concentration of

NaOH doping increased from 2 M to 4 M. The shifting of power density curves in the upward direction with the highest shifting in the central region of the power density curves can be observed upto doping concentration of 4 M NaOH. It indicates very enhancement in power density in the ohmic polarization region (**Figure 5.30**). The power density gets decreased beyond 4 M NaOH doping concentration. The maximum power density of 61.81 mW/cm^2 was obtained at the current density of 140.8 mA/cm^2 for the membrane electrolyte doped with 4 M NaOH concentration i.e., $PT_{5wt.\%}$-7Cy-(4M). The maximum power density of 33.51 mW/cm^2, 50.26 mW/cm^2 and 47.20 mW/cm^2 were obtained for the membrane electrolyte $PT_{5wt.\%}$-7Cy-(2M), $PT_{5wt.\%}$-7Cy-(6M), and $PT_{5wt.\%}$-7Cy-(8M), respectively (**Table 5.13**). The membrane electrolyte doped in 4 M NaOH i.e. $PT_{5wt.\%}$-7Cy-(4M), exhibited the highest maximum power density (61.81 mW/cm^2), even though the NaOH uptake of $PT_{5wt.\%}$-7Cy-(6M) membrane was highest at 6 M NaOH doping concentration (33.64 wt.%). It is seen from **Table 5.13** that the ionic conductivity of $PT_{5wt.\%}$-7Cy-(4M) membrane electrolyte was found to be highest ($9.26\pm0.03 \times 10^{-3}$ S cm^{-1}), whereas the $PT_{5wt.\%}$-7Cy-(6M) membrane electrolyte showed lower ionic conductivity of $6.37\pm0.04 \times 10^{-3}$ Scm^{-1}.

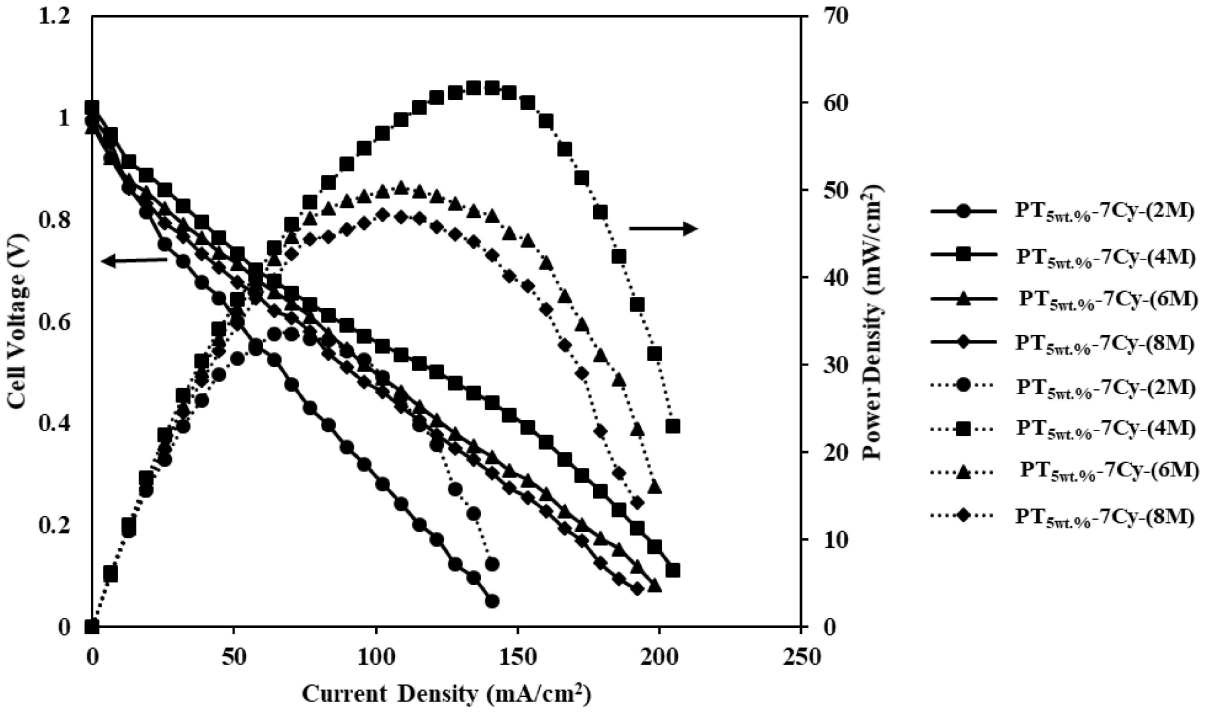

Figure 5.30 The polarization and power density curve of DSBFC for different NaOH concentration of $PT_{5wt.\%}$-7Cy at the cell temperature of 30 ºC. Anode and cathode loading was 1 mg/cm^2 and 2 mg/cm^2, respectively. Solid line-polarization curves; dotted line-power density curve.

Table 5.13 Maximum power density and current density for different NaOH doping concentration for $PT_{5wt.\%}$-7Cy-(X) (where, X ranging from 2M to 8M NaOH) at the cell temperature of 30 ºC**.**

Type of membrane electrolyte	**Maximum power density (mW/cm^2)**	**Current density at maximum power density (mA/cm^2)**
$PT_{5wt.\%}$-7Cy-(**2M**)	33.51	70.4
$PT_{5wt.\%}$-7Cy-(**4M**)	**61.81**	**140.8**
$PT_{5wt.\%}$-7Cy-(**6M**)	50.26	108.8
$PT_{5wt.\%}$-7Cy-(**8M**)	47.20	102.4

The very high mobility of hydroxyl ion at a moderate NaOH doping concentration of 4 M may be due to moderate NaOH uptake of 22.38 wt. % with sufficient water content (65.8 wt.%) which

resulting in very high ionic mobility of OH^- ions within the membrane electrolyte matrix. When the PVA-TEOS membrane was doped with 6 M NaOH, the ionic mobility OH^- ions may have been low due to extremely high NaOH uptake (33.64 wt. %) and low water uptake (45.66 wt. %). It may result in the poor ionic conductivity and thus, the performance of the membrane electrolyte $PT_{5wt.\%}$-7Cy-(6M) in DSBFC was also not promising. The performance studies of membrane electrolyte doped in various concentration of NaOH shows that the 4 M NaOH doping concentration is the optimum value.

5.2.2.3 Effect of TEOS concentration on DSBFC performance

Figure 5.31 shows the polarization and power density curves with varying TEOS concentration/loading in PVA-TEOS, keeping the NaOH doping concentration fixed at optimum value (4 M) and freeze-thaw cycle 7 (optimum). The TEOS content was varied from 5 wt. % to 15 wt. %. The incorporation of TEOS in the PVA membrane matrix enhanced the water uptake, NaOH uptake (**Table 5.6)** and ionic conductivity (**Table 5.9**). It is seen from **Figure 5.31** that the power density gets increased from 61.81 mW/cm^2 to 66.96 mW/cm^2 with the increase in TEOS content from 5 wt. % to 10 wt. % in the membrane matrix. However, further increase in TEOS content to 15 wt. %, the power density gets reduced to 47.37 mW/cm^2 (**Table 5.14)**. The highest peak power density for the membrane electrolyte $PT_{10wt.\%}$-7Cy-(4M) may be due to the highest ionic conductivity ($9.67\pm0.04 \times 10^{-3}$ Scm^{-1}) of the $PT_{10wt.\%}$-7Cy-(4M) membrane electrolyte. It is seen that the ionic conductivity of the membrane electrolyte increases with the increase in the amount of TEOS in the PVA-TEOS membrane (**Table 5.9**). This is because of the high hydrophilic characteristic of TEOS.

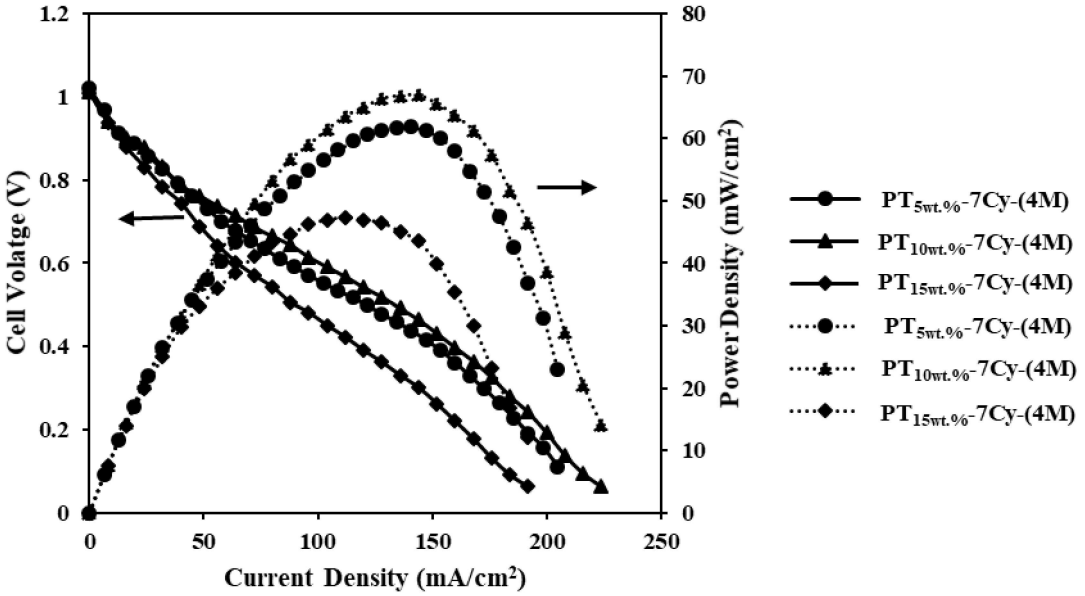

Figure 5.31 The polarization and power density curve of DSBFC for different TEOS wt. % of the PT-7Cy membrane electrolyte doped in 4 M NaOH at the cell temperature 30 ^{o}C. Anode and cathode loading was 1 mg/cm^2 and 2 mg/cm^2, respectively. Solid line-polarization curve; dotted line-power density curve.

Table 5.14 Maximum power density and current density with varying loading of TEOS in the membrane electrolyte at the cell temperature of 30 ^{o}C.

Type of membrane electrolyte	**Maximum power density (mW/cm^2)**	**Current density at maximum power density (mA/cm^2)**
PT$_{5wt.\%}$-7Cy-(4M)	61.81	140.8
PT$_{10wt.\%}$-7Cy-(4M)	**66.96**	**144**
PT$_{15wt.\%}$-7Cy-(4M)	47.37	112

Moreover, the TEOS surface contains many hydroxyl groups, which significantly improve the capacity to retain NaOH (Yang et al. 2011). Thus, the TEOS content of 10 wt. % in the membrane matrix resulting in the highest ionic conductivity (9.67 ±0.04× 10^{-3} Scm^{-1}). On the other hand, a

very high TEOS loading of 15 wt. % resulted in low ionic conductivity, which may be due to the brittle nature of membrane electrolytes at very high TEOS loading. The dependency of ionic conductivity with TEOS content has already been discussed in the **section 5.2.1.4.3** (page no. 130).

5.2.2.4 Effect of temperature on DSBFC performance

The effect of cell temperature on the cell performance in terms of power density and current density were studied using the best membrane electrolyte $PT_{10wt.\%}$-7Cy-(4M) obtained at the optimized synthesized condition as it gives the highest ionic conductivity ($9.67\pm0.04 \times 10^{-3}$ Scm^{-1}) among all synthesized membrane electrolyte (**Table 5.9**). **Figure 5.32** shows the performance characteristics of DSBFC using the best membrane electrolyte ($PT_{10wt.\%}$-7Cy-(4M) for varying cell temperatures ranging from 30 ^oC to 70 ^oC. It is seen from **Figure 5.32** that the maximum power density increases with the increase in cell temperature from room temperature (30 ^oC) to 60 ^oC. However, the power density goes down with further increase in cell temperature beyond 60 ^oC. It is well known that the electrode reaction kinetics increases with the increase in cell temperature, thus increasing cell current density. Further, the activation loss at the electrode gets reduced at the higher temperature. Moreover, when the cell temperature raises, the anolyte viscosity decreases, thus enhancing the ionic mobility. As a result, ohmic loss decreases and electrolyte conductivity increases (Celic et al. 2008). Due to these, at the cell temperature of 60 ^oC, the maximum power density obtained was 85.19 mW/cm^2, which is the highest of all cell temperatures.

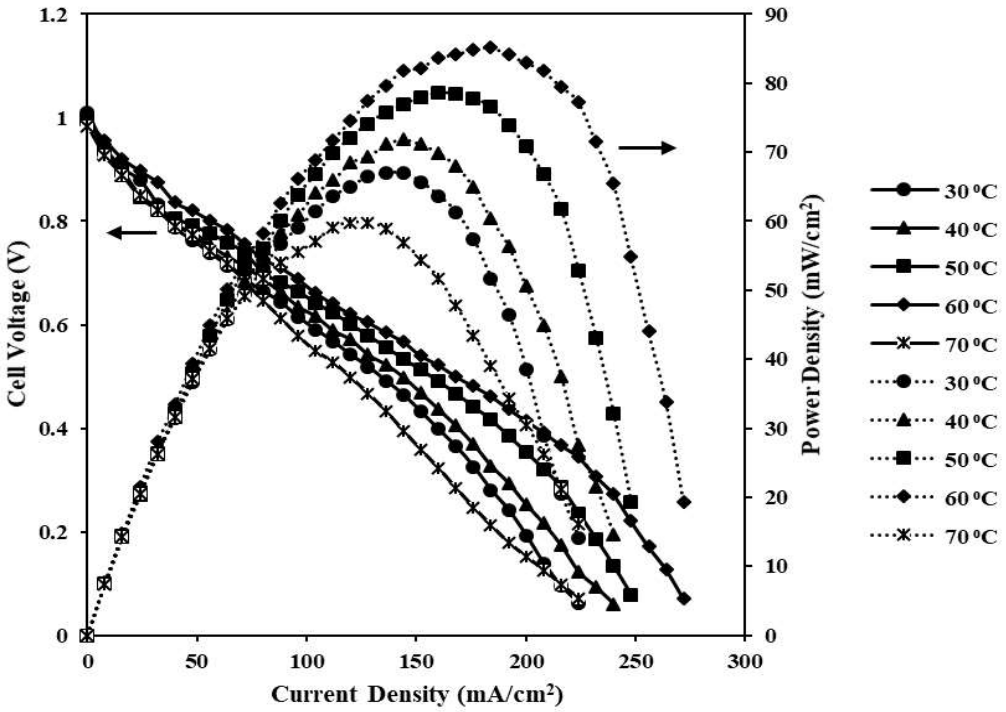

Figure 5.32 The polarization and power density curve of DSBFC for PT $_{10\ wt\ \%}$-7Cy-(4M) membrane electrolyte at various temperatures. Anode and cathode loading was 1 mg/cm^2 and 2 mg/cm^2, respectively. Solid line-polarization curve; dotted line-power density curve.

Table 5.15 Maximum power density and current density at different cell temperatures for the membrane electrolyte PT$_{10wt.\%}$-7Cy-(4M).

Cell temperature (°C)	**Maximum power density (mW/cm^2)**	**Current density at maximum power density (mA/cm^2)**
30 °C	66.96	144
40 °C	71.85	144
50 °C	78.56	160
60 °C	**85.19**	**184**
70 °C	59.77	128

It should be noted that very high cell temperature of 70 ^{o}C produced a lower power density of 59.77 mW/cm^2. It may be due to the dryness of the cathode at very high temperatures (70 ^{o}C), the ion transport decreases at the electrode layer. Similarly, electrolyte dehydration occurs at relatively higher temperatures, increasing cell resistance (Lobato et al. 2007, Tran et al. 2021). Moreover, borohydride crossover and borohydride hydrolysis come into existence at high temperature (Cheng et al. 2006b). Thus, the optimum cell temperature of 60 ^{o}C was recorded for the highest cell performance in terms of power density (**Table 5.15**).

5.2.3 Performance study of NaOCl as oxidant in DSBFC using physically crosslinked membrane electrolyte

5.2.3.1 Cathode reduction in half cell

5.2.3.1.1 Effect of scan rates

The effect of scan rates on the electrochemical reduction of sodium hypochlorite was thoroughly studied to determine the optimal value of scan rate. The optimum value of scan rate was further used to determine the optimum values of various electrode parameters, such as the effect of electrocatalyst loading, the effect of sodium hypochlorite concentration and effect of supporting electrolyte concentration, i.e., NaOH. **Figure 5.33** shows cyclic voltammetry for the electrochemical reduction of 2 M sodium hypochlorite mixed in 1 M NaOH solution at varying scan rate. The electrocatalyst used was commercial Pt/C_{HSA}, which had a loading of 1 mg/cm^2. In the CV study, the peaks in the backward scan corresponds to the electrochemical reduction of sodium hypochlorite. It is seen from **Figure 5.33** that there are three prominent peaks are observed in the backward scan due to electrochemical reduction reaction. It is clearly seen from **Figure 5.33** that the reduction peaks current density increases with increase in the scan rate from 10 mV/s to

50 mV/s. Moreover, the peak position/peak potential shifted to more (-)ve axis side when scan rate was increased.

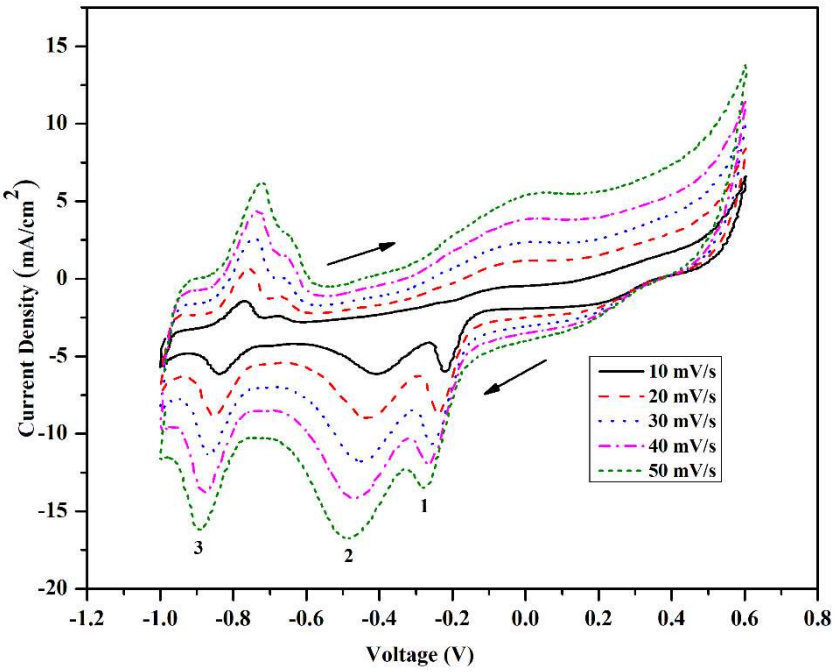

Figure 5.33 Cyclic voltammetry for Pt/C cathode at loading of 1 mg/cm^2 at different scan rate using 2 M NaOCl mixed in 1 M NaOH solution.

Table 5.16 Voltage and current density of the reduction peaks for the scan rate of 10 mV/s and 50 mV/s.

Scan Rate	**10 mV/s**			**50 mV/s**		
Reduction Peak	**1st peak**	**2nd peak**	**3rd peak**	**1st peak**	**2nd peak**	**3rd peak**
Voltage (V)	-0.216	-0.405	-0.837	-0.275	-0.485	-0.893
Current Density (mA/cm^2)	5.82	6.12	6.24	13.53	16.7	16.1

In the electrochemical reduction, sodium hypochlorite is consumed, a concentration gradient between the bulk phase and the electrode surface is created, and a diffusion barrier develops. The scan rate influences the thickness of the diffusion barrier. When the scan rate is slow (10 mV/s),

there is enough time for the diffusion barrier to become wider than the faster scan rates (Panjiara and Pramanik 2020b). As a result, the mass transfer resistance for the transport of NaOCl molecules from bulk to the electrode surface will be significant at slow scan rates, resulting in low peak current density (Singh and Pramanik 2023).

On the other hand, at a rapid scan rate, the thickness of the diffusion layer will be smaller, resulting in a more prominent peak current density due to low resistance to mass transfer of sodium hypochlorite molecule (Panjiara and Pramanik 2020b). The shifting of peak potential towards the more (-)ve axis may be due to the higher activation overpotential at higher scan rates (Zhang et al. 2014). When compared the CV of 50 mV/s with the CV of 10 mV/s, a prominent shifting in the peak potentials are observed. Althogh, overpotential is little high for the scan rate of 50 mV/s, the peak current density at this scan rate is highest giving prominent peaks for all electrochemical reactions. Thus, the CV of 50 mV/s is considered to explain the probable electrochemical reduction reaction of NaOCl taking place at the cathode and is also the basis for all the CV studies in the preceding sections. As per the published literature, the electrochemical reduction reaction of NaOCl in alkaline medium occurs in a single step as already shown in Equation 2.4 (page no. 48) (Kjeang et al. 2008, Cardenas-Valencia et al. 2007). Martins et al. 2018 reported the peaks at approximate -0.2 V corresponds to the electrochemical reduction reaction of NaOCl in alkaline medium. In the present study, a prominent reduction peak in the backward scan rate at the position of -0.275 V for the scan rate of 50 mV/s is observed (**Table 5.16**) and it may be due to the reduction of NaOCl as presented in Equation 2.4 (Martins et al. 2018).

There are two more peaks at the backward scan were clearly observed. No such studies are found in open literature search to explain these two additional peaks. However, there is high possibilities

of NaOCl decomposition (Kim et al. 2016) (Equation 5.1) followed by electrochemical reduction of O_2 via two-step two-electron transfer mechanism as already presented in the Equation 2.6 and 2.7 (page no. 50) (Rathoure and Pramanik 2016) and also in **Figure 5.34.**

$$NaOCl \rightarrow 2NaCl + O_2 \quad (5.1)$$

The reduction peaks at -0.485 V and -0.893 V for the scan rate of 50 mV/s are corresponds to the O_2 reduction (Equation 2.6 and 2.7). Rathoure and Pramanik also reported that the peaks at around -0.4 V and -0.8 V correspond to the two step reduction of O_2 in alkaline medium (Rathoure and Pramanik 2016).

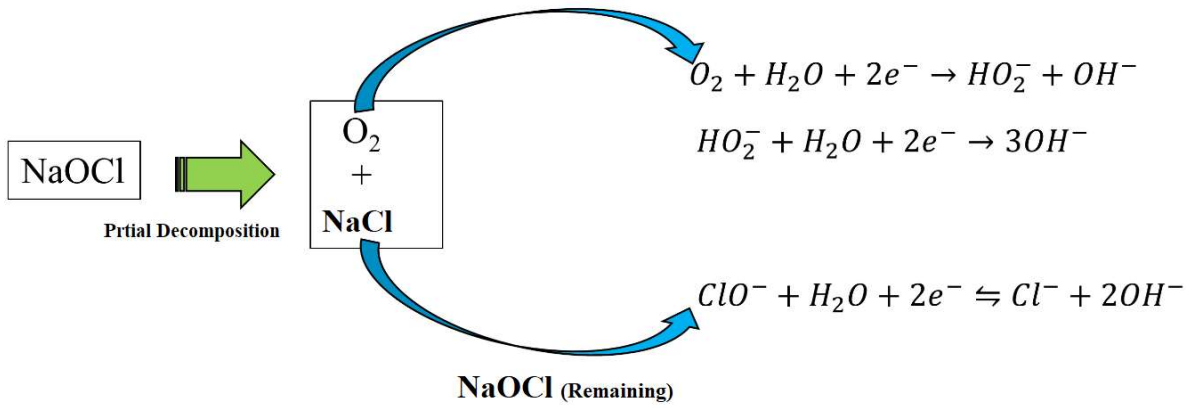

Figure 5.34 Schematic of the possible reduction reaction routes of the sodium hypochlorite.

5.2.3.1.2 Effect of sodium hypochlorite concentration

Figure 5.35 shows the cyclic voltammogram of varying concentration of oxidant sodium hypochlorite mixed in fixed 1 M NaOH concentration at a san rate of 50 mV/s. It is seen from the **Figure 5.35,** the reduction peak current density in the backward scan rises as the NaOCl concentration rises from 1 M to 2 M and then decreases when the NaOCl concentration was

increased from 2 M to 2.5 M. The highest peak current density for NaOCl reduction (Equation 2.4) (page no. 48) of 17.5 mA/cm^2 at a peak current density of -0.269 V was obtained for the NaOCl concentration of 2 M. Whereas, the highest oxygen electrochemical reduction (Equation 2.6 & 2.7) (page no. 50) peak current density of 33.5 mA/cm^2 at a voltage of -0.93 V and 28.7 mA/cm^2 at -0.541 V were obtained for the NaOCl concentration of 2 M. The peak current density for the concentrations 1 M, 1.5 M and 2.5 M were always lower than the 2 M NaOCl (**Table 5.17)**. The initial rise in the reduction current density upto 2 M NaOCl may be due to the improved cathode kinetics with more NaOCl molecules at this optimum (2 M) NaOCl concentration, causing more molecules to split and comes up with increased current density (Gupta and Pramanik 2019b). The current density decreases beyond 2 M NaOCl may be due to less availability of water molecules at the active catalyst site (Panjiara and Pramanik 2022, Yadav and Pramanik 2024b). As the presence of water molecule is very much essential as per reduction reaction (Equation 2.4) (page no. 48).

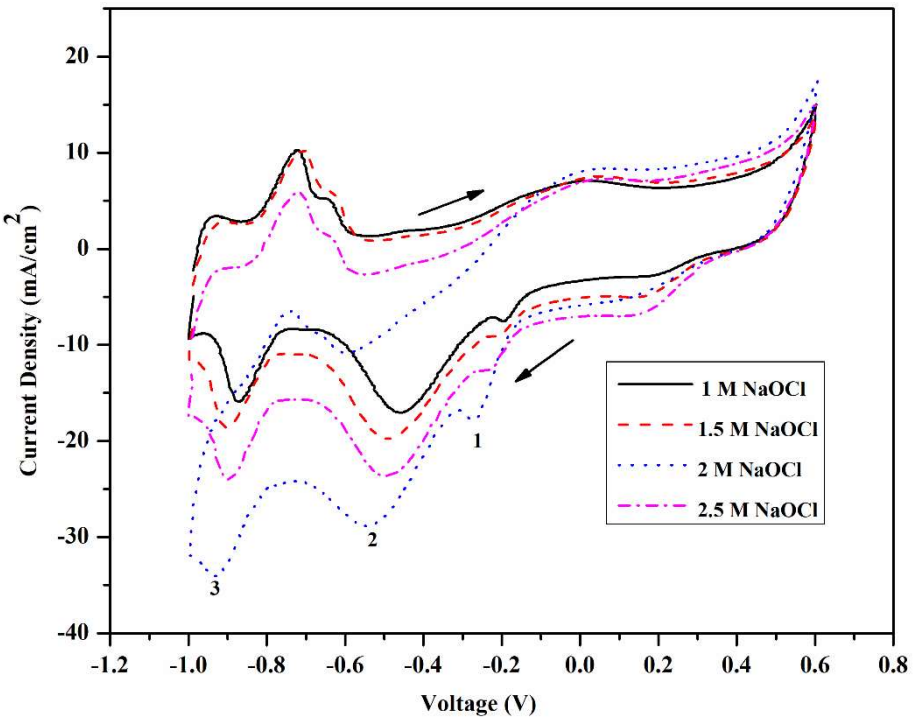

Figure 5.35 Cyclic voltammetry for different concentration of NaOCl mixed in 1 M NaOH solution using 2 mg/cm^2 Pt/C electrocatalyst at scan rate of 50 mV/s.

Table 5.17 Voltage and current density of the reduction peaks at different NaOCl concentration.

NaOCl concentration	**1 (M)**			**1.5 (M)**			**2 (M)**			**2.5 (M)**		
Reduction Peak	**1st peak**	**2nd peak**	**3rd peak**	**1st peak**	**2nd peak**	**3rd peak**	**1st peak**	**2nd peak**	**3rd peak**	**1st peak**	**2nd peak**	**3rd peak**
Voltage (V)	-0.194	-0.460	-0.871	-0.207	-0.481	-0.899	-0.269	-0.541	-0.930	-0.225	-0.497	-0.896
Current density (mA/cm^2)	7.3	17.1	15.8	9.0	19.8	18.4	17.5	28.7	33.5	12.6	23.7	23.7

5.2.3.2 Chronoamperometry

The chronoamperometry test of the electrocatalyst Pt/C (2 mg/cm^2) was done in the solution prepared by 2 M NaOCl mixed in 1 M NaOH solution. The CA test was done to study the stability loss under certain test conditions. The main purpose of this study is see if there is rapid catalyst poisoning for electrochemical reduction in the sodium hypochlorite solution. **Figure 5.36** shows the chronoamperometry tests for the electrochemical reduction of 2 M NaOCl solution mixed in 1 M NaOH on the surface of the Pt/C electrocatalyst having loading of 2 mg/cm^2 at different potential.

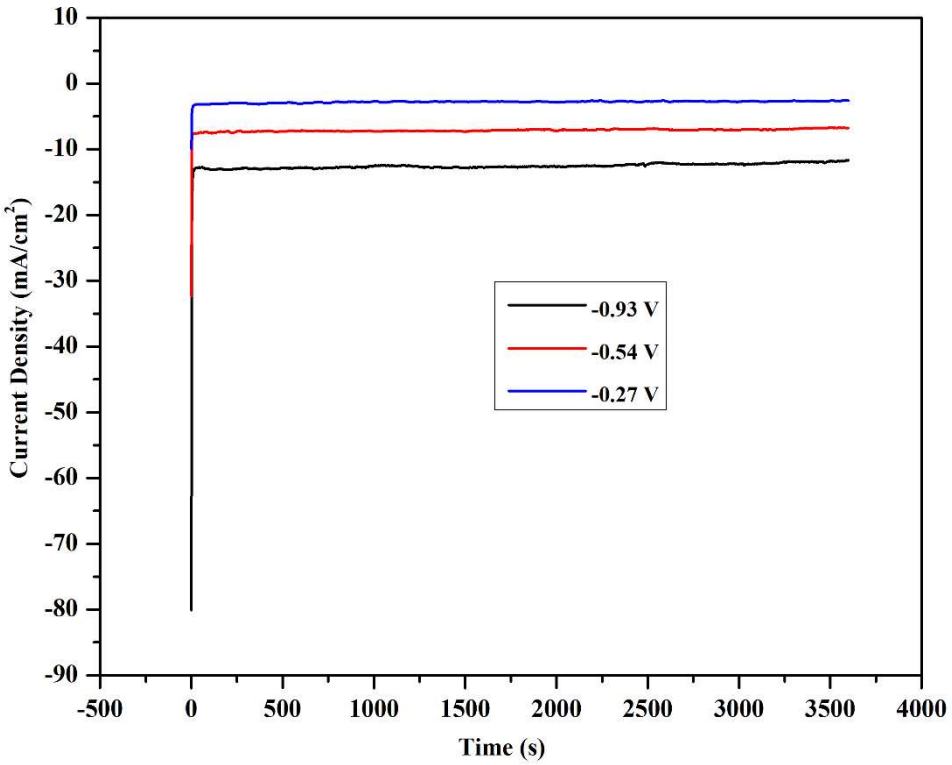

Figure 5.36 Chronoamperometry test for the electrochemical reduction of 2 M NaOCl solution mixed in 1 M NaOH on the surface of Pt/C (2 mg/cm^2) electrocatalyst at -0.93 V vs. Ag/AgCl, -0.54 V vs. Ag/AgCl and -0.27 V vs. Ag/AgCl at room temperature 30 ^{o}C.

The reference potential of -0.93 V, -0.54 V and -0.27 V for chronoamperometry test were obtained from CV results (**Figure 5.35**). It is observed from **Figure 5.36** that the current for electrochemical reduction of sodium hypochlorite decreases rapidly and then became stable. The diffusional effects are the main reason for the sudden drop in current. The Pt/C electrocatalyst demonstrate the quite stable characteristic for electrochemical reduction in alkaline sodium hypochlorite solution which can be seen by stable current generation during the chronoamperometry test (**Figure 5.36**). It can also be seen from **Figure 5.36** that the current density for electrochemical reduction of the alkaline sodium hypochlorite was highest at the lower potential of -0.93 V.

5.2.3.3 Single cell studies

5.2.3.3.1 Effect of NaOCl concentration

Figure 5.37 shows the polarization and power density curve of the DSBFC using alkaline $NaBH_4$ of 1 M $NaBH_4$ mixed in 4 M NaOH as fuel at anode and alkaline NaOCl as oxidant of various concentration at cathode. The NaOH doped physically crosslinked PVA-TEOS membrane was used as solid electrolyte for the transport of ions from cathode to anode side. The Pt/C of 1 mg/cm^2 was used as the anode side and the electrocatalyst loading 2 mg/cm^2 was used as cathode side. The power density curve and polarization curve were shifted upward when the NaOCl concentration was increased from 0.5 M to 2 M NaOCl. Further increase in the NaOCl concentration to 2.5 M, the decrease in the performance of the DSBFC was observed in terms of power density. The maximum power density of 58.80 mW/cm^2 at current density of 120 mA/cm^2 was obtained for the 2 M NaOCl concentration.

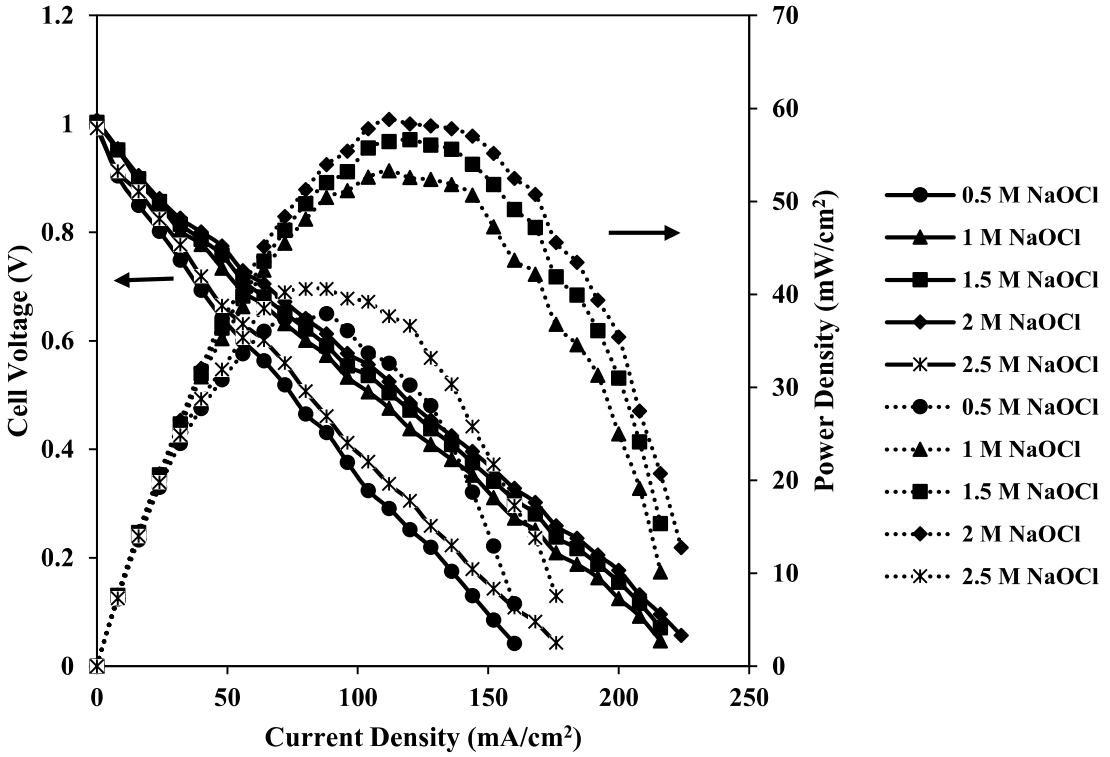

Figure 5.37 Polarization and power density curve of the DSBFC using various concentration of NaOCl mixed in 1 M NaOH to the cathode side at fixed anode and cathode loading of 1mg/cm^2 and 2 mg/cm^2; Anode flow rate 3 ml/min and cathode flow rate 4 ml/min: cell temperature 30 ^{o}C; Solid line – Polarization curves; Dotted line – Power density curves.

Table 5.18 Maximum power density and corresponding current density with varying concentration of the oxidant (NaOCl) mixed in 1 M NaOH solution at the cell temperature of 30 ^{o}C.

NaOCl Concentration	**0.5 M**	**1 M**	**1.5 M**	**2 M**	**2.5 M**
Maximum Power Density (mW/cm^2)	37.92	53.31	56.64	58.80	40.56
Current density at maximum power density (mA/cm^2)	88	112	120	112	80

However, the lower power density of 40.56 mW/cm^2 at current density of 80 mA/cm^2 was obtained for 2.5 M NaOCl concentration. The maximum power density of 37.92 mW/cm^2, 53.31 mW/cm^2 and 56.62 mW/cm^2 were obtained for the NaOCl concentration of 0.5 M, 1 M and 1.5 M, respectively (**Table 5.18**). The improvement in the cell performance on increasing the NaOCl concentration is due to the improve in the cathode reaction kinetics. The decrease in the performance in terms of power density at higher concentration (2.5 M) may be due to less availability of water molecule at active catalyst site (You et al. 2006, Yadav and Pramanik 2024b). It should be noted that CV studies (**Figure 5.35**) also showed the highest peak current density at the NaOCl concentration of 2 M.

5.2.3.3.2 Effect of temperature on the DSBFC performance

The effect of the cell temperature on the DSBFC was investigated keeping the all other cell condition at their optimum values. It is seen from **Figure 5.38**, the performance of the DSBFC improves with increase in cell temperature upto 60 ^{o}C where increase in cell temperature, the polarization and curve and power density curve shifted upward (**Figure 5.38**). The maximum power density of 69.44 mW/cm^2 was obtained for the cell temperature 60 ^{o}C (**Table 5.19**). Whereas, the highest temperature of 70 ^{o}C produced lower peak power density of 60.28 mW/cm^2. It is commonly known that the electrode reaction kinetics increases with the increasing cell temperature, and thus, cell current density increases. Furthermore, when the temperature rises, the activation loss at the electrode decreases. Moreover, the anolyte viscosity also reduces, resulting in better ionic mobility at elevated temperatures. As a result, the ohmic loss is reduced and electrolyte conductivity is increased. The performance of the DSBFC decreases beyond 60 ^{o}C in terms of power density. The decrease in the power density at a very high temperature of 70 oC

may be due to decomposition of $NaBH_4$ (Cao et al. 2009) at the anode and NaOCl at the cathode (Kim et al. 2016), reducing the fuel and oxidant efficiency. Furthermore, borohydride crossover and borohydride hydrolysis occur at high temperatures (Cheng et al. 2006b). As a result, the optimal cell temperature of 60 ^oC was determined for the best cell performance in terms of power density.

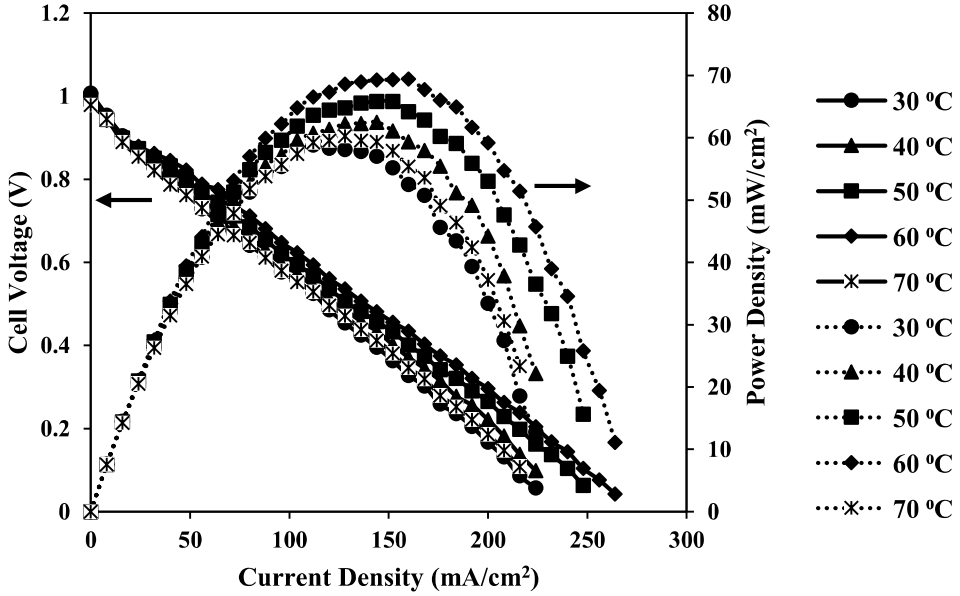

Figure 5.38 The polarization and power density curve of DSBFC using 2 M NaOCl mixed in 1 M NaOH for varying cell temperature at the fixed fuel and oxidant flow rate of 3 ml/min and 4 ml/min; Solid line – Polarization curves; Dotted line – Power density curves.

Table 5.19 Maximum power density and corresponding current density with varying cell temperature.

Cell Temperature (oC)	**30**	**40**	**50**	**60**	**70**
Maximum power density (mW/cm^2)	58.80	62.49	65.81	69.44	60.28
Current density at maximum power density (mA/cm^2)	112	144	152	160	128

5.2.4 Optimization of process parameter via RSM

5.2.4.1 Anova analysis and model development

Table 5.20 represents the various set of 17 experimental results of response variable (maximum power density) as suggested by BBD model. The experimentally determined power density are close enough to the predicted value derived from the model. The closeness of the experimental and predicted values of power density validates the reliability of RSM model. The maximum power density of 66.96 mW/cm^2 was achieved when DSBFC was operated with TEOS loading of 10 wt. %, NaOH doping concentration of 4 M and freeze-thaw cycle of 7 (**Table 5.20**, 4^{th} Run). However, the lowest power density of 28.66 mW/cm^2 was achieved at TEOS loading of 15 wt. %, NaOH doping concentration of 2 M and freeze-thaw cycle of 7 (**Table 5.20**, 5^{th} Run). **Table 5.21** presents the results of the statistical analysis conducted on the power density of the glycerol electrooxidation reaction. This analysis was performed using the quadratic model and the analysis of variance (ANOVA) technique. The sum of squared represents the deviation of the data values from the mean. On the other hand, Df represents the degree of freedom for the model, which is determined by the number of model terms and intercepts minus one. The mean square is calculated as the ratio of the sum of squares divided by the degrees of freedom, and it serves as an estimation of the variance of the model. On the basis of the values of two parameters, namely F-value and P-value, the significance of each independent variable to the response is assessed. The F-value for each term is a statistical test used to assess the relationship between the variance associated with the term in question and the residual variance.

Tabe 5.20 BBD arrangement of the DSBFC using three independent variables and corresponding predited and experimental response value.

Run	Freeze-thaw cycle	NaOH doping concentration (M)	TEOS loading (wt. %)	Power density (mW/cm^2)	
				Actual/Experimental value	Predicted value
1	5	4	5	53.37	53.00
2	9	6	10	47.18	46.80
3	7	6	15	41.98	42.30
4	7	4	10	66.96	66.46
5	7	2	15	28.66	28.19
6	7	4	10	66.23	66.46
7	9	4	5	43.18	43.39
8	7	4	10	66.1	66.46
9	5	6	10	53.12	53.02
10	9	2	10	30.91	31.01
11	5	2	10	35.98	36.66
12	7	4	10	66.42	66.46
13	7	6	5	50.26	50.73
14	5	4	15	43.07	42.86
15	7	4	10	66.58	66.46
16	7	2	5	33.01	32.70
17	9	4	15	40.23	40.60

It is the ratio of the mean squares for the term and residual. The regression model, model coefficient, and lack of fit were tested using the ANOVA (**Table 5.21**). The obtained p-value for this model is less than 0.0001, indicating a high level of statistical significance. Additionally, the higher F value of 946.66, further supports the significance of the model. The quadratic model is selected based on its significantly low P-value, high value of F, and a difference of less than 0.2 between the adjusted R^2 and predicted R^2 for the quadratic model. The R^2 value plays a crucial role in determining the effectiveness of the model. A value beyond 0.75 indicates that the model exhibits strong and satisfactory performance (Panjiara and Pramanik, 2020a). The variance analysis conducted on **Table 5.21** revealed that the estimated values for R^2 and adjusted R^2 were

0.9992 and 0.9981, respectively. The model exhibiting a low standard deviation (SD) of 0.59 and a regression coefficient R^2 of 0.9992, which is in close proximity to unity, suggests that the projected power density values were precise and closely aligned with the actual data. The R^2 value of 0.9992 also indicates that the experimental variables account for 99.92% of the total power density variation and that there is a high correlation between the experimental data and the model anticipated ones. The term "Adeq Precision" refers to the signal-to-noise ratio, and a value greater than 4 is generally required. The "Adeq Precision" value of 84.181 in the current investigation demonstrates satisfactory precision. Furthermore, the decreased coefficient of variation (CV% = 1.19) indicates to the quality of the experimental design.

The other term for this model is referred to as "lack of fit," which is characterized by a p-value greater than 0.05, indicating ‘Not singnificant’. The implication of the suggested model is that it aligns well with the experimental data. Additionally, it suggests that the independent variables have significant impacts on the dependent variable (power density) of DSBFC. Additionally, it is beneficial to comprehend the relationship between the dependent variable and the independent variable (Choudhary and Pramanik, 2021). It is seen from **Table 5.21** that the P-value of the linear term A, B and C is less than 0.05 which indicates the great impact of these variable on the power density of DSBFC. The P-value for the interaction terms AC and BC was found to be less than 0.05, indicating a statistically significant influence of these interaction factors on the power density. In contrast, the P-value for the interaction factor AB was determined to be 0.6414, exceeding the significance level of 0.05. The statistical significance of the quadratic terms (A^2, B^2, and C^2) is indicated by the P-values less than 0.05. This suggests that there is a non-linear

association between each variable and the power density. The F-values for the significant terms A, B, and C in the regression models are 205.32, 1505.31, and 244.01, respectively.

Table 5.21 The response surface second order model of the ANOVA analysis.

Source	**Sum of squares**	**Degree of freedom (Df)**	**Mean squares**	**F-value**	**P-value (Prob > F)**	**Remark**
Model	2923.30	9	324.81	946.66	< 0.0001	significant
A-Freeze-Thaw cycle	70.45	1	70.45	205.32	< 0.0001	
B-NaOH doping concentration	516.49	1	516.49	1505.31	< 0.0001	
C-TEOS loading	83.72	1	83.72	244.01	< 0.0001	
AB	0.081	1	0.081	0.24	0.6414	
AC	13.51	1	13.51	39.36	0.0004	
BC	3.86	1	3.86	11.25	0.0122	
A^2	344.87	1	344.87	1005.13	< 0.0001	
B^2	1016.19	1	1016.19	2961.68	< 0.0001	
C^2	652.14	1	652.14	1900.68	< 0.0001	
Residual	2.40	7	0.34			
Lack of fit	1.95	3	0.65	5.81	0.0612	Not significant
Pure Error	0.45	4	0.11			
Correlation Total	2925.70	16				
SD	0.59					
Mean	49.03					
CV%	1.19					
R^2	0.9992					
Adjusted R^2	0.9981					
Predicted R^2	0.9891					
Adeq. precision	84.181					

The power density of the direct sodium borohydride fuel cell (DSBFC) is influenced by three factors, namely factors A, B, and C. In terms of their impact on the response, it can be observed that factor B has the greatest influence, followed by factor C, and then factor A. Additionally,

when considering the interaction terms, it is found that the interaction between factors A and C (i.e., AC) has a greater influence on the response compared to the interaction between factors B and C (i.e., BC), and the interaction between factors A and B (i.e., AB). The second order regression model equation in terms of actual factor which can be used to find maximum power density of DSBFC by relating dependent variable and independent variable are given below:

$$\text{Power density (Y)} = -147.6098 + 28.497\text{A} + 36.319\text{B} + 8.415\text{C}$$

$$-0.035\text{AB} + 0.183\text{AC} - 0.098\text{BC} - 2.262\text{A}^2 - 3.883\text{B}^2 - 0.497\text{C}^2 \qquad (5.2)$$

Where A, B and C denotes the freeze-thaw cycle, NaOH doping concentration and TEOS loading, respectively. In Equation 5.2, a positive sign preceding the term implies that the influence of the term is in favour of the response. Conversely, a negative sign indicates an adeverse impact on the response. It can be seen from Equation 5.2 that the terms A, B, C, AC have the positive effect on the power density as it has positive coefficient, while the terms AB, BC, A^2, B^2, C^2 have a negative effect on the power density of DSBFC as it has negative coefficient.

Figure 5.39 shows the graph of actual (experimental) vs predicted power density of the RSM model for the direct sodium borohydride fuel cell (DSBFC). The straight line shows the predicted power density by the model and coloured points indicate the experimental value of the power density for DSBFC. The red colour is the indication of the highest power density, while the blue colour is the indication of the lowest power density. It is seen from **Figure 5.39** that the experimental values are very close to the predicted values as given by the model. In the present model, the correlation coefficient (R^2) for the DSBFC power density is determined to be 0.9992.

This high number suggests a strong agreement between the predicted value obtained by the Response Surface Methodology (RSM) and the experimental data.

$$R^2 = 0.9992$$

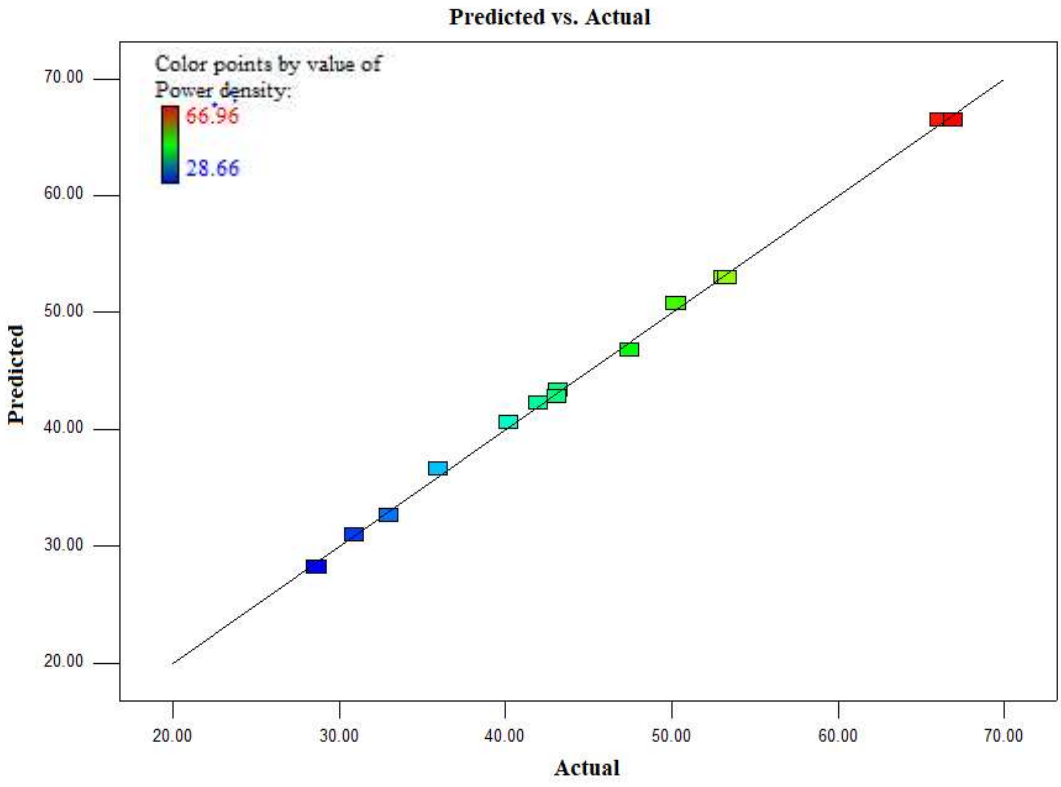

Figure 5.39 Actual vs predicted power density of the RSM model for DSBFC.

Figure 5.40 depicting the relationship between residuals and predicted power density values, provides insight into the accuracy of model prediction. The scattering of the studentized residuals over the displayed area and the fact that no one value deviates significantly from the x-axis red line indicate a continuous range of residuals across the graph. The value of each residual point

exhibits minor variations along the x-axis and the slight fluctuation confirms the constant variance assumptions.

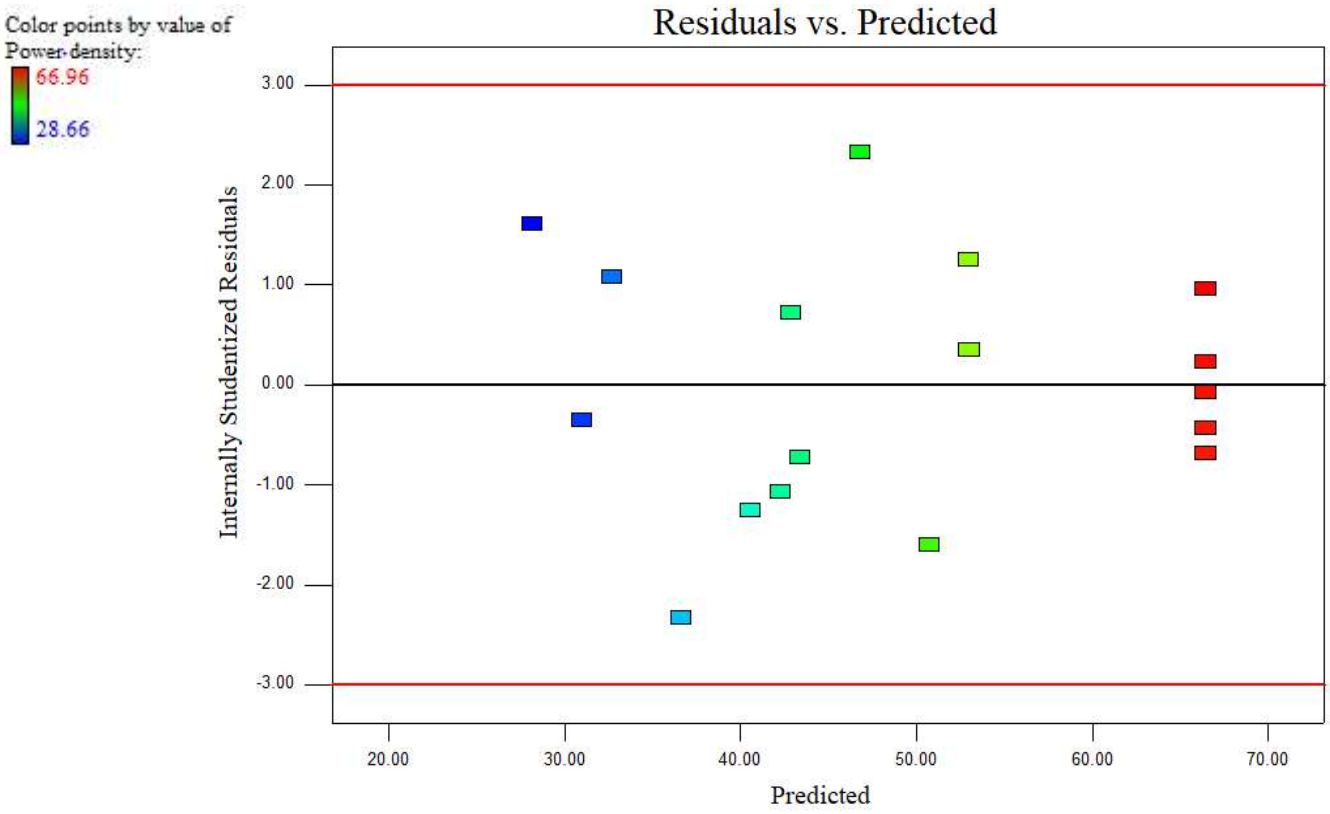

Figure 5.40 The residual vs predicted power density of the RSM model for DSBFC.

5.2.4.2 Effect of various parameter and its optimization

The effect of various parameter i.e., freeze-thaw cycle (A), NaOH doping concentration (B) and TEOS loading (C) was examined and determined their optimized value. The two-dimensional contour plot and three-dimensional plot of the power density of DSBFC as fuction of two independent variables keeping the other third variable fixed were plotted and studied. An infinite number of the grouping of two independent variables while keeping others fixed are represented by three-dimensional plot. The graphical representation between power density (response) and the

independent process variables is generated by second-order polynomial regression Equation 4.2. The values of the power density are shown by the different color codes on the three-dimensional plots.

5.2.4.2.1 Combined effect of freeze-thaw cycle and NaOH doping concentration

Figure 5.41 shows the effect of the membrane synthesis variables freeze-thaw cycle (A) and NaOH doping (B) on the response i.e., power density of DSBFC, keeping TEOS loading fixed. The two-dimensional contour plot and three-dimensional contour plot generated by RSM for the combined effect of A and B on the response, are shown in **Figure 5.41**a and **Figure 5.41**b, respectively. The other operating parameters of DSBFC like, $NaBH_4$ concentration, anode loading, cathode loading were fixed at the optimum values which were obtained from experiment.The fuel supplied was 1 M $NaBH_4$ mixed in 4 M NaOH at the anode side and pure oxygen was supplied at the cathode side. The anode and cathode electrocatalyst loading were 1 mg/cm^2 and 2 mg/cm^2, respectively. The DSBFC was operated at a room temperature of 30 ^oC. The freeze-thaw cycle was varied from 5 cycles to 9 cycles. The NaOH doping concentration was varied from 2 M to 6 M. It was observed that the DSBFC performance in terms of power density increases as the freeze-thaw cycle is increased from 5 cycles to 7 cycles. Beyond 6.86 (≈ 7) cycles, the power density goes down. The initial increase in power density upto 6.86 (≈ 7) cycles may be due to an increase in the amorphous nature of the membrane resulted from the high interaction between PVA and TEOS, which eventually increases the ionic conductivity of the PVA-TEOS membrane electrolyte and, hence, the power density of the DSBFC (Yadav and Pramanik 2024a).

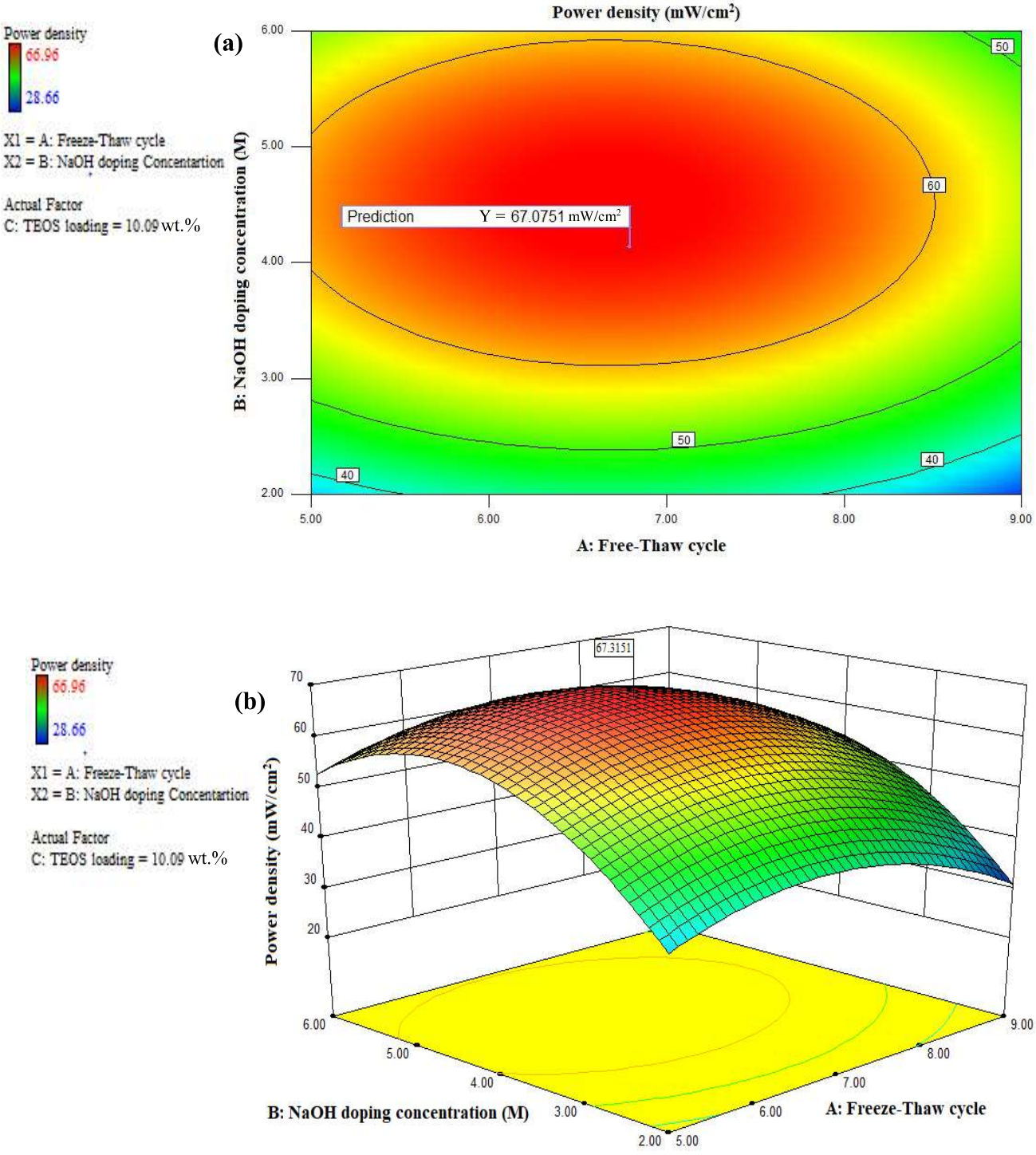

Figure 5.41 The effect of freeze-thaw cycle and NaOH doping concentration on the power density of DSBFC at fixed TEOS loading of 10.09 wt. % are shown in (a) two dimensional contour plot (b) three dimensional contour plot.

The power density of the DSBFC decreases at a high freeze-thaw cycle due to high crosslinking between PVA and TEOS, which led to a decrease in water uptake, NaOH uptake and eventually ionic conductivity (Yadav and Pramanik 2024a).

It was also found that the power density of DSBFC gets affected by NaOH doping concentration of the membrane electrolyte. The presence of hydroxyl ion is essential for the ionic conductivity of the PVA-TEOS membrane electrolyte. The PVA-TEOS membrane was immersed in the NaOH solution for 24 h to make it OH^- conducting. The concentration of NaOH doping within the membrane matrix is an important parameter which greatly affects the ionic conductivity of the membrane electrolyte. The NaOH doping concentration was varied from 2 M to 6 M. The power density of DSBFC increases as the NaOH doping concentration increases from 2 M to 4.25 M. Beyond 4.25 M, the power density starts decreasing. The ionic conductivity of the PVA-TEOS membrane electrolyte increases as the NaOH doping concentration increases from 2 M to 4 M (Yadav and Pramanik 2023), which may lead to an increase in the power density of the DSBFC. The increase in the ionic conductivity of the membrane electrolyte may be due to an increase in NaOH uptake. The ionic conductivity of the PVA-TEOS membrane electrolyte falls at higher concentrations of NaOH doping (i.e., beyond 4.25 M). This decrease in ionic conductivity may be attributed to a reduction in water uptake (Gupta and Pramanik 2019a, Yadav and Pramanik 2023). The higher ionic conductivity of the membrane electrolyte is favoured by the intricate balance between water and NaOH in the membrane electrolyte matrix (Kim et al. 2004). The lower ionic conductivity at higher NaOH doping concentration may lead to a decrease in the power density of the direct sodium borohydride fuel cell. The optimum doping concentration of 4.25 M NaOH and 6.86 (≈ 7) cycle of freeze-thaw operation resulting in highest power density of 67.731 mW/cm^2.

The red colour area in **Figure 5.41**a and in **Figure 5.41**b is the area of the optimum value of independent variable i.e., freeze-thaw cycle and the NaOH doping concentration which resulted in optimum power density.

5.2.4.2.2 Combined effect of TEOS loading and freeze-thaw cycle

The effect of TEOS loading (C) and freeze-thaw cycle (A) on the maximum power density of the DSBFC at fixed and optimum NaOH doping concentration of 4.25 M are illustrated by two-dimensional plot and three-dimensional plot in **Figure 5.42**a and **Figure 5.42**b, respectively. The TEOS loading was varied from 5 wt. % to 15 wt. % and freeze-thaw cycle was varied from 5 to 9 cycles. It is seen from **Figure 5.42**a and **Figure 5.42**b that the power density increases as the TEOS loading increases from 5 wt. % to 10.09 wt. % and freeze-thaw cycle from 5 to 6.86 (≈ 7) at fixed NaOH doping concentration of 4.25 M. The increase in power density is indicated by enhancement in the red zone as the TEOS loading increases from 5 wt. % to 10.09 wt. % at fixed NaOH doping concentration of 4.25 M. The power density of the DSBFC starts to decrease beyond 10.09 wt. % of TEOS loading as indicated by the change in zone colour from red to green in **Figure 5.42**a and **Figure 5.42**b. It is seen from the published literature that the power density increases due to the increase in the ionic conductivity of the membrane electrolyte when the TEOS loading is increased (Gupta and Pramanik 2019a, Yang et al. 2011, Das et al. 2015). The improve in the ionic conductivity of the membrane electrolyte is promoted by increase in water uptake and NaOH uptake (Das et al. 2015). The water uptake of the PVA-TEOS membrane electrolyte is enhanced by the hygroscopic properties of TEOS. Additionally, the NaOH uptake is increased due to NaOH retaing ability of TEOS (Yang et al. 2011).

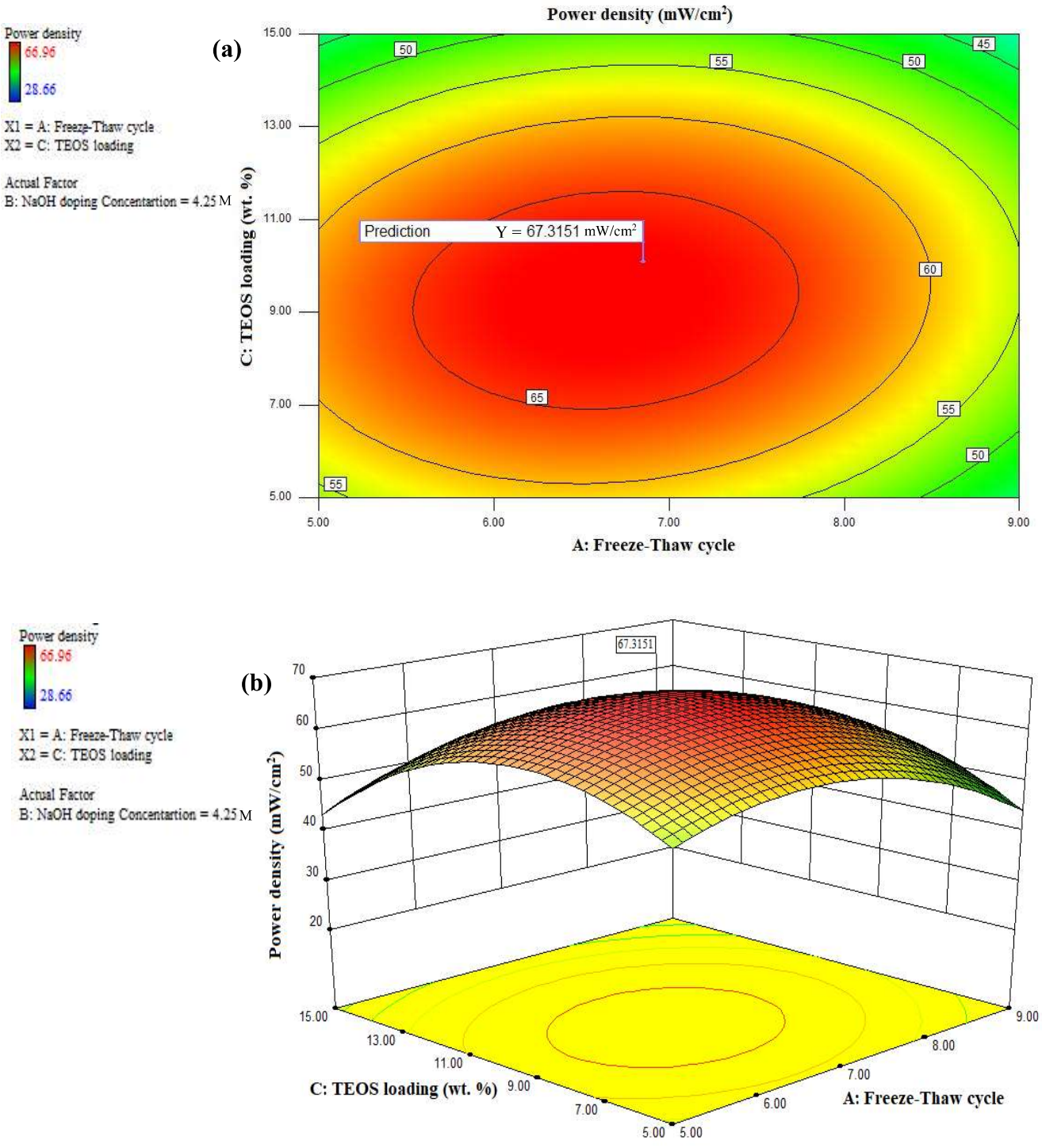

Figure 5.42 The effect of TEOS loading and freeze-thaw cycle on the power density of DSBFC at fixed NaOH dopig concentration of 4.25 M are shown in (a) two dimensional contour plot (b) three dimensional contour plot.

However, at very high TEOS loading i.e., beyond 10.06 wt. %, the power density of the DSBFC decreases due to decrease in water uptke, NaOH uptake and thus, the ionic conductivity of the PVA-TEOS membrane electrolyte. At higher TEOS loading, the degree of crosslinking between PVA and TEOS is significantly increased, resulting in a more compact membrane structure. Consequently, this leads to a reduction in both water uptake and NaOH uptake (Yang et al. 2011). The similar effect of freeze-thaw cycle on the DSBFC performance as discussed earlier in the previous **section 5.2.4.2.1** was observed when freeze-thaw cycle was varied from 5 to 9 cycle. The optimum value of 10.09 wt. % and 6.86 (≈ 7) cycle produced highest power density of 67.731 mW/cm^2.

5.2.4.2.3 Combined effect of NaOH doping concentration and TEOS loading

The two-dimensional and three-dimensional RSM plots of the effect of NaOH doping concentration and TEOS loading on the power density of the DSBFC with the fixed optimum freeze-thaw cycle of 6.86 (≈ 7) are shown in **Figure 5.43**a and **Figure 5.43**b, respectively. The NaOH doping concentration was varied from 2 M to 6 M and TEOS loading was varied from 5 wt. % to 15 wt. %. It is seen from **Figure 5.43**a and **Figure 5.43**b that the power density of DSBFC increases as the NaOH doping concentration increases from 2 M to 4.25 M. The power density starts decreasing beyond 4.25 M. The reason for the increase in the power density upto 4.25 M NaOH doping concentration and then further reduction in power density beyond 4.25 M, is already discussed in the previous **section 5.2.4.2.1** (page no. 167). The effect of TEOS loading on the DSBFC was similar as discussed earlier in the **section 5.2.4.2.2** (page no.170).

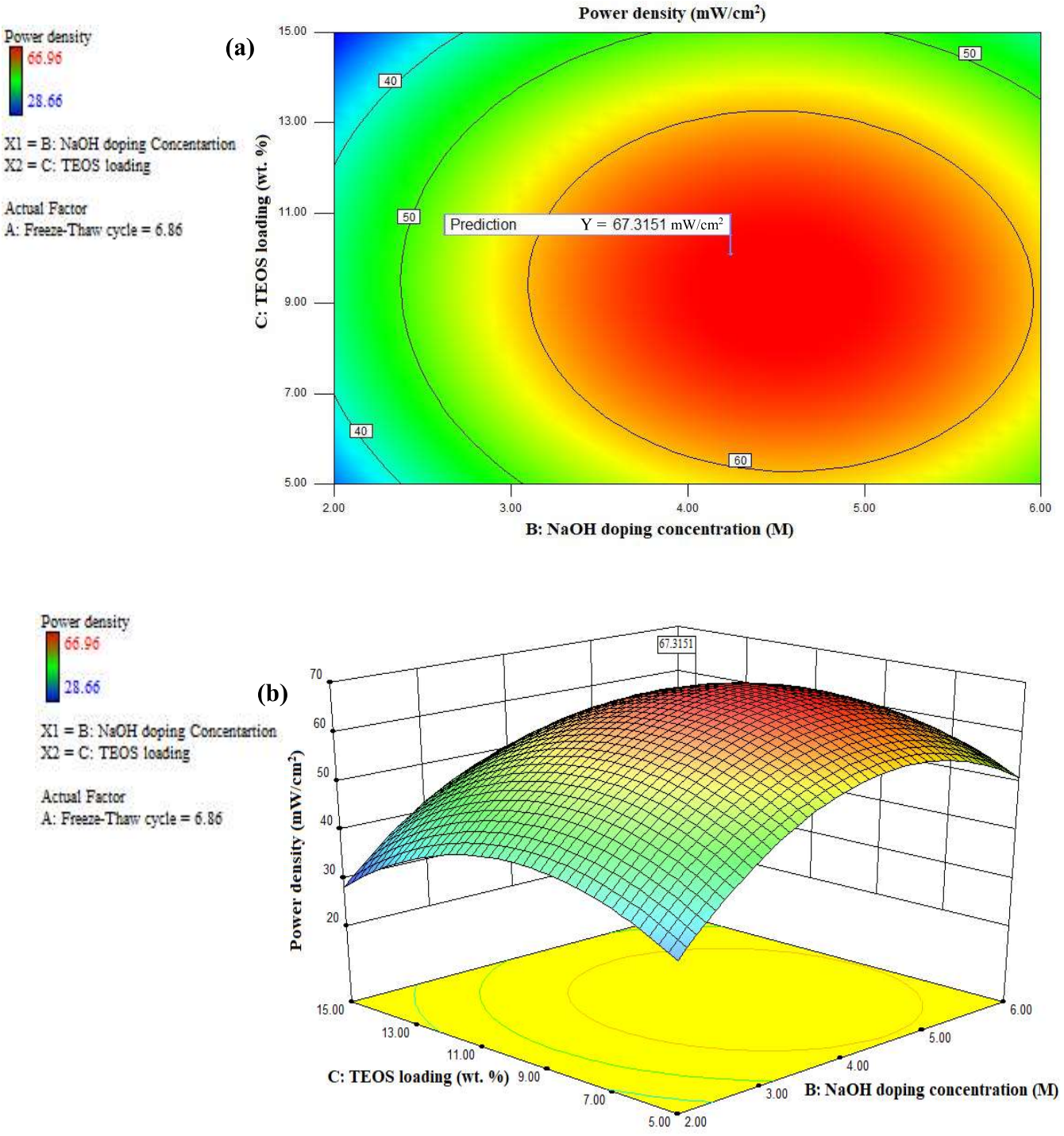

Figure 5.43 The effect of NaOH doping concentration and TEOS loading on the power density of DSBFC at a fixed freeze-thaw cycle of 6.86 (≈ 7) are shown in (a) two-dimensional contour plot (b) three-dimensional contour plot.

The red zone depicted in **Figure 5.43**a and **Figure 5.43**b of the RSM plot represents the maximum power density achieved when the DSBFC is operated at the optimum dping concentration of 4.25 M and optimum TEOS loading of 10.09 wt. %. This optimum value is observed when the freeze-thaw cycle is fixed at around 6.86 (≈ 7).

5.2.4.2.4 Verification of the model

The effective parameters to synthesize the PVA-TEOS membrane electrolyte was optimized to achieve the highest power density from the direct sodium borohydride fuel cell. The effective parameters of the PVA-TEOS membrane electrolyte were the the freeze-thaw cycle (A), NaOH doping concentration (B) and TEOS loading (C). The perturbation graph (**Figure 5.44**) demonstrates the effect of a single variable on the response value power density while keeping all other variables constant. The optimum parameters for achieving the highest power density from the direct sodium borohydride fuel cell (DSBFC) using RSM Design Expert 7.0 are presented in **Figure 5.44**. The optimum value of the freeze-thaw cycle, NaOH doping concentration and TEOS loading were 6.86 (≈ 7), 4.25 M and 10.09 wt. %, respectively. The highest power density predicted by RSM Design Expert 7.0, corresponding to the optimum value of the independent variable, was 67.31 mW/cm^2.

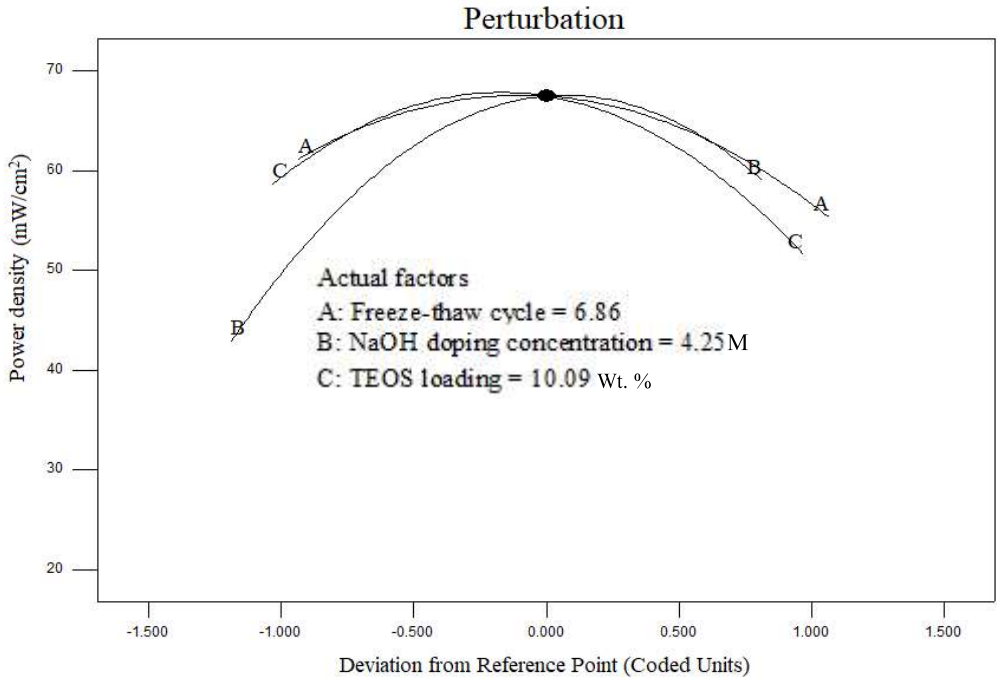

Figure 5.44 Detection of the optimum point from the perturbation curve for the maximum power density of DSBFC.

To validate the predicted outcomes of the model, three further confirmation experiments were conducted using the predicted optimum condition on the same DSBFC setup. **Table 5.22** and **Figure 5.45** show the final outcomes of these tests. **Table 5.22** shows that there is no substantial difference between the highest power density observed in the experimental results and the power density predicted for the DSBFC. An error of 1.51 % was found, lying below the acceptable range of 5 %. This observation supports the notion that the model projection is accurate enough within the 95% prediction interval.

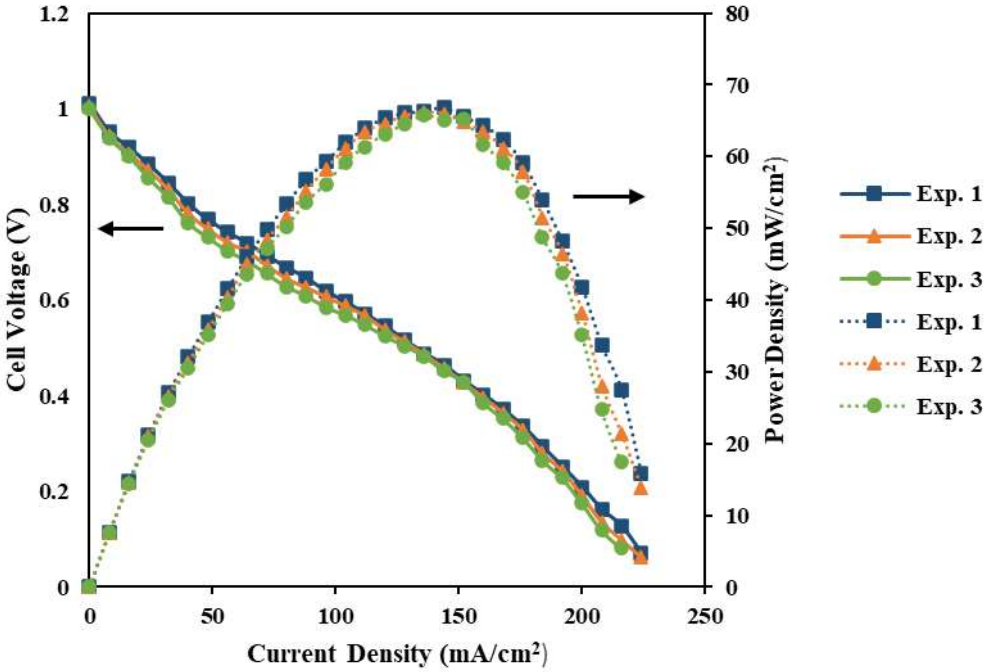

Figure 5.45 Polarization and power density curve of three repeated experiments of the DSBFC at optimum parameter conditions predicted by the RSM model.

Table 5.22 Validation test results utilizing optimum independent variable values for the developed second-order equation of the RSM model.

Procees Parameter			**Power density (mW/cm²)**					
Freeze-thaw cycle	**NaOH doping concentration (M)**	**TEOS Loading (wt. %)**	**Model predicted**	**Run 1**	**Run 2**	**Run 3**	**Avg.**	**Error (%)**
6.86 (≈ 7)	4.25	10.09	67.31	66.81	66.09	65.98	66.29	1.51

The three sets of another random condition of the independent variable were also selected to validate the developed RSM model. The predicted values of the power density of the DSBFC were calculated using the established second-order equation (Equation 5.2) and the experimental values of the power density for the same set of random independent variables were obtained from direct

sodium borohydride fuel cell operation (DSBFC). The selected three sets of random conditions are Random condition 1- Freeze-thaw cycle of 7, NaOH doping concentration of 4 M and TEOS loading of 15 wt. %; Random condition 2- Freeze-thaw cycle of 5, NaOH doping concentration of 6 M and TEOS loading of 5 wt. % and Random condition 3- Freeze-thaw cycle of 9, NaOH doping concentration of 6 M and TEOS loading of 5 wt. %. The predicted power density (Response, i.e., Y) of the DSBFC using Random condition 1, Random condition 2 and Random condition 3 were 50.77 mW/cm^2, 46.62 mW/cm^2 and 36.73 mW/cm^2, respectively (**Table 5.23**). **Figure 5.46** represents the polarization and the power density curve of the DSBFC using Random condition 1, Random condition 2 and Random condition 3. The experimental values of the maximum power density for the DSBFC using Ranndom condition 1, Random condition 2 and Random condition 3 were 49.98 mW/cm^2, 45.93 mW/cm^2 and 36.18 mW/cm^2, respectively (**Table 5.23**). The difference between experimental power density and the predicted power density of the DSBFC using the three selected random conditions was found to be minute. The percentage error of the power density were found to be in acceptable range of 1.42 % to 1.56 %. Thus, it can be concluded from the above results that Equation 5.2 obtained from the developed RSM model is well acceptable and it can be used to determine the power density of the DSBFC.

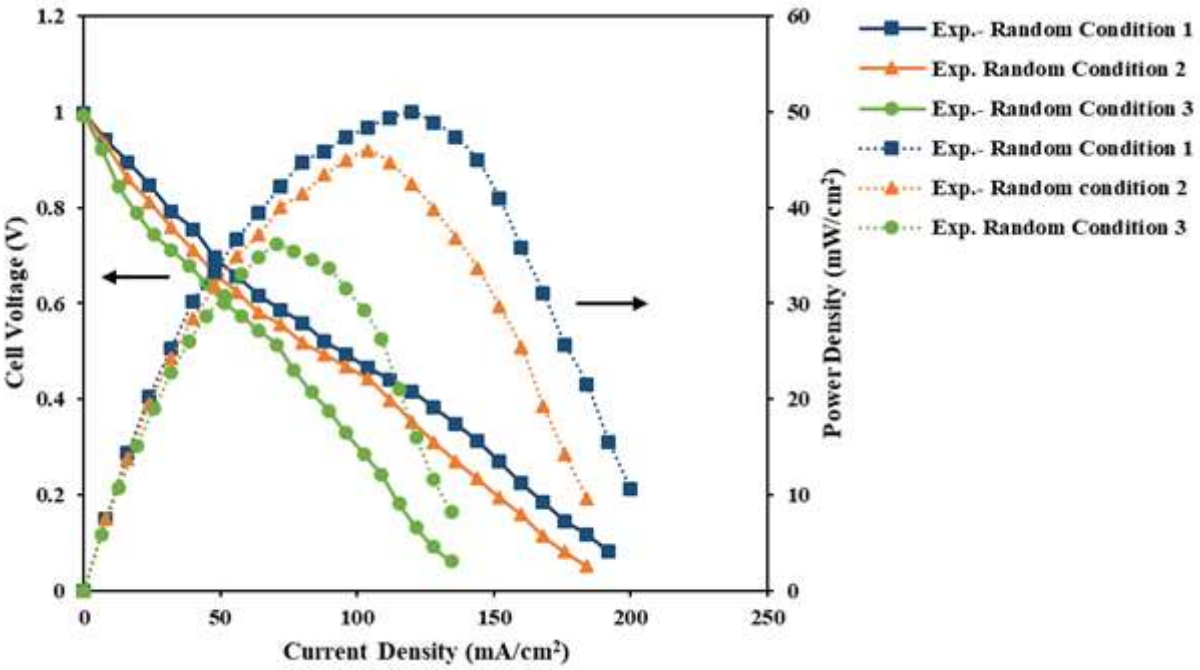

Figure 5.46 Polarization and power density curve of the DSBFC at three different random conditions experiment, i.e., Random condition 1- freeze-thaw cycle- 7, NaOH doping concentration - 4 M and TEOS loading- 15 wt. %; Random condition 2- freeze-thaw cycle-5, NaOH doping concentration-6 M and TEOS loading- 5 wt. %; Random condition 3- freeze-thaw cycle-9, NaOH doping concentration-2 M and TEOS loading- 5wt. %.

Table 5.23 The predicted and experimental power density of DSBFC for the three random condition.

Parameters	Free-Thaw Cycle	NaOH doping Concentration (M)	TEOS loading (wt.%)	Predicted Power Density (Y) (mW/cm^2)	Experimental Power Density (mW/cm^2)	Error (%)
Random Condition-1	7	4	15	50.77	49.98	1.56
Random Condition-2	5	6	5	46.62	45.96	1.42
Random Condition-3	9	6	5	36.73	36.18	1.49

5.2.5 Comparison of the present DSBFC with other reported work

The performance of the best synthesized membrane electrolyte i.e., $PT_{10wt.\%}$-7Cy-(4M) of the present study, is compared with the previously reported research work on the direct sodium borohydride fuel cell (**Table 5.24**). It was found that the performance of the synthesized membrane electrolyte $PT_{10wt.\%}$-7Cy-(4M) in the present study was better than the previously reported many research works in terms of power density, as it is presented in **Table 5.24**. Akay et al. 2018 synthesized the NaOH doped PBI membrane electrolyte. The maximum power density of 38.5 mW/cm^2 was obtained at the cell temperature of 80 ^oC. The reported power density at the cell temperature of 80 ^oC is lower than the present study (85.19 mW/cm^2 at the cell temperature of 60 ^oC). Yang et al. 2008c synthesized the PVA/HAP membrane electrolyte for the application in direct sodium borohydride fuel cells and obtained the maximum power density of 45 mW/cm^2 at cell temperature of 25 ^oC. The Pt-Ru/Ni was used as an anode electrocatalyst and MnO_2/C was used as a cathode electrocatalyst. The power density reported by Yang et al. 2008c is lower than the present study (66.96 mW/cm^2 at 30 ^oC). Wang et al. 2023 reported the performance of alkaline poly (isatin-N-dimethyl piperidinium triphenyl) membrane electrolyte using 1 M $NaBH_4$ in 4 M NaOH as an anode stream and 5 M H_2O_2 in 1.5 M HCl solution as a cathode stream. The maximum power density of 75.5 mW/cm^2 was obtained at cell temperature of 20 ^oC. The electrocatalyst used for the anode and the cathode electrocatalyst was platinum foil (Gaossunion China) of 0.25 cm^2 surface area. The maximum power density reported by Wang et al. 2023 is higher than the present study may be due to the different oxidants and membrane electrolytes used in their study. Huang et al. 2013 reported the maximum power density of 92 mW/cm^2 for the membrane electrolyte PVA/CNT in DSBFC.

Table 5.24 Comparison of the performance of the synthesized membrane electrolyte with published literature in DSBFC.

Membrane electrolyte	**Fuel and oxidants**	**Electrocatalysts**	**Cell Temperature (ºC)**	**MPD** (mW/cm^2)	**References**
PBI-NaOH	**Fuel:** 4 wt.% $NaBH_4$ + NaOH(5 ml/min); **Oxidant:** O_2 (300 ml/min)	**Anode: Pt/C (**Loading: 2 mg/cm^2); **Cathode: Pt/C** (Loading: 1 mg/cm^2)	80	38.5	Akay et al. 2018
PVA/HAP	**Fuel**: 1 M $NaBH_4$ in 4 M NaOH; **Oxidant:** Air	**Anode:** Pt-Ru/Ni foam **Cathode:** MnO_2/C	25	45	Yang et al. 2008c
Poly (isatin-piperidium-terphenyl)	**Fuel:** 1 M $NaBH_4$ in 4M NaOH; **Oxidant**: 5 M H_2O_2 in 1.5 M HCl	**Anode:** Pt foil (0.25 cm^2 active surface area) **Cathode:** Pt foil (0.25 cm^2 active surface area)	20	75.5	Wang et al. 2023
PVA/CNT	**Fuel:** 1 M $NaBH_4$ + 4 M NaOH (130 ml/min); **Oxidant:** O_2 (100 ml/min)	**Anode:** Pt-Ru/C (Loading: 5 mg/cm^2) **Cathode:**Pt/C (Loading:5 mg/cm^2)	30	92	Huang et al. 2013
AEM (University of Cranfield, UK)	**Fuel:** 5 wt.% $NaBH_4$ in 6M NaOH; **Oxidant:** Air	**Anode:** Au (Loading: 0.8 mg/cm^2) **Cathode:**MnO_2	Room Temperature	28	Coowar et al. 2008
$PT_{10wt.\%}$-7Cy-(4M)	**Fuel:** 1 M $NaBh_4$ in 4 M NaOH; **Oxidant**: O_2	**Anode**: Pt/C (Loading: 1 mg/cm^2) **Cathode**: (2 mg/cm^2)	30	66.96	Present work
			60	85.19	

Abbrevations: MPD: Maximum power density; PBI: Polybezimidazole; HAP: Hydroxiapatite; CNT: carbon nanotube; AEM: Anion exchange membrane

The higher performance of the alkaline DSBFC may be due to very high electrode loading, i.e., 5 mg/cm^2, for both anode and cathode with a very high flow rate of fuel i.e., 130 ml/min. The support material for the electrocatalyst was multi-wall carbon nanotube which is having very high surface

area and is very expensive. Similarly, Coowar et al. 2008 used commercial AEM (University of Cranfield, UK) for electrooxidation study of $NaBH_4$ in a single DSBFC. The reported power density was lower (28 mW/cm^2) than the present study work operating at room temperature of 30 ^oC. Thus, it can be concluded that the present synthesized NaOH doped $PT_{10wt.\%}$-7Cy-(4M) is very promising for the direct sodium borohydride fuel cell. The simple freeze-thaw physical crosslinking method followed by NaOH doping was used for the preparation of the PVA-TEOS membrane electrolyte. The maximum power density obtained in the present work at the room temperature (30 ^oC) and little higher temperature (60 ^oC) were also better than that of many other previously reported research work (**Table 5.24**).

5.3 Efficiency of the direct sodium borohydride fuel cell (DSBFC)

The overall efficiency of the DSBFC depends on the various types of individual efficiencies which are calculated for overall efficiency of the fuel cell by multiplication of all the specific individual efficiency (Carrette et al. 2001). The efficiency of the DSBFC is calculated by the following equation (Equation 5.3):

$$\eta_{\mathrm{DSBFC}} = \eta_{\mathrm{r}} \times \eta_{\mathrm{V}} \times \eta_{\mathrm{F}} \times \eta_{\mathrm{U}} \times \eta_{\mathrm{H}} \quad (5.3)$$

The overall efficiency is represented by η_{DSBFC} whereas η_{r} is the thermodynamic efficiency, η_V is the electrochemical efficiency, η_F is the faradic efficiency, η_U is the fuel utilization efficiency and η_H is the heating value efficiency. The thermodynamic efficiency (η_r) of the fuel cell is calculated by the ratio of Gibbs free energy change (ΔG) to change in enthalpy of formation (ΔH) (Larmine and Dicks 2003) (Equation 5.4a). The thermodynamic efficiency of the DSBFC is

determined by using the literature data, (ΔG) = -1267.56 kJ/mol and ΔH = -1392.26 kJ/mol at 25 ^{o}C and 1 atm pressure (Li et al. 2005).

$$\eta_r = \frac{\Delta G}{\Delta H} \tag{5.4a}$$

The electrochemical efficiency is determined by the ratio of operating cell potential to the theoretical cell potential (Equation 5.4b). Theoretical cell potential of the DSBFC is 1.64 V at 25 ^{o}C.

$$\eta_V = \frac{\text{Open circuit voltage}}{\text{Theoretical cell potential}} \tag{5.4b}$$

The ratio of the actual experimental current to the theoretical maximum current is known as Faradic efficiency (η_F) (Equation 5.4c).

$$\eta_F = \frac{\text{Actual current}}{\text{Theoretical current}} \tag{5.4c}$$

Figure 5.9 shows the direct oxidation of $NaBH_4$ in a concentrated alkaline medium (4 M NaOH), indicating the maximum electron generation. However, hydrolysis of $NaBH_4$ to hydrogen gas is unavoidable due to which 7 electrons are utilized per molecule of borohydride electrooxidation instead of theoretical 8 electrons (Pramanik and Rathoure 2016).

The fuel utilization efficiency is defined as the ratio of fuel consumed by the cell to the fuel supplied to the cell (Equation 5.4d). The fuel utilization efficiency (η_U) is considered to be 0.90 (Oh et al. 2015).

$$\eta_U = \frac{\text{Fuel consumed}}{\text{Fuel supplied}} \quad (5.4d)$$

The ratio of the heating value of fuel that is electrochemically transformed to the heating value of all fuel components present in the fuel is known as heating value efficiency. It is 1 for pure fuel. Thus, the overall efficiency is calculated by using Equation 5.3 without using heating value efficiency and is presented in **Table 5.25**. The overall efficiency of the DSBFC is found to be 0.44.

Table 5.25 The efficiency of the DSBFC at room temperature of 25 ^{o}C and atmospheric pressure (1 atm).

Type of efficiency	η_r	η_V	η_F	η_U	η_{DSBFC}
Efficiency	0.91	0.61	0.88	0.90	0.44

5.4 Stability test of direct sodium borohydride fuel cell (DSBFC)

The stability test of the best synthesized membrane i.e., $PT_{10wt.\%}$-7Cy-(4M) obtained at optimum conditions was tested in the direct sodium borohydride fuel cell at the temperature of 30 ^{o}C (**Figure 5.47**). The cell voltage was recorded for the maximum power density of 66.96 mW/cm^2 at current density of 144 mA/cm^2 (i.e., at a total current of 900 mA) for 15 h at a fixed interval of 1 h. It is seen from **Figure 5.47** that the variation of cell potential is very small from the start time to the operating time of 15 h. The initial cell potential of the DSBFC was 0.465 V and the cell potential after 15 h observed to 0.413 V. It is clearly seen that the drop in cell potential is negligible. Thus, it can be concluded that the synthesized membrane electrolyte $PT_{10wt.\%}$-7Cy-(4M) is quite stable for application in direct sodium borohydride fuel cell.

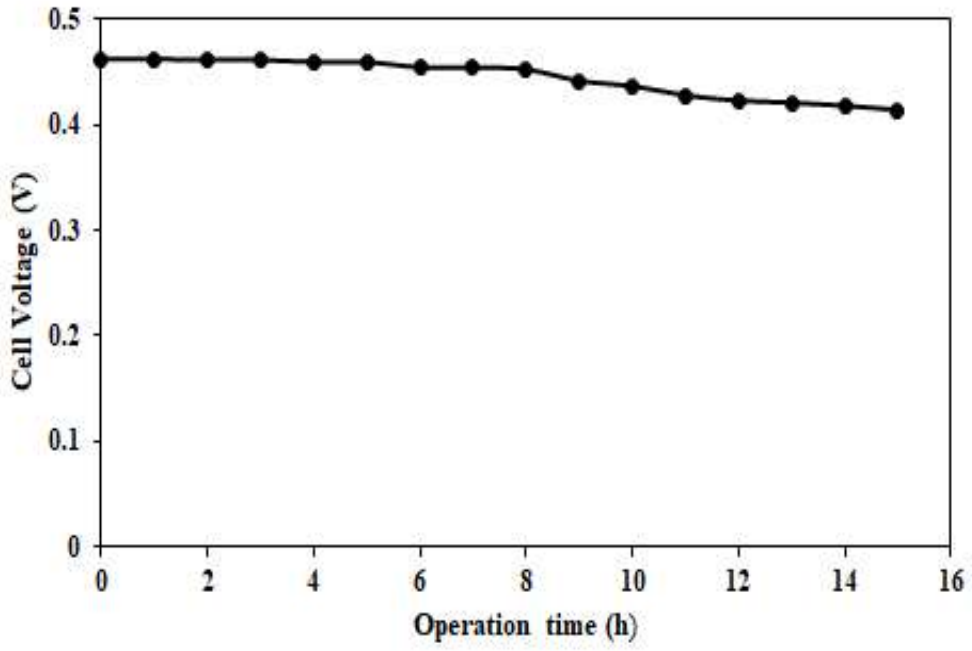

Figure 5.47 Stability test of the PT10wt.%-7Cy-(4M) membrane electrolyte for the DSBFC at optimum condition at cell temperature of 30 ^{o}C.

5.5 Cost analysis of the synthesized membrane electrolyte

The cost of the material used in the preparation of 100 ml PVA-TEOS solution and NaOH doping material is given in appendix **Table C1.** The NaOH doped PVA-TEOS membrane of 3 cm × 3 cm was used for manufacturing a single MEA which was used in the DSBFC study. The membrane electrolyte of four numbers having 3 cm × 3 cm dimension were obtained from 100 ml of PVA-TEOS solution. Thus, the cost of a single membrane used in the fuel cell was $ 0.1574 (**Table C1**). However, the cost of 7.5 cm × 13 cm commercial Nafion™ 117 with the thickness 0.007 in. (product code 915270) supplied by Sigma-Aldrich (https://www.sigmaaldrich.com) is $ 128.51 and thus, the cost of this Nafion™ 117 membrane of 3 cm × 3 cm is estimated to be $ 11.863. It is clear from this cost analysis and subsequent cost comparison between the laboratory synthesized

and commercial membrane electrolyte that the synthesized PV-TEOS membrane is very much cheaper than the commercial Nafion™ 117 membrane.